Using Applied Tracer Tests to Predict

Solute Transport in Fractured Rock Aquifers

Submitted by

Douglas Weatherill BSc (Hons)

as requirement in full for the degree of Doctor of Philosophy in the

School of the Environment

Faculty of Science and Engineering

Flinders University

May 2010

Contents

Summary v

Declaration of Originality vi

Acknowledgements vii

Chapter 1: Introduction 1

Objectives 1

Synopsis of the Remaining Chapters 3

Chapter 2: Applied tracer tests in fractured rock: Can we predict natural gradient solute transport more accurately than fracture and matrix parameters? 3

Chapter 3: Discretising the fracture-matrix interface for accurate simulation of solute transport in fractured rock 4

Chapter 4: Conceptual model choice for dipole tracer tests in fractured rock 5

Chapter 5: Interpreting dipole tracer tests in fractured rock aquifers 6

Chapter 2: Applied tracer tests in fractured rock: Can we predict natural gradient solute transport more accurately than fracture and matrix parameters? 9

Abstract 9

Introduction 10

Theory 14

Methods 16

Forward model 16

Adding noise to the breakthrough curve 17

Parameter estimation with PEST 20

Breakthrough curve characteristics....21
Results....22
Best-fit parameters....24
Predictions....24
Uncertainty comparison: parameter estimation vs prediction....31
Discussion....33
Conclusions....36
Notation and Units....38
References....40
Chapter 3: Discretising the fracture-matrix interface for accurate simulation of solute transport in fractured rock....42
Abstract....42
Introduction....43
Analytical Modelling....46
Numerical Modelling....46
Results....53
Discussion....63
Conclusions....65
Notation and Units....68
References....70
Chapter 4: Conceptual model choice for dipole tracer tests in fractured rock....74
Abstract....74
Introduction....75
Methods....77
Results....84

Discussion 89
Conclusions 92
Notation and Units 95
References 96
Chapter 5: Interpreting dipole tracer tests in fractured rock aquifers 99
Abstract 99
Introduction 100
Generating Synthetic Fracture Networks 102
Numerical Modelling 105
Analytical Modelling 109
Field Tracer Tests 118
Discussion 127
Conclusions 129
Notation and Units 132
References 134
Chapter 6: Concluding Remarks 136
Summary of Findings 136
Further Research 138
Appendix A: Published Papers 141

Summary

Applied tracer tests are used to measure solute transport characteristics of fractured rock aquifers. Whilst not always mentioned in the published literature, the ultimate purpose of the characterisation is to enable prediction of solute transport in the aquifer. The thesis examines the potential for using forced-gradient, applied tracer tests to predict solute transport under natural gradient conditions in fractured rock aquifers.

Analysis of tracer tests to quantify aquifer parameters requires use of an interpretative model. Previously it has been assumed that equivalent single fracture and matrix parameters can be used to represent complex networks of fractures. Given the highly heterogeneous nature of fractured rock aquifers, tracer breakthrough curves often contain detailed features that cannot be fully replicated by comparatively simple analytical models. This thesis examines the parameter and prediction uncertainty that might arise from such discrepancies between fitted breakthrough curves and complex measured data. Comparisons are made between parameters and predictions obtained using different analytical models and the ability of single fracture models to interpret tracer transport in networks of fractures is examined. Methods to improve predictions of solute transport and quantify uncertainty are identified. Also, previously unidentified discretisation requirements are presented to enable accurate simulation of tracer transport in numerical groundwater flow and transport models.

Declaration of Originality

I certify that this thesis does not incorporate without acknowledgement any material previously submitted for a degree or diploma in any university; and that to the best of my knowledge and belief it does not contain any material previously published or written by another person except where due reference is made in the text.

Douglas Weatherill

Acknowledgements

I must say a big thank you to my supervisors, Professor Craig Simmons (Flinders University) and Professor Peter Cook (CSIRO Land and Water) for their scientific guidance, patience and endless support. Their constructive criticism helped me along the road of scientific discovery and development that is the PhD process. Both are brilliant scientists. Craig has been an inspiration throughout my entire university education, from my undergraduate degree, to supervising my Honours project and now supervising my PhD. He gives more than is required and it is greatly appreciated. I look back fondly on the long days spent in the Clare Valley with Peter as we waited for tracer to arrive!

Neville Robinson's assistance programming and mathematical aspects of the thesis was greatly appreciated. Neville was always willing to discuss my work when needed.

Thank you to William Sanford (Colorado State University) for allowing me to visit CSU and for teaching me the technical aspects required to run an applied tracer test.

Finally, thank you to my extremely patient partner Jodie. I would not have managed to finish this thesis without your support and encouragement.

Chapter 1: Introduction

Objectives

The occurrence of contaminants in groundwater systems has created a need for means to characterise the aquifer properties affecting solute transport. Applied tracer tests enable in-situ measurement of solute transport and a means to estimate aquifer parameters. Tests conducted under a forced hydraulic gradient enable more rapid measurement of tracer breakthrough than could be achieved under ambient flow conditions and so these types of tests are usually preferred. The interpretation of tracer tests in fractured rock aquifers presents a challenge due to their highly heterogeneous nature. There is little in the published literature regarding the uncertainty that is inherent in aquifer parameters interpreted from tracer tests in fractured rock. Perhaps more importantly, the accuracy of predictions of solute transport using made using these inferred aquifer parameters is not understood.

The broad objectives of this thesis are to:

1) evaluate how accurately aquifer parameters can be determined from tracer test data, given the inability of analytical models to completely describe the complex nature of fractured rock and associated tracer breakthrough curves;
2) quantify the impact of parameter and interpretative model uncertainty on predictions of solute transport under lower hydraulic gradients;

3) identify the most effective ways to improve the accuracy of predictions of solute transport in fractured rock aquifers made using tracer test data;

The next four chapters are presented in the form of self-contained scientific papers. They comprise two papers which have been published in international journals and two papers which have been prepared ready for submission to journals. The chapters/papers are as follows:

Weatherill, D, Cook, PG, Simmons, CT and Robinson, NI, 2006. Applied tracer tests in fractured rock: Can we predict natural gradient solute transport more accurately than fracture and matrix parameters? Journal of Contaminant Hydrology 88, 289-305. **(Chapter 2)**

Weatherill, D, Graf, T, Simmons, CT, Cook, PG, Therrien, R, and Reynolds, DA, 2008. Discretizing the fracture-matrix interface to simulate solute transport. Ground Water 46(4), 606-615. **(Chapter 3)**

Weatherill, D, McCallum, JL, Simmons, CT, Cook, PG, Robinson, NI. Conceptual model choice for dipole tracer tests in fractured rock. In preparation. **(Chapter 4)**

Weatherill, D, Simmons, CT, Cook, PG. Interpreting dipole tracer tests in fractured rock aquifers. In preparation. **(Chapter 5)**.

Each of the following chapters contains a review of relevant literature in the introductory phases. Copies of the two published papers are provided in Appendix A.

Synopsis of the Remaining Chapters

The following presents a synopsis of the four chapters and their main scientific contributions.

Chapter 2: Applied tracer tests in fractured rock: Can we predict natural gradient solute transport more accurately than fracture and matrix parameters?

Applied tracer tests provide a means to estimate aquifer parameters in fractured rock. The traditional approach to analysing these tests has been using a single fracture model to find the parameter values that generate the best fit to the measured breakthrough curve. In many cases, the ultimate aim is to predict solute transport under the natural gradient. Usually, no confidence limits are placed on parameter values and the impact of parameter errors on predictions of solute transport is not discussed. The assumption inherent in this approach is that the parameters determined under forced conditions will enable prediction of solute transport under the natural gradient. The parameter and prediction uncertainty that might arise from analysis of breakthrough curves obtained from forced gradient applied tracer tests is examined. By adding noise to an exact solution for transport in a single fracture in a porous matrix, multiple realisations of an initial breakthrough curve are created. A least squares fitting routine is used to obtain a fit to each realisation, yielding a range of parameter values rather than a single set of absolute values. The suite of parameters is then used to make predictions of solute transport under lower hydraulic gradients and the uncertainty of estimated parameters and subsequent predictions of solute transport is compared. Results show that predictions of breakthrough curve

characteristics (first inflection point time, peak arrival time and peak concentration) for groundwater flow speeds orders of magnitude smaller than that at which a test is conducted can sometimes be determined even more accurately than the fracture and matrix parameters. This paradigm/philosophy has not been explored in previous literature.

Chapter 3: Discretising the fracture-matrix interface for accurate simulation of solute transport in fractured rock

This paper is not targeted at addressing the overall research aims of the thesis. Rather, the paper is a by-product of work presented in chapter 5, in which applied tracer tests are simulated in fractured rock using a numerical model. During that process it became apparent that extremely fine spatial discretisation was required in the matrix material immediately adjacent the simulated fractures. This had not been previously identified in the literature. Chapter 3 is the result of investigation into the causes and occurrences of the need for such fine discretisation.

This paper examines the required spatial discretisation perpendicular to the fracture-matrix interface (FMI) for numerical simulation of solute transport in discretely-fractured porous media. The discrete fracture finite element model HydroGeoSphere and a discrete fracture implementation of MT3DMS were used to model solute transport in a single fracture and the results were compared to an analytical solution. To match analytical results on the relatively short timescales simulated in this study, very fine grid spacing perpendicular to the FMI, of the scale of the fracture aperture, is necessary if advection and/or

dispersion in the fracture are high compared to diffusion in the matrix. The requirement of such extremely fine spatial discretisation has not been previously reported in the literature. In cases of high matrix diffusion, matching the analytical results is achieved with larger grid spacing at the FMI. Cases where matrix diffusion is lower can employ a larger grid multiplier moving away from the FMI. The very fine spatial discretisation identified in this study for cases of low matrix diffusion may limit the applicability of numerical discrete fracture models in such cases.

Chapter 4: Conceptual model choice for dipole tracer tests in fractured rock

Applied tracer tests provide a means to estimate fracture and matrix parameters that determine solute transport in fractured rock. Dipole tracer tests utilise an injection-extraction well pair to create a forced hydraulic gradient, allowing tests to be conducted more rapidly than natural gradient tests. Tracer breakthrough is analysed using an analytical model to find the parameters that generate the best fit to the data. This study explores the differing interpretation that can be drawn from a tracer test when analysed with two different models; one assuming a dipole, the other a linear flow field. The two models are able to produce almost identical breakthrough curves for a range of scenarios. Comparison of the parameters required to create matching breakthrough curves demonstrates the non-uniqueness of the 1-D and dipole interpretations, resulting in large parameter uncertainty. Considering that neither of the conceptual models incorporates the complexity of a real fracture network, it is expected that analytically interpreted parameters may be as different, or more

different from reality as they are from those interpreted with a different analytical model. Given the complex nature of fractured rock systems and the many unknown fracture and matrix properties involved therein, this study highlights the benefit of incorporating multiple conceptual models in the analyses of dipole tracer tests conducted in fractured rock.

Chapter 5: Interpreting dipole tracer tests in fractured rock aquifers

Dipole tracer tests, where transport of applied tracer is measured in a steady state flow field between an injection-extraction well pair, provide a means to measure solute transport through in-situ aquifer material. A dipole flow field allows sampling of a large volume of aquifer and the forced gradient enables rapid measurement of tracer transport. The measured tracer breakthrough curve is used to infer aquifer properties, usually using an analytical model. For tests conducted in fractured rock aquifers it is usually assumed that equivalent single fracture and matrix parameters can be used to represent the whole network. The extent to which the complex geometry of a fracture network affects the interpretation of a dipole tracer test is not known.

The previous chapter examined the different interpretations that can arise when using two single fracture analytical models. This study builds on those results to look at the performance of the models when used to interpret tracer tests conducted in networks of fractures. The first part of this study examines the performance of two single fracture analytical models when used to interpret simulated dipole tracer tests conducted in hypothetical three-dimensional fracture networks. Initially a single dipole tracer test is simulated numerically in

a hypothetical fracture network. The analytical models are calibrated to the modelled tracer breakthrough curve and used to predict solute transport under a much lower hydraulic gradient. The predicted solute transport is then compared to the 'real' simulated transport. In this way the consequences of the single fracture approximation and associated flow geometry of the two interpretative analytical models are identified. Both the analytical models are able to produce good fits to the initial tracer test data, but the predictive performance of the models decreases as they are used to predict transport under increasingly lower hydraulic gradients. The study then examines how the predictive capability of the analytical models is improved if additional information is available to calibrate them. The value of the following is examined: (a) an extra tracer test at either higher or lower hydraulic gradient, (b) an additional tracer with a different diffusion coefficient included in the initial tracer test and (c) knowledge of the length of the shortest fracture flow path between the injection and extraction wells (rather than an assumption of a straight line). Results indicated that predictions could be most improved by conducting an additional test at a lower injection and extraction rate.

The second section of this study applies the methodology used in the hypothetical fracture networks to real dipole tracer tests conducted in the Clare Valley, South Australia. Application of the methodology to the field environment introduces additional variations between the assumptions of the analytical models and the reality of the field setting. In correlation with the results for the synthetic fracture networks, the predictive performance of the calibrated single fracture models was found to decrease as the hydraulic gradient of predictive

scenarios was decreased. However, hydraulic data indicated that the application of dipoles at different pumping rates resulted in significantly different dewatering of the aquifer near the extraction well and therefore tests at different hydraulic gradients were not sampling the same fracture pathways between the well pair. This phenomenon, combined with the findings from the hypothetical fracture networks suggests that dipole tracer tests in unconfined aquifers should be performed at the lowest feasible pumping rates where the aim is to predict solute transport under ambient groundwater flow conditions.

Chapter 2: Applied tracer tests in fractured rock: Can we predict natural gradient solute transport more accurately than fracture and matrix parameters?

The work presented in this chapter can be found in the following:

Weatherill, D, Cook, PG, Simmons, CT and Robinson, NI, 2006. Applied tracer tests in fractured rock: Can we predict natural gradient solute transport more accurately than fracture and matrix parameters? Journal of Contaminant Hydrology 88, 289-305.

Abstract

Applied tracer tests provide a means to estimate aquifer parameters in fractured rock. The traditional approach to analysing these tests has been using a single fracture model to find the parameter values that generate the best fit to the measured breakthrough curve. In many cases, the ultimate aim is to predict solute transport under the natural gradient. Usually, no confidence limits are placed on parameter values and the impact of parameter errors on predictions of solute transport is not discussed. The assumption inherent in this approach is that the parameters determined under forced conditions will enable prediction of solute transport under the natural gradient. This paper considers the parameter and prediction uncertainty that might arise from analysis of breakthrough curves obtained from forced gradient applied tracer tests. By adding noise to an exact solution for transport in a single fracture in a porous matrix we create multiple realisations of an initial breakthrough curve. A least squares fitting routine is

used to obtain a fit to each realisation, yielding a range of parameter values rather than a single set of absolute values. The suite of parameters is then used to make predictions of solute transport under lower hydraulic gradients and the uncertainty of estimated parameters and subsequent predictions of solute transport is compared. The results of this study show that predictions of breakthrough curve characteristics (first inflection point time, peak arrival time and peak concentration) for groundwater flow speeds orders of magnitude smaller than that at which a test is conducted can sometimes be determined even more accurately than the fracture and matrix parameters.

Introduction

Applied tracer tests provide a means to estimate aquifer parameters in fractured rock. Tests conducted under a forced hydraulic gradient, for example Novakowski et al. (1985) and Sanford et al. (2002), enable more rapid measurement of tracer breakthrough than could be achieved under ambient flow conditions and so these types of tests are usually preferred.

Many fractured rock tracer tests are analysed with a single fracture model, regardless of whether they were conducted in a single fracture or through a network of fractures. The model may be optimised to fit the breakthrough curve but the parameters, and indeed the model itself, may not be a good representation of reality. An extreme case is when multiple peaks are observed such as those reported by Abelin et al. (1991) and Jakob and Hadermann (1994). A single flow path model can never describe such a system correctly, although a best-fit model could be obtained. Similarly, the choice of whether to

model variable apertures, ambient flow and other processes will impact upon the integrity of the interpretation.

Complex models incorporating many processes and therefore many parameters have greater potential to generate non-unique solutions, whereas simpler models may not be able to adequately match the data. Thus due to the complex nature of fractured rock, analysis of tracer tests conducted in fracture networks is subject to the potential for large errors in the analysis phase, as well as the measurement errors associated with any experimental procedure. Maloszewski and Zuber (1983) go as far as saying *"The great number of non-disposable parameters make a correct interpretation of tracer experiments impossible."* Knowing that our models are always a simplification of reality, it is probably optimistic to place exact values on the parameters obtained from them. There may be many parameter sets that will generate an approximation to a breakthrough curve, but a conventional best-fit inversion approach yields a single set of parameters. For example, for a dipole tracer test in an isolated fracture Novakowski et al. (1985) present parameter values of effective fracture aperture and dispersivity based on a single fracture model with no matrix diffusion. The authors state that due to the goodness of the fit over the entire data range and the sensitivity of the model to dispersivity that their fit is unique, but they do not quantify the errors on the parameters. Similarly, for a dipole tracer test in a fracture network Sanford et al. (2002) present best-fit parameter values for fracture path length, fracture aperture, maximum water velocity and dispersivity for a single fracture model with dispersion and matrix diffusion. Whilst these authors show that different parameter values do not match the

measured breakthrough curves quite as well as the best fit parameters do, they do not quantify the errors on the parameter values. Numerous examples of analyses of tracer tests can be found in the literature in which the absolute parameter values that optimise the fit between a modelled breakthrough curve and the measured one are found. Whilst some authors make comparisons between these parameter values and those obtained using other means or at other sites, errors are rarely quantified. With many assumptions made in analysing tracer test data, it is valuable to obtain a range of parameter sets that fit the data within a prescribed tolerance level and to ascertain the uncertainty on these estimations. This is likely to be more useful than a set of absolute parameter values where error or uncertainty is not known at all.

There is an additional factor that warrants attention. Typically, forced gradient tracer tests are conducted to enable prediction of solute transport under the natural gradient (such as leakage from a waste disposal site). The fracture and matrix parameters obtained from the inversion process are usually a step towards prediction at lower velocities. Yet we have been unable to find any previous studies which have considered the effect that the errors on these parameters may have for prediction. If prediction is the ultimate aim then the errors on the predictions are important.

This paper considers the uncertainty on parameters and predictions that might arise from analysis of breakthrough curves obtained from forced gradient applied tracer tests. In order to simulate the complexity observed in field data, we add noise to an exact solution to create multiple realisations of an initial

breakthrough curve simulated using the analytical solution of Tang et al. (1981). The best fit for each realisation is found using a least squares fitting routine, yielding a range of parameter values rather than a single set of absolute values. The suite of parameters is then used to make a range of predictions of solute transport under lower hydraulic gradients. The uncertainty of estimated parameters from tracer test breakthrough curves and subsequent predictions of solute transport at lower groundwater velocities are compared.

Although this study interprets data generated with a particular single fracture model, the same process is applicable to other models. The purpose of this study is not to provide an absolute description of the behaviour of solute transport in fractured rock, but rather to demonstrate that the uncertainty associated with solute transport predictions under natural gradients may, in some cases, be smaller than the uncertainty of parameters estimated from breakthrough curves. This paradigm/philosophy has not been explored in previous literature.

The objectives of this study are to identify:

1) How accurately individual parameters can be determined from a breakthrough curve;
2) How accurately can predictions be made of solute transport under lower hydraulic gradients using parameters obtained from fitting a forced gradient breakthrough curve;
3) How the uncertainties on parameters compare to those on predicted solute transport.

Theory

Tang et al. (1981) present a solution for solute transport in a single fracture with geometry as outlined in Figure 2.1. Fluid flow occurs within the fracture only whilst solute transport occurs both within the fracture and the porous matrix. The solution incorporates solute transport via advection, longitudinal mechanical dispersion and molecular diffusion in the fracture, adsorption onto the face of the matrix, diffusion and adsorption within the matrix and radioactive decay. Tang et al. (1981) describe transport in the fracture as:

$$\frac{\partial c}{\partial t}+\frac{v}{R}\frac{\partial c}{\partial z}-\frac{D}{R}\frac{\partial^2 c}{\partial z^2}+\lambda c-\left.\frac{\theta D'}{bR}\frac{\partial c'}{\partial x}\right|_{x=b}=0 \qquad 0\le z\le\infty \tag{2.1}$$

where c = solute concentration (ML^{-3}), t = time (T), v = water velocity (LT^{-1}), R = face retardation coefficient, z = spatial coordinate along the fracture, D = hydrodynamic dispersion coefficient in the fracture (L^2T^{-1}), λ = radioactive decay constant (T^{-1}), θ = matrix porosity (-), b = half fracture aperture (L), D' = diffusion coefficient of solute in the matrix (L^2T^{-1}) and x = spatial coordinate perpendicular to the fracture axis (L). D is defined to be $\alpha v + D^*$ where α = dispersivity and D^* = diffusion coefficient of solute in water and D' is defined as τD^*.

The Laplace transformed solution to the problem as presented by Tang et al. (1981) is:

$$\frac{d^2\bar{c}}{dz^2}-\frac{v}{D}\frac{d\bar{c}}{dz}-\frac{R}{D}\left\{p+\lambda+\frac{\sqrt{p+\lambda}}{A}\right\}\bar{c}=0 \tag{2.2}$$

where

$$A=\frac{bR}{\theta\sqrt{R'D'}} \tag{2.3}$$

and *R'* = matrix retardation coefficient.

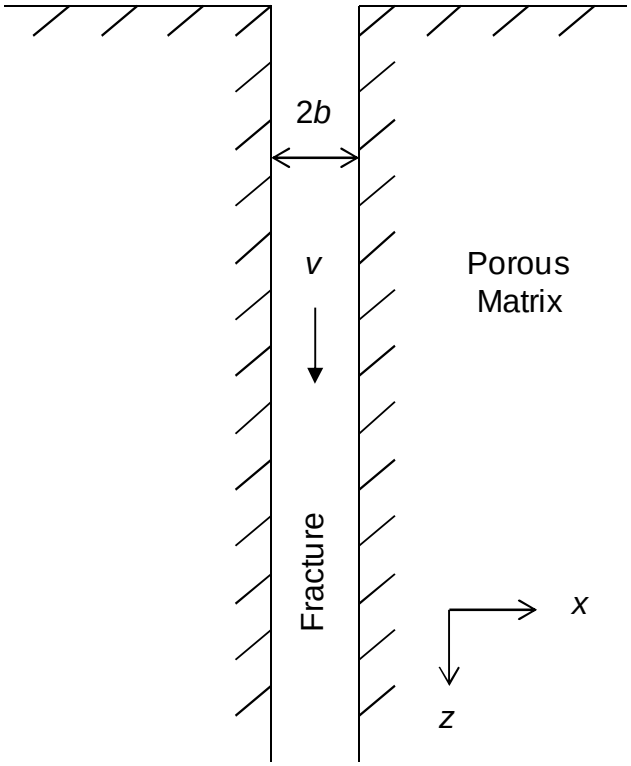

Figure 2.1 The fracture-matrix system after Tang et al. (1981) showing fracture aperture (2*b*) and water flow (*v*).

We solved the Tang et al. (1981) expression by numerical Laplace transform inversion using the accurate and robust routine of Piessens and Huysmans (1984). The solution method was verified by reproducing the analytical results presented in Fig. 9 and Fig. 10 of Tang et al. (1981) and checking with a series solution for finite length fractures Robinson and Sharp (1997).

It can be seen from Equation 2.2 that for a solute that does not decay or sorb (λ = 0, *R* = 1, *R'* = 1) the only parameters affecting the solute concentration in the fracture are *v*, *D* and *A*. These represent the three processes of advection,

dispersion and matrix diffusion respectively. By assuming that hydrodynamic dispersion within the fracture is dominated by the mechanical dispersion component (ie $\alpha v >> D^*$) the 6 parameters (v, α, D^*, θ, τ and b) can be reduced to v, α and A, where A is now simplified to $A = b/\theta D'^{1/2}$.

Methods

Forward model

The Tang et al. (1981) analytical solution for solute transport in a single fracture was used to generate breakthrough curves for seven initial parameter sets (see Table 2.1 for parameter values). Parameters for the base case were chosen to be similar to results presented in the literature. The other six parameter sets were chosen by increasing and decreasing the three variable parameters, v, α and A. In all cases, an input tracer pulse duration of1 hour was used, breakthrough curves were measured at a distance z = 10 m along the fracture, retardation constants were set to 1 and radioactive decay was set to zero. The breakthrough curves were defined by 16 equally (temporally) spaced data points over one day.

Parameter Set	$2b$ (m)	D' (m^2/d)	θ (-)	α (m)	v (m/d)	z (m)	A ($d^{-1/2}$)	β (-)
Base Case	10^{-4}	10^{-4}	0.02	1	100	10	0.25	1.26
Low α	10^{-4}	10^{-4}	0.02	0.001	100	10	0.25	40.00
High α	10^{-4}	10^{-4}	0.02	2	100	10	0.25	0.89
Low A	10^{-4}	10^{-4}	0.04	1	100	10	0.125	5.06
High A	10^{-4}	10^{-4}	0.01	1	100	10	0.5	0.32
Low v	10^{-4}	10^{-4}	0.02	1	50	10	0.25	2.53
High v	10^{-4}	10^{-4}	0.02	1	200	10	0.25	0.63

Table 2.1 Initial parameters used for each of the parameter sets

Adding noise to the breakthrough curve

In order to determine the sensitivity of the breakthrough curves to different hydrogeologic parameters, 100 realisations were generated from each parameter set, each with different added random noise of a specified level (ranging from 5% to 20%) added to each data point. The effect of the applied noise level is examined in this study. By progressively increasing the number of realisations employed, it was found that 100 realisations were more than sufficient to achieve converged average fitted parameters.

We first attempted to understand how such noise might appear in field tracer experiments. Clearly, the interpreted differences between a real breakthrough curve and any mathematical fit (herein after called “noise”) are a function of numerous factors including (1) measurement error in instruments, field data collection and subsequent analyses, (2) the choice of conceptual and hence mathematical model used to fit the field data, (3) the inherent complexity (at many spatial and temporal scales) in heterogeneous geologic field settings that is not captured by the mathematical model employed, and (4) the fitting algorithms and convergence criteria used to define when an optimised fit to the data has been obtained. An analysis of typical tracer test results presented by Sanford et al. (2002) reveals an average residual of 19% (with residual mode = 2 to 4%) for bromide and 18% (with residual mode = 6 to 8%) for helium, where the residual is defined as the absolute value of $(c_{measured} - c_{modelled})/c_{measured}$. In comparing these average and modes, it is clear that the average is somewhat larger owing to a small number of data points which have large associated residuals. This comparison with field data is fairly crude and is based upon one

case only. However, it suggests that the level of noise applied in this study is indeed likely in a field based scenario. It was difficult to determine what distribution these residuals followed due to the limited number of points in the breakthrough curves. This problem is expected to arise in the analysis of most, if not all, previously published breakthrough curves due to the typically limited number of measurement points and a resultant inability to construct the precise statistical distribution of residuals. To the authors best knowledge the nature of such residuals (i.e., discrepancies between measured and modelled data) are rarely, if ever, known and have not been the subject of previous investigation. Therefore, the choice of noise type used in this study (white noise) might be arbitrary, but the aim of this study is intended to be demonstrative rather than absolutely quantitative. Therefore, the key trends and outcomes of the study are expected to be qualitatively similar regardless of the choice of noise distribution employed.

Random numbers were obtained using a random number generator in which each random number had an equal probability of falling anywhere between 0 and 1 (white noise). The level of noise was specified such that the maximum deviation from the initial data was a chosen percentage of the initial data value itself. This process is illustrated in Figure 2.2, where the initial data for the base case is shown as well as a realisation of the data with 20% noise added. The best-fit breakthrough curve for the realisation does not pass directly through the initial data points, but is similar to the initial curve. Adding noise creates a fit that is not the absolute best fit to the initial data, but that still approximates it.

Repeating this process creates a range of similar breakthrough curves that approximate the initial data.

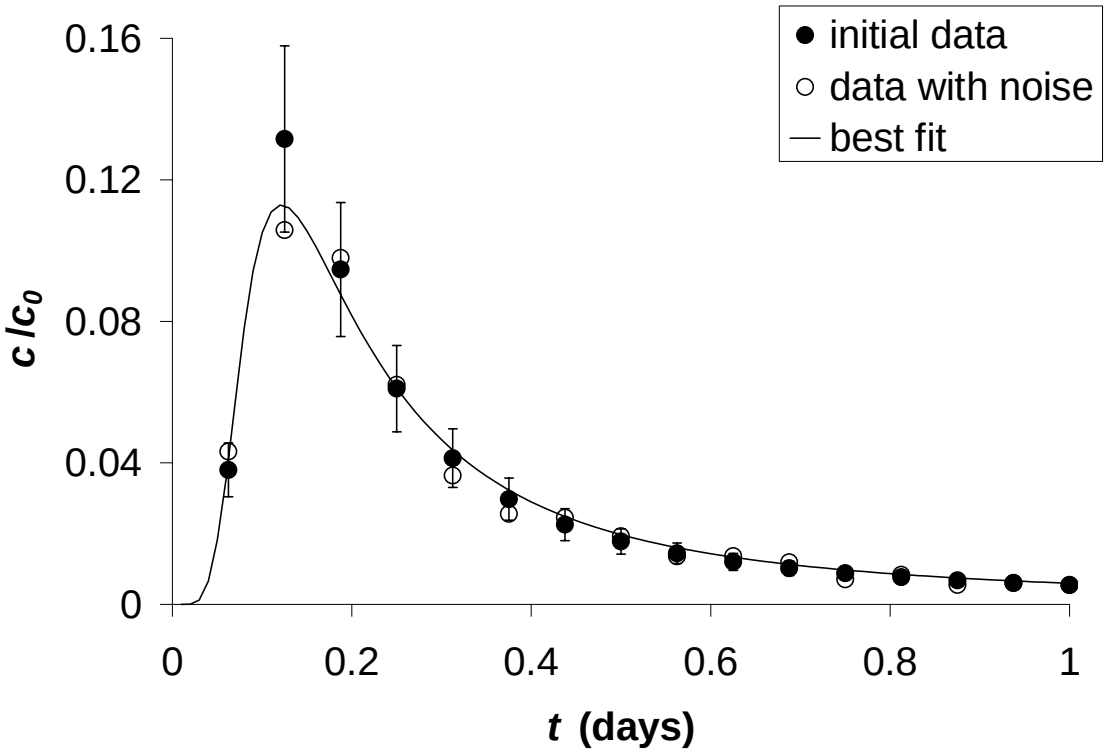

Figure 2.2 Initial data for the base case (with 20% error bars) and a realisation of the data with 20% noise added. The best fit to the realisation is shown as the solid line.

It should be noted that the number of data points and the noise applied to them affects the parameter estimation process. As the number of data points increases, the range of fits to the data decreases and the realisations more closely approximate the forward model. Also the higher the noise level, the greater the range of fits to the data.

Parameter estimation with PEST

PEST (Doherty, 2004) is a model-independent parameter estimation program. PEST finds the parameters that minimise the squared sum of weighted residuals between the target and fitted data values. In our study, equal weighting was assigned to all data values. PEST has a number of ways of determining when it has found optimal parameter values (or done the best it can). The ideal termination criterion is that the objective function (squared sum of weighted residuals) reaches zero. This means that the parameters have been found such that the modelled values exactly match the measured values. This cannot always be achieved, so other termination criteria are required. In our study, if 4 iterations pass since the lowest objective function value, or if the lowest 4 objective function values are within 0.005, relative to the minimum objective function, of each other, PEST stops. Otherwise if 4 iterations pass in which the largest relative parameter value change has been less than or equal to 0.01, PEST terminates execution. As a final criterion for ending execution, PEST will stop after 30 iterations. For further detail on PEST, the reader is referred to Doherty (2004).

During the fitting process, bounds must be placed on the parameters. In order to find a representative range of possible fits to the data, large bounds were placed on the parameters so that they would not interfere with the parameter estimation process, except in cases where parameters must be logically bounded (ie α, v, $A \geq 0$).

Breakthrough curve characteristics

In order to quantify the differences between breakthrough curves, properties that would describe the shape and behaviour of a breakthrough curve were required. Three characteristics were used; time to the first inflection point (t_{i1}), time to the peak concentration (t_p) and the peak concentration (c_p). These three characteristics are the most basic descriptors of a breakthrough curve and can most easily be obtained from tracer test data. Other indicators such as mass recovery may be more difficult to quantify accurately and harder to interpret due to mass losses that result from non-recovered tracer, long breakthrough curve tails resulting from the flow geometry induced by the forced gradient and/or matrix diffusion. Thus, mass recovery, whilst theoretically determinable was not used here due to the complications associated with quantifying it under field conditions.

In order to quantify the spread of parameter values and subsequent predictions of the breakthrough characteristics, the coefficients of variation (*CV* = standard deviation / mean) of parameter values and predicted characteristics were found for each set of realisations. This enables uniform and consistent comparison of the confidence in different estimated parameters/predictions regardless of their numerical values.

In order to determine the accuracy of predictions based on parameters obtained under a forced gradient (high water velocity), breakthrough curves were generated using parameters from each of the best-fit realisations at several slower groundwater flow velocities. It is assumed here that the hydraulic

pressures associated with the different hydraulic gradients have no effect on the fracture apertures or other physical properties of the system other than to change the flow velocity of water in the fracture. Characteristics t_{i1}, t_p and c_p were determined at v_{pr} = 1, 0.3, 0.1, 0.03, 0.01, 0.003, 0.001, 0.0003 and 0.0001 where:

$$v_{pr} = \frac{v_{prediction}}{v_{test\ (fitted)}} \tag{2.4}$$

where $v_{prediction}$ = prediction water velocity (LT^{-1}) and $v_{test\ (fitted)}$ = fitted water velocity under the forced gradient (LT^{-1}).

Scaling down to v_{pr} = 0.0001 is sufficient to cover the scaling required for most current forced gradient tracer tests. Love et al. (2002) quote hydraulic gradients ranging from 0.005 to 0.1 for a fractured rock catchment. Consider a tracer test conducted between two wells 10 m apart in such a system. In order to require a scaling factor of v_{pr} = 0.0001, a head difference of 500 m to 10 000 m between the two wells would need to be imposed. This head difference is unrealistically large and therefore suggests that the range of v_{pr} employed in this study more than adequately covers the range likely to be encountered in realistic field settings.

Results

Figure 2.3 shows the breakthrough curves for the seven initial parameter sets outlined in Table 2.1. In fractured rock systems, particularly where the porosity of the matrix is greater than the fracture porosity, solute transport over long time scales is dominated by matrix diffusion. By applying a forced gradient, tracer

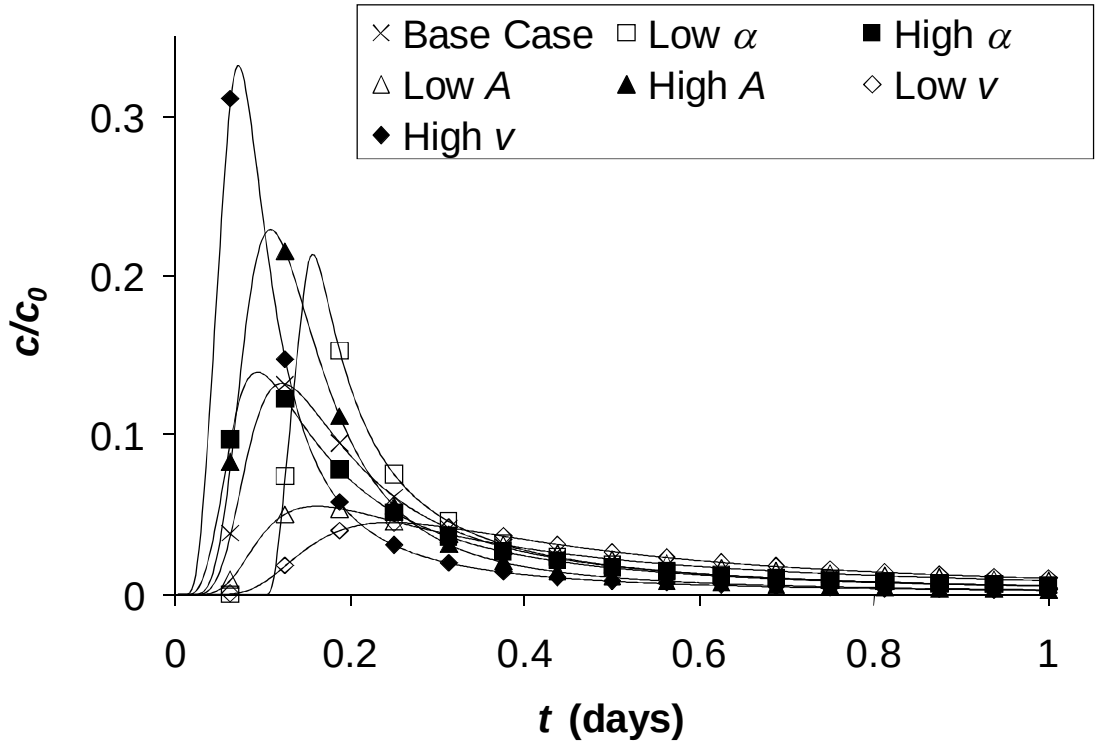

Figure 2.3 Initial breakthrough curves for the parameter sets, each consisting of 16 data points over 1 day. Parameter values are given in Table 2.1.

tests increase the impact of dispersion and are less sensitive to diffusion. In order to assess the predictive capability of parameters obtained under forced conditions it was necessary to cover a range of diffusive to dispersive scenarios under the forced gradient. Lever and Bradbury (1985) quantify the relative importance of diffusion and dispersion by the ratio of time scales over which each spreads solute, defined as:

$$\beta = \frac{z^{3/2}}{4A^2 v\sqrt{\alpha}} \tag{2.5}$$

Values less than one indicate that dispersion dominates whilst values greater than one indicate the dominance of diffusion. Whilst the Lever and Bradbury (1985) approach treats diffusion and dispersion as independent processes, in

contrast to the coupled solution of Tang et al. (1981), it gives an indication of the relative dominance of the processes. The parameters chosen for this study cover a range of diffusive versus dispersive scenarios, with β ranging from 0.316 to 40, with the base case close to unity at 1.26. A complete set of values for β is presented in Table 2.1.

Best-fit parameters

Figure 2.4 shows the range in optimised parameter values obtained for the base case with noise levels of 5%, 10%, 15% and 20%. As would be expected, increased noise broadens the range of possible parameter values for α, v and A. For the case of dispersivity, it can be seen that at a 20% noise level one standard deviation (0.472 m) is almost half as large as the average parameter value (1.07 m) itself. The average values for α, v and A remain close to the initial values despite the range of values increasing. However, if sufficient noise was applied, the parameter bounds may be reached (ie α, v, $A \geq 0$) causing parameter biasing.

Predictions

Predictions of solute transport under slower groundwater velocities were made using the same solute source duration and the best-fit parameters for each realisation (with water velocity scaled by v_{pr}). Figure 2.5 (a) shows the initial data points for the base case and best-fit breakthrough curves for the first ten realisations with a noise level of 20%. All breakthrough curves could be considered to fit the initial data. The noise bounds are shown to indicate the

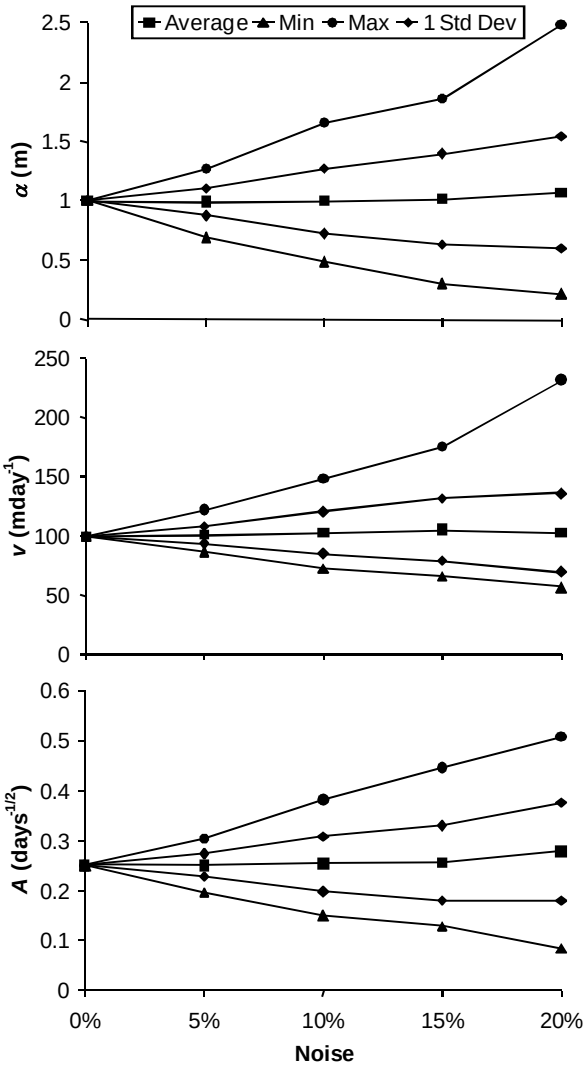

Figure 2.4 Best-fit parameters for 100 realisations of the base case with noise of 5%, 10%, 15% and 20% for (a) dispersivity, (b) water velocity and (c) matrix diffusion term. Averages, minimum, maximum and average +/- 1 standard deviation are shown.

maximum possible variability for the realisations, all of which lie within this range. Figures 2.5 (b), (c), (d) and (e) show the predicted breakthrough curves for the same ten realisations at v_{pr} = 0.1, 0.01, 0.001 and 0.0001 respectively. As velocity decreases, solute arrives at later times (increased t_{i1} and t_p) and at lower concentrations (c_p). As would be expected, the breakthrough curves are less similar as the prediction velocity differs more from the test velocity (ie. v_{pr}

gets smaller). However, the rate at which the overall shape of the breakthrough curves differ appears to decrease at low v_{pr}. This observation is confirmed by examination of the predicted breakthrough curve characteristics t_{i1}, t_p and c_p.

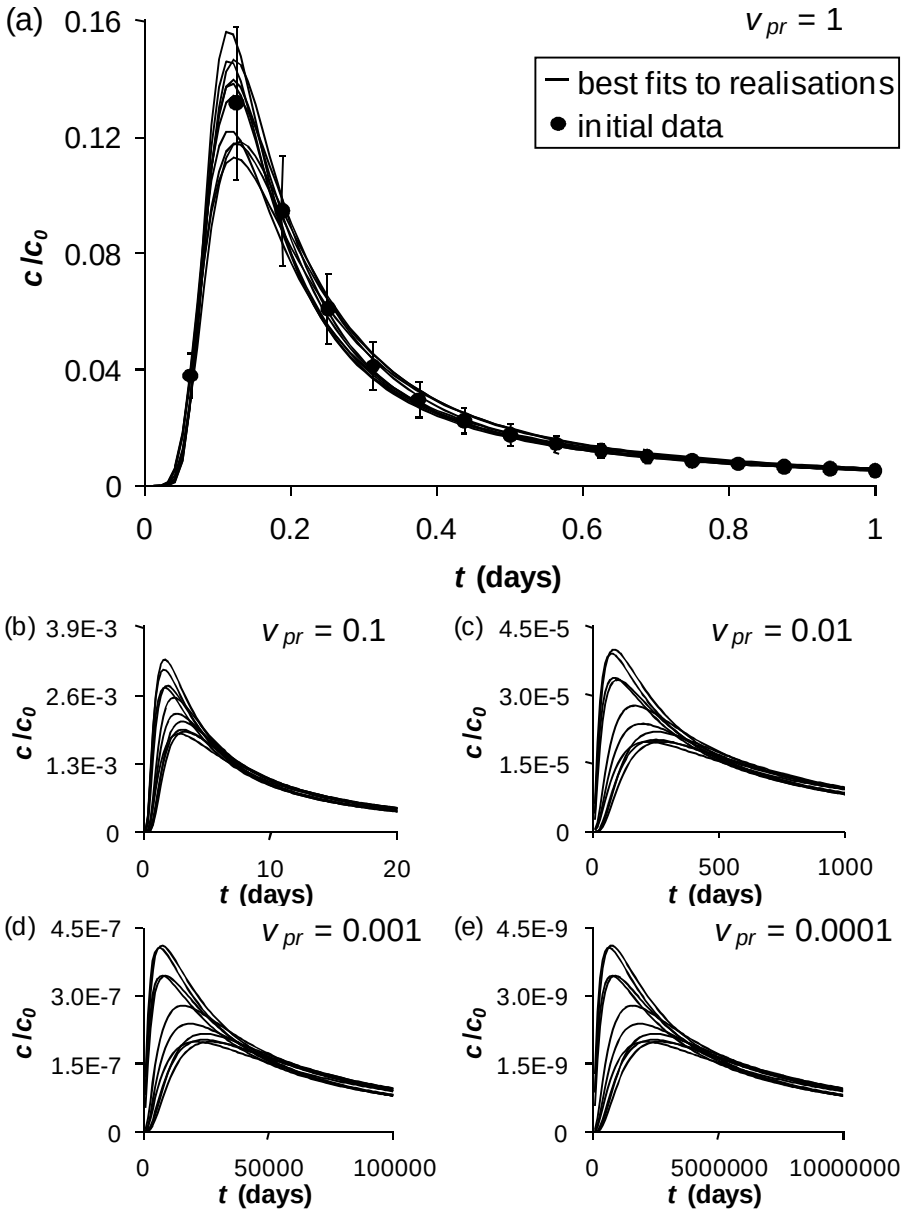

Figure 2.5 (a) Initial data points (with 20% error bars) for the base case and the best-fit breakthrough curves for realisations 1-10 (of 100) with 20% noise. Predictions for realisations 1-10 for v_{pr} = (b) 0.1, (c) 0.01, (d) 0.001 and (e) 0.0001.

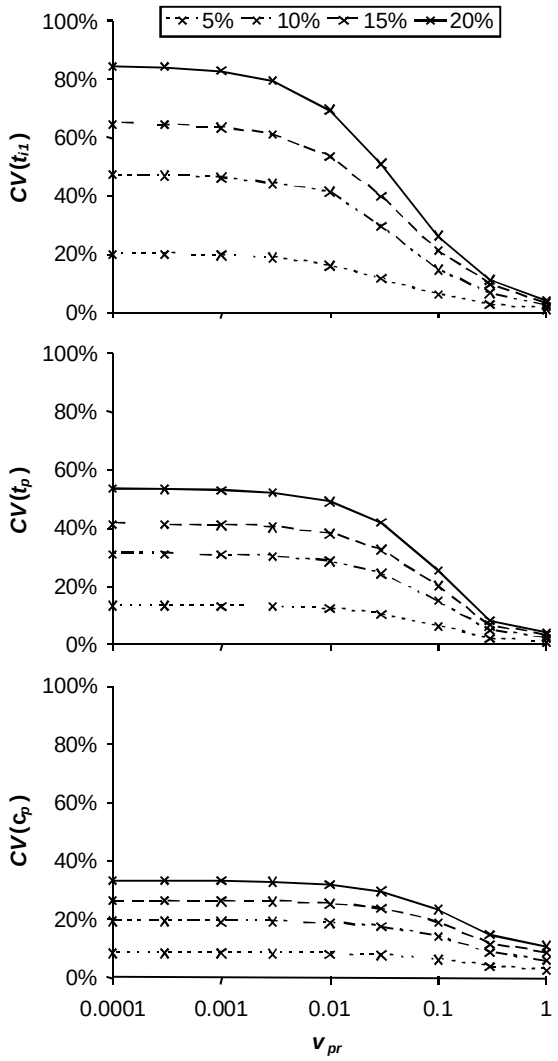

Figure 2.6 Base case coefficient of variation of (a) t_{i1}, (b) t_p and (c) c_p as a function of v_{pr} with noise of 5%, 10%, 15% and 20%. After an initially rapid increase *CV* levels off at low v_{pr} for all characteristics and noise levels.

Coefficients of variation of predicted values of t_{i1}, t_p and c_p as a function of v_{pr} are presented in Figure 2.6. All three characteristics behave in a similar manner. Greater noise increases the uncertainty of all predictions. Also, *CV* increases as v_{pr} decreases from 100%, but plateaus at lower values of v_{pr}. It should be pointed out that the data is plotted on a log scale and $\partial CV/\partial v_{pr}$ is non-zero, but very small and constant at low v_{pr}. As mentioned earlier, the range of

v_{pr} values covered in this study is greater than that which would be used in current practice. The plots cannot be extrapolated back to v_{pr} = 0 as this is meaningless. The plateauing is explained by the lessening impact of dispersivity on the solution at lower velocity. The behaviour asymptotes towards one in which only *v* and *A* have an impact. For example, in the 20% noise case, the *CV* values are 44% for α, 32% for *v* and 36% for *A*. With the dispersion coefficient dominated by αv, as velocity decreases, so does the dispersion coefficient. In addition, slower water flow allows greater matrix diffusion, increasing the dominance of *A* on the solution. Overall at lower water velocity (and lower v_{pr}) the solution is governed more by the better constrained parameters (*A* and *v*) and less by the poorest defined (α).

In order to demonstrate the range of predicted values around the actual values, Figure 2.7 shows the average predicted characteristic values normalised by the actual values with error bounds of +/- one standard deviation. The range of predictions is best constrained at the test speed and broadens with decreasing v_{pr}. Minor biasing of average predictions is evident. Both averages and ranges of predictions plateau for lower v_{pr}.

To test whether the results obtained for the base case apply more generally, a further 6 parameter sets were tested using the same procedure used for the base case, but with decreased and increased α, *A* and *v* (Table 2.1). Figure 2.8 shows the behaviour of the predicted transport characteristics. As with the base case, breakthrough curve characteristics for all parameter sets display a

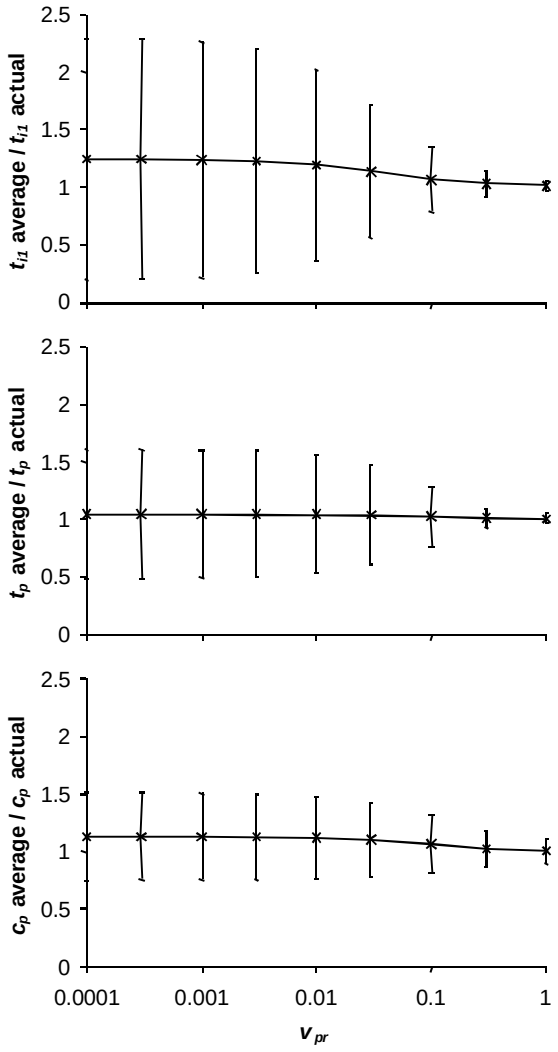

Figure 2.7 Base case (noise = 20%) average values for (a) t_{i1}, (b) t_p and (c) c_p, normalised by the actual values, as a function of v_{pr}. Therefore 1 represents the correct value for a characteristic. Error bars indicate ±1 standard deviation from the average.

decrease in certainty with decreasing v_{pr} and then a levelling at the lowest values of v_{pr}. Each of the parameter sets reaches a different level of uncertainty. It should be pointed out that as v_{pr} is a function of the water velocity at the test speed, identical values of v_{pr} for the altered v cases do not correspond to the same prediction velocities.

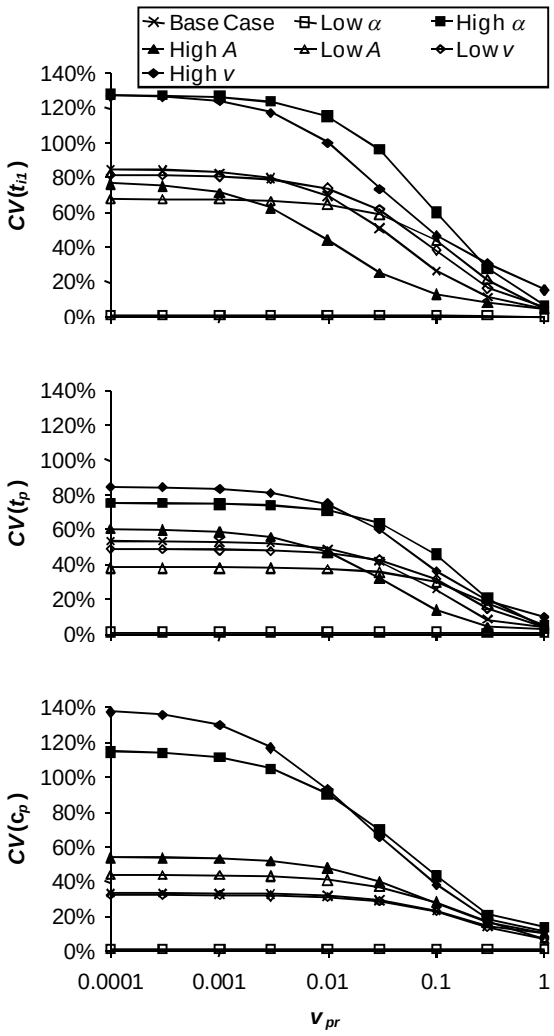

Figure 2.8 Coefficient of variation (noise = 20%) of (a) t_{i1}, (b) t_p and (c) c_p as a function of v_{pr} for all parameter sets. After an initial increase *CV* of all characteristics for all parameter sets levels off at low v_{pr}.

The level of uncertainty on the predictions of solute transport under slower velocities depends on the uncertainty in the parameters themselves and on the dominance of the individual parameters at the different prediction velocities. It may be possible to constrain a particular parameter very well at the test speed, but that parameter may have less impact on transport at the prediction speed. The relative contributions of dispersion in the fracture and diffusion in the matrix

at the test and prediction velocities and the degree to which they can be identified determines the accuracy of the predictions.

Uncertainty comparison: parameter estimation vs prediction

Having determined the uncertainty on the parameters and the predicted breakthrough curve characteristics under different flow velocities, we can now compare the two. Figure 2.9 shows *CV* for parameters α, *v* and *A* and the predicted breakthrough curve characteristics t_{i1}, t_p and c_p (at v_{pr} = 0.0001) for all the parameter sets with 20% noise as well as 5%, 10% and 15% noise levels for the base case. For each of the base case scenarios t_{i1} is the least well constrained predicted characteristic and is less constrained than the parameters. t_p is better constrained and almost as well defined as the parameters. c_p is the most constrained predicted characteristic and even better constrained than α and *A* and almost as constrained as *v*. Whilst the individual values vary, many of the other parameter sets display better constrained predicted characteristics than estimated parameter values.

In the low *A* case all three characteristics can be predicted with greater certainty than the individual parameters themselves can be determined. However, in the high *A* case the opposite is observed. The β parameter used by Lever and Bradbury (1985) can be used to explain this. A comparison of the uncertainty on predicted characteristics relative to parameters with respect to β shows a trend. By counting the number of predicted characteristics that are better constrained than all the corresponding parameters (Figure 2.9) we see that the low *A* case (β = 5.06) has 3, the low *v* case (β = 2.53) has 1 but all other scenarios have at

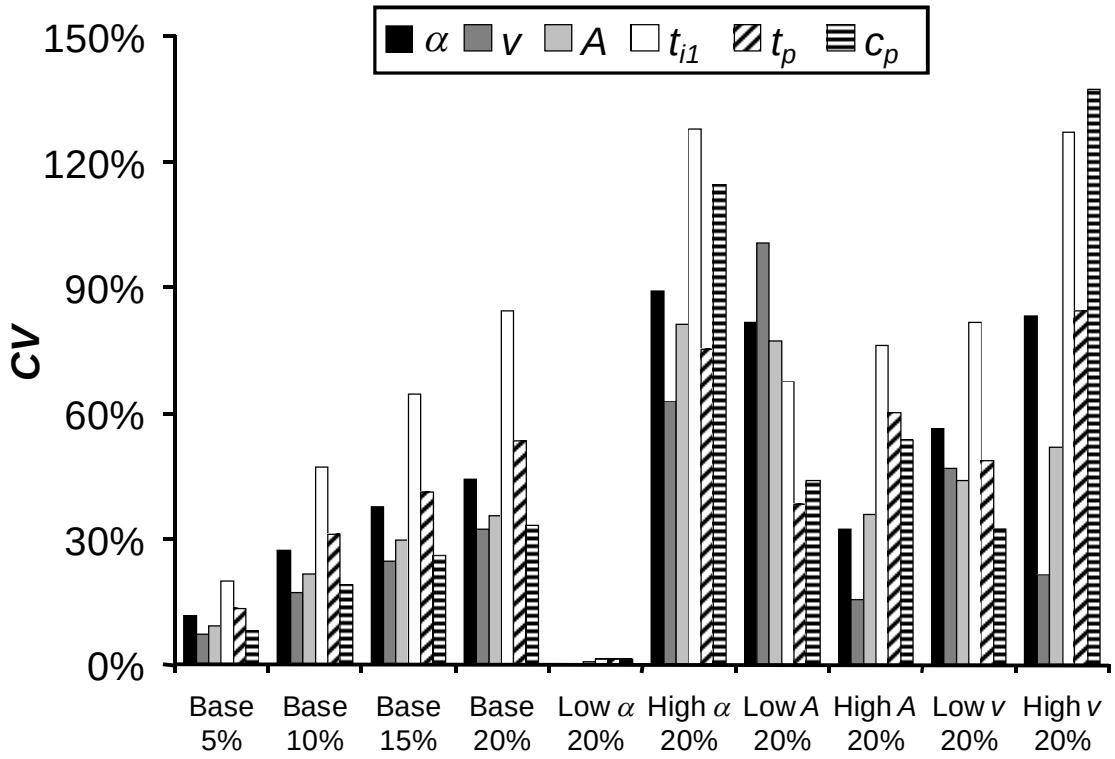

Figure 2.9 Coefficient of variation of parameters α, v and A and predictions (at v_{pr} = 0.0001) of t_{i1}, t_p and c_p for all parameter sets (noise = 20%) and at noise = 5%, 10% and 15% for the base case.

least 1 parameter better constrained than the predicted characteristics. According to their β values, the low A and low v scenarios are relatively diffusive. Generally the degree to which the predictions of characteristics can be constrained relative to the parameters seems to be controlled by β. Scenarios with high β values (more diffusive) tend to yield better constrained predictions of characteristics than parameters and scenarios with low β values (more dispersive) yield less constrained predictions of characteristics than parameters. Furthermore, as natural gradient predictions are dominated by diffusion, tests conducted under more diffusive conditions will yield greater constrained predictions of breakthrough characteristics. This can be seen in Figure 2.8,

where the least constrained predictions of characteristics occur for the high α and high *v* cases.

Discussion

This study has demonstrated that by accepting a range of fits to a simulated forced gradient breakthrough curve, not only can bounds be placed on the parameters themselves, but also on predicted solute transport under the natural gradient. Furthermore the uncertainty on the predicted transport characteristics can be lower than that on the individual parameters. This has important implications for our ability to predict solute transport in fractured rock. Essentially, the results suggest that we are able to conduct a tracer test under a forced gradient 4 orders of magnitude larger than the natural gradient and use the results to predict transport under the natural gradient with errors on peak arrival time of typically $CV(t_p)$ = 40 % to 60%.

Results have shown that tracer tests in which β is large give the best predictions of solute transport under low gradients (where diffusion dominates). In the field, the only parameter in β that can be controlled is *v*. Therefore as would be expected, the lower the velocity of a test is, the better the predictions of solute transport under the natural gradient will be.

Besides the physical test conditions, a number of factors affect the uncertainty on estimated parameters and subsequent predictions of solute transport. The convergence criteria used in the optimisation process determine the accuracy of the fit to each realisation. The number of data points and the noise level applied

to them affect the range of estimated parameters and predictions. Whilst the absolute uncertainties are determined by these choices, we are interested in the relative uncertainties and general trends of parameters and predictions and have shown that they are of a similar magnitude and that in some cases, resultant predictions have less uncertainty than the individual constituent parameters.

This previously unreported behaviour provides positive support for the use of forced gradient tests to predict transport under natural gradient conditions. It was necessary to determine whether this behaviour was real and not a numerical artifact of the solution procedure used in the modelling process. To do this we compare our numerical implementation of the Tang et al. (1981) solution with the zero-dispersivity solution presented by Lever and Bradbury (1985). The dispersivity for the low dispersion case in this study was chosen to be very low to enable comparison with the Lever and Bradbury (1985) analytical solution. The solution for t_p presented in Equation 5.1 of Lever and Bradbury (1985) is:

$$t_p = \frac{z^2}{6}\left(\frac{1}{A^2 v^2}\right) + \frac{z}{v} \tag{2.6}$$

By applying the formula for variance of a linear function:

$$Var\left(U = \sum_i a_i P_i\right) = \sum_i a_i{}^2 Var(P_i) + \sum_i \sum_{\neq j} a_i a_j Cov(P_i P_j) \tag{2.7}$$

letting $a_1P_1 = z^2/6A^2v^2$, $a_2P_2 = z/v$ and assuming z is accurately known, variance of the peak arrival time is:

$$Var(t_p) = \frac{z^4}{36} Var\left(\frac{1}{A^2 v^2}\right) + z^2 Var\left(\frac{1}{v}\right) + \frac{z^3}{3} Cov\left(\frac{1}{A^2 v^2}, \frac{1}{v}\right) \quad (2.8)$$

where *Var* = variance and *Cov* = covariance.

In the low dispersivity case, a comparison of the actual $Var(t_p)$ at v_{pr} = 0.0001 with that calculated from the variances of the fracture and matrix parameters using Equation 8 provides a means to check the validity of the *CV*s generated by the model. To four significant figures, the variances are identical ($Var(t_p)$ = 6.109 x 10^9 days). Thus, the results of the Tang et al. (1981) and Lever and Bradbury (1985) solutions are in excellent agreement and this provides further evidence in support of not only the Tang et al. (1981) numerical solution employed here but also the findings of this study more generally.

This study is a demonstration of a paradigm. As such, it is limited in that both the initial breakthrough curves and fits were generated using a particular model, the single fracture solution of Tang et al. (1981). However, the philosophy behind this work can be extended to all conceptual models of solute transport in fractured rock systems. Indeed, given that the choice of model itself may be the biggest source of error, multiple models could be incorporated into the process. In a field scenario, tracer may travel in complicated flow geometries through channels in multiple fractures with different properties. Whilst tracer tests are usually analysed using single flow-path models (with various flow geometries incorporated), there has been no definitive study to determine the validity and errors associated with this approach for tracer tests conducted on fracture networks. This should form the subject of future investigations.

Conclusions

The key findings of this study are:

1. As the hydraulic gradient decreases, the uncertainty of solute transport predictions does not increase significantly. In particular, this study has shown that a 4 order of magnitude scaling reduction in v results in no worse than an 85 % CV on t_p but that CVs on the order of 40 % - 60 % are typical. This result is not intuitively obvious and is an important finding that has consequences for scaling forced gradient tracer tests in hydrogeology.
2. The uncertainty of solute transport predictions under a natural gradient is typically similar to the uncertainty of the parameters estimated from forced gradient breakthrough curves, and importantly, it is occasionally better. This result suggests that an uncertainty analysis may be more useful than is commonplace in the interpretation of field based tracer tests. Whilst it is typical to only determine the best fit to observed data, these findings suggest that determining the range of acceptable fits is important in understanding the range of both acceptable fitting parameters and hence subsequent predictions of solute transport that are likely.
3. Tracer tests conducted under more diffusive conditions (high β) yield better predictions of solute transport under the natural gradient. In practical terms, v is usually the most easily controllable parameter in β. Therefore, to maximise β to improve predictability necessarily involves conducting tracer tests at the lowest forced gradients that are practically feasible.

4. Therefore, forced gradient applied tracer tests may be a valuable means of estimating solute transport under natural gradients in fractured rock providing that an appropriate choice of interpretational conceptual model is made.

Further work is required to explore how uncertainties on parameter estimation and subsequent predictions at lower velocities are affected by the choice of interpretative conceptual model. This may be a fundamental limitation and clearly warrants further investigation.

Notation and Units

A	matrix diffusion term	$T^{1/2}$
b	half fracture aperture	L
c	solute concentration	ML^{-3}
c'	solute concentration in the matrix	ML^{-3}
Cov	covariance	-
CV	coefficient of variation	-
D	hydrodynamic dispersion coefficient	L^2T^{-1}
D^*	diffusion coefficient of solute in water	L^2T^{-1}
D'	diffusion coefficient of solute in matrix	L^2T^{-1}
R	face retardation coefficient	-
R'	matrix retardation coefficient	-
t	time	T
t_p	peak arrival time	T
v	water velocity	LT^{-1}
Var	variance	-
v_{pr}	prediction water velocity / test water velocity	-
$v_{prediction}$	prediction water velocity	LT^{-1}
$v_{test\ (fitted)}$	fitted water velocity under the forced gradient	LT^{-1}
x	spatial coordinate perpendicular to the fracture axis	L
z	spatial coordinate along a fracture	L
α	longitudinal dispersivity	L

β	ratio of diffusive to dispersive time scales	-
θ	matrix porosity	-
λ	radioactive decay constant	T^{-1}
τ	tortuosity	-

References

Abelin, H., Birgersson, L., Moreno, L., Widen, H., Agren, T. and Neretnieks, I., 1991. A large-scale flow and tracer experiment in granite 2. Results and interpretation. Water Resources Research, 27(12): 3119-3135.

Doherty, J., 2004. PEST: Model-Independent Parameter Estimation. Watermark Numerical Computing, Brisbane, Australia.

Jakob, A. and Hadermann, J., 1994. INTRAVAL Finnsjon Test - modelling results for some tracer experiments. PSI-Bericht No. 94-12, PSI (Paul Scherrer Institut), Wurenlingen.

Lever, D.A. and Bradbury, M.H., 1985. Rock-matrix diffusion and its implications for radionuclide migration. Mineralogical Magazine, 49: 245-254.

Love, A.J., Cook, P.G., Harrington, G.A. and Simmons, C.T., 2002. Groundwater flow in the Clare Valley. DWR02.03.0002, Department for Water Resources, Adelaide.

Maloszewski, P. and Zuber, A., 1983. Interpretation of artificial and environmental tracers in fissured rocks with a porous matrix. In: I.A.E.A. (Editor), Isotope Hydrology 1983, Vienna, Austria, pp. 635-651.

Novakowski, K.S., Evans, G.V., Lever, D.A. and Raven, K.G., 1985. A field example of measuring hydrodynamic dispersion in a single fracture. Water Resources Research, 21(8): 1165-1174.

Piessens, R. and Huysmans, R., 1984. Algorithm 619. Automatic numerical inversion of the Laplace transform. Association of Computer Machinery Transactions on Mathematical Software, 10: 348-353.

Robinson, N.I. and Sharp, J.M., 1997. Analytical solution for solute transport in a finite set of parallel fractures with matrix diffusion. CMIS C23/97, CSIRO, Adelaide.

Sanford, W.E., Cook, P.G. and Dighton, J.C., 2002. Analysis of a vertical dipole tracer test in highly fractured rock. Ground Water, 40(5): 535-542.

Tang, D.H., Frind, E.O. and Sudicky, E.A., 1981. Contaminant transport in fractured porous media: analytical solution for a single fracture. Water Resources Research, 17(3): 555-564.

Chapter 3: Discretising the fracture-matrix interface for accurate simulation of solute transport in fractured rock

The work presented in this chapter can be found in the following:

Weatherill, D, Graf, T, Simmons, CT, Cook, PG, Therrien, R, and Reynolds, DA, 2008. Discretizing the fracture-matrix interface to simulate solute transport. Ground Water 46(4), 606-615.

Abstract

This paper examines the required spatial discretisation perpendicular to the fracture-matrix interface (FMI) for numerical simulation of solute transport in discretely-fractured porous media. The discrete fracture finite element model HydroGeoSphere (Therrien et al. 2005) and a discrete fracture implementation of MT3DMS (Zheng 1990) were used to model solute transport in a single fracture and the results were compared to the analytical solution of Tang et al. (1981). To match analytical results on the relatively short timescales simulated in this study, very fine grid spacing perpendicular to the FMI, of the scale of the fracture aperture, is necessary if advection and/or dispersion in the fracture are high compared to diffusion in the matrix. The requirement of such extremely fine spatial discretisation has not been previously reported in the literature. In cases of high matrix diffusion, matching the analytical results is achieved with larger grid spacing at the FMI. Cases where matrix diffusion is lower can employ a larger grid multiplier moving away from the FMI. The very fine spatial

discretisation identified in this study for cases of low matrix diffusion may limit the applicability of numerical discrete fracture models in such cases.

Introduction

Recent computational and theoretical advances have allowed the development of numerical codes for simulating solute transport in fractured rock. A range of models have been suggested which encompass differing complexity in fracture geometry and the interaction of solutes between fractures and the rock matrix. In a review paper, Neuman (2005) summarises a range of conceptual models for flow and transport in fractured rock. Diodato (1994) presents a compendium of the available numerical models for flow in fractured media. Equivalent porous media (EPM) and multiple-continuum approaches allow solutions which are relatively rapid computationally, but are not always suitable on smaller spatial and temporal scales due to the conceptual simplifications they employ. Neuman (2005) states that a single continuum model of flow and transport in fractured rock is usually inadequate. Discrete fracture models, whilst more demanding computationally, allow simulation of complex fracture networks where the interaction between fractures and the matrix cannot be simplified to an EPM or multiple-continuum approach. A range of discrete fracture models exists, incorporating a variety of physical and chemical processes. Whilst current computing capabilities can limit the application of such models to small scale simulations, they are of benefit in studying system processes and phenomena that occur on the smaller scale. Examples of discrete fracture models capable of simulating solute transport include FRACTRAN (Sudicky and McLaren 1998), HydroGeoSphere (Therrien et al. 2005), MAGNUM-2D (England et al. 1986),

MOTIF (Chan et al. 1999a, 1999b), PORFLOW (Runchal 2002), SWIFT (HSI-GeoTrans 2000) and TRACR3D (Travis and Birdsell 1991). Examples of numerical simulations of solute transport in discretely-fractured porous media with matrix diffusion are found in Grisak and Pickens (1980), Sudicky and McLaren (1992), Therrien and Sudicky (1996), VanderKwaak and Sudicky (1996), Reynolds and Kueper (2002) and Graf and Therrien (2005).

Solute transport in fractured rock is typically characterised by rapid advection within the fractures and minimal advection in the matrix. Much slower solute transport can occur by diffusion into porous matrix material thereby complicating the simulation of mass transport by introducing an additional timescale. Slough et al. (1999) found that longitudinal grid discretisation of fracture elements, particularly at fracture intersections, can have a significant impact on simulated DNAPL transport paths and rates in fracture networks. Additionally, when matrix diffusion is modelled, grid discretisation in the matrix must be fine to correctly simulate the high concentration gradients that develop between fractures and the matrix (Sudicky and McLaren 1992). Previous numerical studies have matched analytical solutions for solute transport in fractured rock despite using grid spacing at the fracture-matrix interface (FMI) that is much larger than the fracture aperture. For example, Sudicky and McLaren (1992) used a grid spacing of 25 mm perpendicular to fractures of aperture 0.1 mm when matching the analytical solution of Sudicky and Frind (1982), equating to elements 250 times the size of the fracture aperture. Cook et al. (2005) matched chlorofluorocarbon-12 (CFC-12) concentrations modelled with the analytical solution of Sudicky and Frind (1982) in a 0.1 mm fracture using a grid spacing

of 25 mm (250 x fracture aperture). In contrast, Reynolds and Kueper (2002) used a much finer discretisation of 100 μm when modelling DNAPL migration in fractures of apertures from 15 to 50 μm (2 to 7 x fracture aperture). To date there has been no systematic study of the spatial discretisation required for accurate simulation of solute transport in fractured rock as a function of the parameter values employed in the model domain, in particular the relative strength of longitudinal advection and dispersion in the fracture to transverse diffusion in the matrix.

This study compares concentrations simulated with the discrete fracture model HydroGeoSphere (Therrien et al. 2005) and a discrete fracture implementation of MT3DMS (Zheng 1990) to those computed with the analytical solution of Tang et al. (1981) for transport in a single fracture embedded in a porous rock matrix. Two aspects of spatial discretisation were investigated: (1) the discretisation of the elements closest to the fracture (Δx_{min}), and (2) the grid multiplier perpendicular the fracture (m_x). The work of Sudicky and McLaren (1992) and Cook et al. (2005) focussed on scenarios where diffusion is higher than that in this study, and demonstrated that over long simulation times relatively coarse discretisation is adequate when advection and mechanical dispersion within the fracture are small compared to diffusion in the adjacent matrix. In contrast, this study examines a scenario with relatively fast fluid flow in the fracture which reduces potential for matrix diffusion. Such conditions can occur when simulating transport on a small spatiotemporal scale and/or under high hydraulic gradients such as those encountered in some tracer tests.

Quantitative relationships are developed between β (a ratio of the timescales for dispersion and advection in the fracture to diffusion in the matrix) and Δx_{min} and m_x to guide discretisation principles. This study demonstrates that when both fracture and matrix domains are modelled with a discrete fracture model not only do spatial grids have to be fine at the FMI, but in cases of low matrix diffusion they need to be on the scale of the fracture aperture to accurately simulate solute transport, not only within the matrix, but also within the fracture. Even where matrix diffusion is deemed to be physically unimportant over relevant timescales, inappropriate discretisation will lead to an over prediction of matrix diffusion and subsequently to an underestimation of advective/dispersive transport within the fracture. This required level of spatial discretisation has not previously been reported in the literature. Another result reported here is that dispersive scenarios can employ a larger grid multiplier moving away from the FMI than diffusive scenarios.

Analytical Modelling

The geometry and solution for the model presented by Tang et al. (1981) is outlined in Chapter 2 (see Figure 2.1 and equations 2.1, 2.2 and 2.3) and is not repeated here.

Numerical Modelling

The discrete fracture fluid flow and solute transport model HydroGeoSphere (Therrien et al. 2005) was used to simulate solute transport in the fracture-matrix system presented by Tang et al. (1981). The control volume finite element (CVFE) method was used to discretise both the flow and transport

equations with full upstream weighting of advective flux terms. The discretised equations are solved using the WATSIT iterative solver package of general sparse matrices (Clift et al. 1996) and a conjugate gradient stabilised (CGSTAB) acceleration technique (Rausch et al. 2005). HydroGeoSphere represents discrete fractures with 2-D planes of connected nodes that already form part of the 3-D grid for the porous medium. The fracture and matrix domains are thus coupled by their co-location and by requiring that their corresponding hydraulic heads and concentrations be equal.

The discretised solute transport equations used by HydroGeoSphere can be simplified for a non-sorbing, non-decaying, non-reactive solute in fully saturated media. For the porous medium:

$$\left[(\theta c)_i^{L+1}-(\theta c)_i^{L}\right]\frac{V_i}{\Delta t}=\varepsilon\left(\sum_{j\in\eta_i}c_{(ij+1/2)}^{L+1}\gamma_{ij}\left(h_j^{L+1}-h_i^{L+1}\right)+\sum_{j\in\eta_i}\chi_{ij}\left(c_j^{L+1}-c_i^{L+1}\right)\right)+ \\ (1-\varepsilon)\left(\sum_{j\in\eta_i}c_{(ij+1/2)}^{L}\gamma_{ij}\left(h_j^{L+1}-h_i^{L+1}\right)+\sum_{j\in\eta_i}\chi_{ij}\left(c_j^{L}-c_i^{L}\right)\right)+\Omega_{ex}^{L+1}V_i \tag{3.1}$$

and for fractures:

$$\left[c_{fi}^{L+1}-c_{fi}^{L}\right]\frac{2ba_i}{\Delta t}=\varepsilon\left(2b\sum_{j\in\eta_{fi}}c_{f(ij+1/2)}^{L+1}\gamma_{fij}\left(h_{fj}^{L+1}-h_{fi}^{L+1}\right)+\sum_{j\in\eta_{fi}}\chi_{fij}\left(c_{fj}^{L+1}-c_{fi}^{L+1}\right)\right)+ \\ (1-\varepsilon)\left(2b\sum_{j\in\eta_{fi}}c_{f(ij+1/2)}^{L}\gamma_{fij}\left(h_{fj}^{L+1}-h_{fi}^{L+1}\right)+\sum_{j\in\eta_{fi}}\chi_{fij}\left(c_{fj}^{L}-c_{fi}^{L}\right)\right)+\Omega_f^{L+1}a_i$$

(3.2)

where: a_i = area associated with fracture node i (L^2), h = hydraulic head (L), V_i = region or control volume associated with porous medium node i (L^3), γ_{ij} = term arising from discretisation and describing fluid flow between i and j (L^2T^{-1}), η_i = the set of nodes connected to node i, χ_{ij} = term arising from discretisation and

describing diffusive/dispersive solute flux between *i* and *j* (L^3T^{-1}), Ω = solute exchange rate between fracture and porous medium domains (T^{-1}) and ε = finite difference time weighting factor (-). Subscript *f* denotes a fracture property, subscripts *i* and *j* denote a property of node *i* or *j* respectively and superscript *L* denotes the time level, with *L*+1 corresponding to the time level for which the solution is sought.

The first term on the right hand side (RHS) of equations (3.1) and (3.2) describes solute transport due to advection. The second term on the RHS describes the flux that results from dispersive and diffusive processes. The last term incorporates mass exchange fluxes between porous medium and fracture domains due to the requirement for their concentrations at common nodes to be equal. In equations (3.1) and (3.2), the concentration terms $c_{(ij+1/2)}$ and $c_{f(ij+1/2)}$ depend on the type of spatial weighting used for the advective term between nodes *i* and *j.* For example, $c_{(ij+1/2)}$ and $c_{f(ij+1/2)}$ are equal to the average concentration between nodes *i* and *j* for the central weighting scheme. Prior to solving the transport equations, HydroGeoSphere first solves the fluid flow equation for the two domains and simulation errors that result from inadequate spatial discretisation of the FMI are generated in the second term of the RHS. When simulating solute transport in a coupled system where transport rates have the potential to vary by orders of magnitude between the two domains (fracture and matrix) it is obvious that inadequate discretisation in the matrix could lead to simulation errors in the fractures.

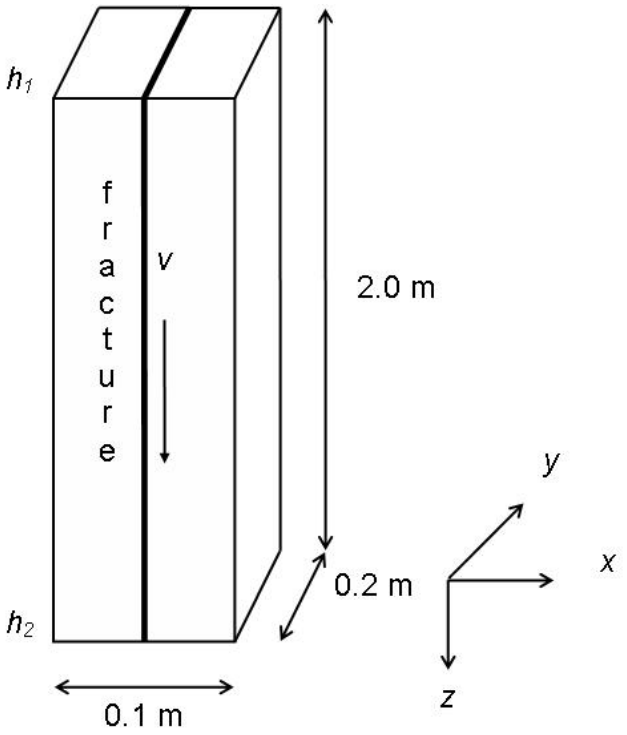

Figure 3.1 Geometry of the numerical model.

Figure 3.1 illustrates the model domain used to simulate the fracture-matrix system. A finite element grid was used to discretise the model domain measuring X = 0.1 m, Y = 0.2 m and Z = 2 m. A single fracture of aperture $2b$ = 1.2 x 10^{-4} m was located at x = 0. No flow (or solute flux) boundary conditions were imposed on all boundaries except the upper and lower faces (z = 0 m and z = 2 m) where specified heads were applied such that the flow rate in the fracture was 0.75 m/day. A specified concentration of 1 was applied to the fracture nodes at z = 0 m. A regular grid spacing of Δz = 0.01 m was used parallel to flow in the fracture and two 0.1 m elements were used in the y dimension (although the problem is essentially 2D). In the x dimension, perpendicular to the FMI, symmetrical variable grid spacing was used such that:

$$\Delta x = m_x^{(n-1)} \Delta x_{min} \tag{3.3}$$

where: Δx = grid spacing in the x direction (L), m_x = grid spacing multiplier in the x direction (-), n = integer element counter where element number 1 borders the fracture centre (-) and Δx_{min} = the minimum element size occurring at n = 1 (L).

Spatial discretisation is often conducted in accordance with the grid Peclet number:

$$Pe_g = \frac{|v|\Delta z}{D' + \alpha |v|} \tag{3.4}$$

As diffusion is typically much smaller than mechanical dispersion ($D' << \alpha |v|$) Pe_g can be simplified to $\Delta z/\alpha$. Depending on the numerical scheme used the necessary Peclet criterion will vary. However, for numerical stability it is usually recommended that Pe_g be less than around 4 (Anderson and Woessner 1992) up to as high as 10 (Huyakorn and Pinder 1983) when central weighting of the advective term is used, which is the case for the simulations presented here. For the chosen grid, Pe_g is 0.0132 along the fracture. As flow only occurs in the z direction, Pe_g is not applicable for the other dimensions.

Temporal discretisation was conducted using HydroGeoSphere's variable time-stepping procedure with a Crank-Nicolson implicit finite difference scheme in time, with ε = 0.5 in equations (3.1) and (3.2). Once a solution at time L is found, the next time-step is determined by:

$$\Delta t^{L+1} = \frac{c_{max}}{\max \left| c_i^{L+1} - c_i^{L} \right|} \Delta t^{L} \tag{3.5}$$

where c_{max} = specified maximum change in concentration desired in a time-step and c_i = calculated concentration at node i. This procedure allows the model to

increase time-steps when there are only small changes in concentration and similarly reduce them when rapid changes occur. Thus computation time is reduced without decreasing numerical accuracy. This study used a very small initial time-step of 0.01 s and a target concentration change per time-step of c_{max} = 0.01. A maximum time-step of 1000 s and maximum time-step multiplier of 2 were imposed. Model output was generated every 0.4 days for a total duration of 4 days.

To provide a check on the performance and accuracy of HydroGeoSphere, the solute transport model MT3DMS (Zheng 1990) was also used to simulate the system depicted in Figure 3.1. The linked combination of MT3DMS and the USGS flow code MODFLOW is one of the most commonly used and widely accepted approaches for modelling flow and solute transport in the subsurface. In the majority of cases, this combination of models is used to simulate flow and transport in fractured media utilising the EPM approach, however it is fully capable of simulating a discrete fracture formulation at very fine grid spacings. The problem was solved using a third order accurate total variation diminishing (TVD) scheme. An identical model domain was used for the MT3DMS simulations. Discretisation in the *y* and *z* directions was identical to that used in HydroGeoSphere. Discretisation perpendicular to the fracture was slightly different as MT3DMS uses a block-centred rather than point-centred grid. In all cases elements of width $2b = 1.2 \times 10^{-4}$ m and 100 % porosity were used for the fracture. The minimum discretisation in the matrix (Δx_{min}) was varied and a grid multiplier of 1.5 was used. An initial time-step of 0.001 s and a time-step multiplier of 1.1 were used with a maximum time-step of 100 s.

Model parameters for HydroGeoSphere and MT3DMS simulations were chosen to match those used by Tang et al. (1981) who in turn successfully replicated the earlier numerical results of Grisak and Pickens (1980). Those were $2b$ = 1.2 x 10^{-4} m, D' = 10^{-6}, 10^{-7}, 10^{-8}, 10^{-9}, 10^{-10} and 0 cm^2s^{-1}, v = 0.75 $mday^{-1}$, α = 0.76 m and θ = 0.35. The range of diffusion coefficients covers typical values for free diffusion in water (10^{-6} cm^2s^{-1}) through to diffusion in tortuous rock (10^{-11} cm^2s^{-1}). In addition, a matrix hydraulic conductivity of 10^{-50} ms^{-1} was used to ensure water flow in the matrix was negligible. Model parameters, grid and time-stepping specifications are summarised in Table 3.1. Grids employing different spatial discretisation were used to model the Tang et al. (1981) problem. Unless otherwise stated $\Delta x_{min} = 2b$ = 1.2 x 10^{-4} m and m_x = 2.

2*b* (m)	0.00012
***D'* (cm^2/s)**	10^{-6} to 10^{-10}, 0
***v* (m/d)**	0.75
α (m)	0.76
θ (-)	0.35
Δh (m)	0.001658219
***z* (m)**	0.76
***t* (d)**	4.0
***X* (m)**	0.1
***Y* (m)**	0.2
***Z* (m)**	2.0
Δx_{min} (m)	0.00012
Δy (m)	0.1
Δz (m)	0.01
m_x (-)	2

Table 3.1 Model parameters and base grid specifications for HydroGeoSphere simulations. Note: Δh is measured across the entire model length *Z*, not the distance over which transport is measured, *z*.

Results

HydroGeoSphere results are now presented for a range of grid discretisations. They are compared with results obtained using the commonly used MT3DMS model.

Figure 3.2 illustrates the effect of spatial discretisation perpendicular to the FMI (Δx_{min}). Concentration contours of 0.2, 0.4, 0.6 and 0.8 are shown after 4 days for a solute with a high matrix diffusion coefficient of 10^{-8} cm^{2}s^{-1}. The elements

closest to the fracture were of size Δx_{min} = (a) 200*b*, (b) 20*b* and (c) 2*b*. In most groundwater models, even the coarsest grid in case (a) would be considered

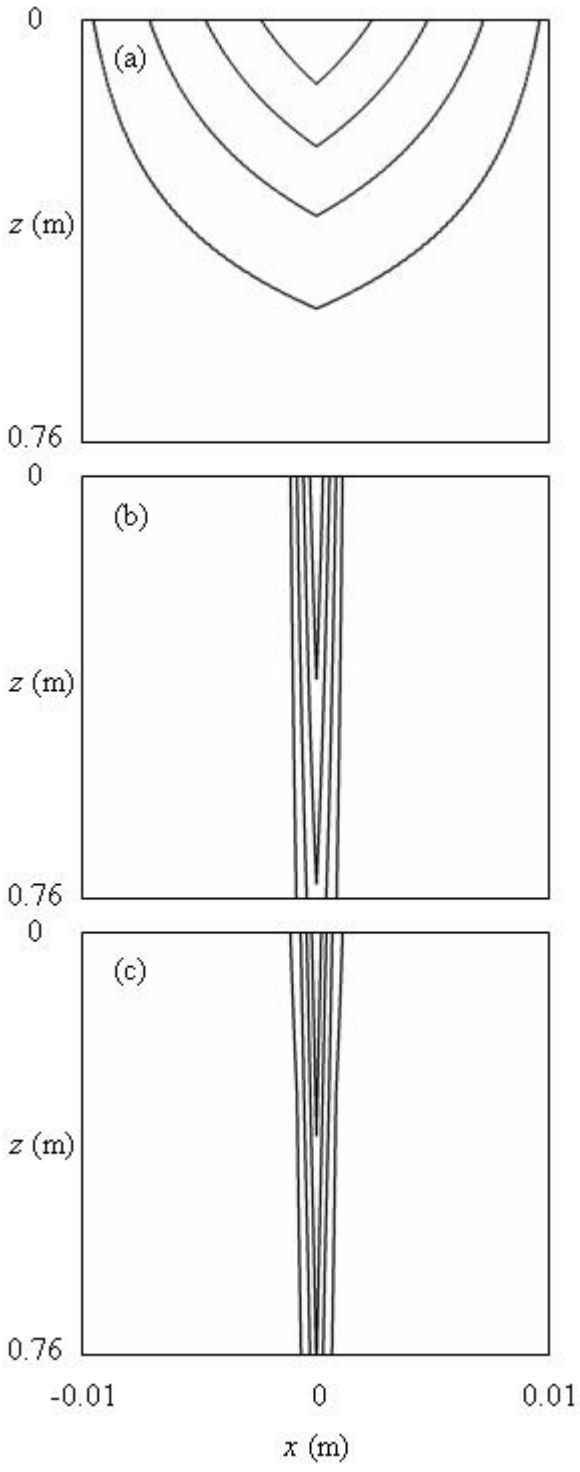

Figure 3.2 Concentration contours (0.2, 0.4, 0.6 and 0.8) after 4 days for D' = 10^{-8} cm^2s^{-1} with Δx_{min} = (a) 200*b*, (b) 20*b* and (c) 2*b* where 2*b* = 120 μm.

extremely fine. The results shown in case (c) were found to match the analytical solution whilst the larger elements used in cases (a) and (b) are clearly not fine enough to correctly model the system.

Figure 3.3 compares the analytical solution of Tang et al. (1981) with corresponding numerical results both (a) along the fracture and (b) in time when using $\Delta x_{min} = 20b$ and $2b$. Results for the finer grid ($\Delta x_{min} = 2b$) are close to the analytical solution for both $D' = 10^{-10}$ and 10^{-6} cm^2s^{-1}. The coarser grid ($\Delta x_{min} = 20b$) is able to reproduce the analytical solution for $D' = 10^{-6}$ cm^2s^{-1} but is clearly unable to match the analytical solution of the less diffusive scenario where $D' = 10^{-10}$ cm^2s^{-1}.

A sensitivity analysis was conducted to assess whether the numerical schemes chosen for the simulations had contributed to the requirement for such fine discretisation at the FMI. All possible combinations of control volume finite element / Galerkin finite element / finite difference discretisation techniques with upstream / central / downstream advective weighting and central (Crank-Nicolson) / fully implicit time weighting were tested in HydroGeoSphere. Simulations were run for $D' = 10^{-10}$ cm^2s^{-1} with $\Delta x_{min} = 2b$ and $20b$ and concentrations compared after 4 days at $z = 0.76$ m. In results not shown here, all numerical combinations produced good results when $\Delta x_{min} = 2b$, falling within 2 % of the analytical solution and 0.052 % of each other. All combinations produced very poor results when $\Delta x_{min} = 20b$, falling 25% from the analytical solution, but within 0.17 % of each other. Therefore it is apparent that

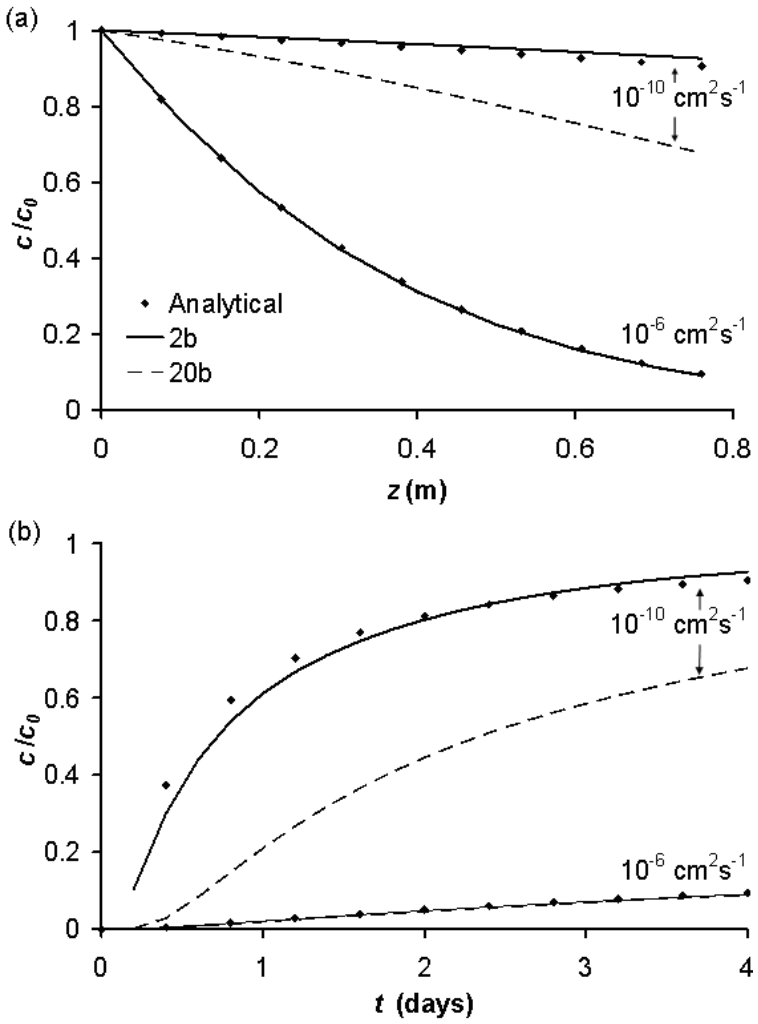

Figure 3.3 Comparison of the HydroGeoSphere concentrations for Δx_{min} = 20*b* and 2*b* with the analytical solution for *D'* = 10^{-10} and 10^{-6} cm^2s^{-1}: (a) concentration along the fracture at *t* = 4 days and (b) concentration with time at *z* = 0.76 m.

regardless of the numerical methods used to calculate the solution in HydroGeoSphere, a very fine grid is required at the FMI to match the analytical solution under the physical conditions simulated in the model.

MT3DMS results presented in Figure 3.4 confirm that the HydroGeoSphere results are not a code specific phenomenon. It is immediately obvious that both models require extremely fine discretisation to match analytical results for low

diffusion coefficients but that less strict discretisation requirements can be tolerated for a higher diffusion coefficient. It is also of interest to note the performance of MT3DMS when the element size immediately adjacent to the fracture is 200*b*, which is still a fine grid compared to that used for most field scale simulations. The predicted migration of the solute through the fracture is severely underestimated, in particular for the case with lower diffusion ($D' = 10^{-10}$ cm^2s^{-1}). Erroneously, the value of the diffusion coefficient itself has little effect on the model prediction, further emphasising the importance of fine grid discretisation in discrete fracture modelling. Given the results for the range of numerical schemes tested in HydroGeoSphere, plus the TVD scheme used in MT3DMS, it appears that the requirement for fine gridding at the FMI under conditions of low diffusion is neither a phenomenon of the codes nor the numerical schemes utilised in them.

Figure 3.5 shows simulated concentrations normalised by their corresponding analytical values as a function of $\Delta x_{min}/2b$. It is readily apparent that highly diffusive cases are able to achieve better agreement between numerical and analytical solutions for larger element sizes but that for low diffusivity cases, $\Delta x_{min}/2b \approx 1$ is required for a match. All cases converge once $\Delta x_{min}/2b$ reduces

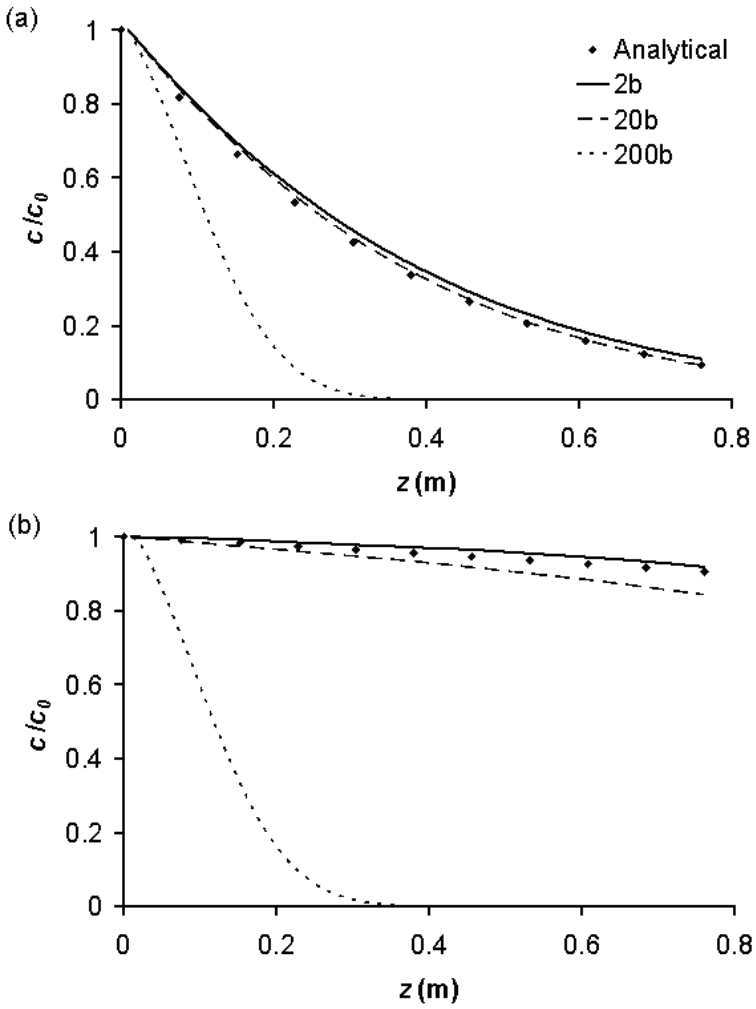

Figure 3.4 Comparison of MT3DMS results with the analytical solution for concentration along the fracture at t = 4 days: (a) D' = 10^{-6} and (b) 10^{-10} cm^2s^{-1}.

to 1 (Δx_{min} = 2b) but the converged values of $c_{modelled}/c_{Tang}$ are not all exactly 1. This could be due to the approximation made in the analytical model that diffusion occurs only perpendicular to the FMI. In reality, diffusion creates arrowhead-like concentration contours that are inherently 2-D in nature, as can be seen in Figure 3.2. Such a concentration distribution creates concentration gradients that are not perpendicular to the fracture wall as is assumed in the

analytical approach used by Tang et al. (1981). Thus, minor discrepancies should be expected, especially for large diffusion coefficients.

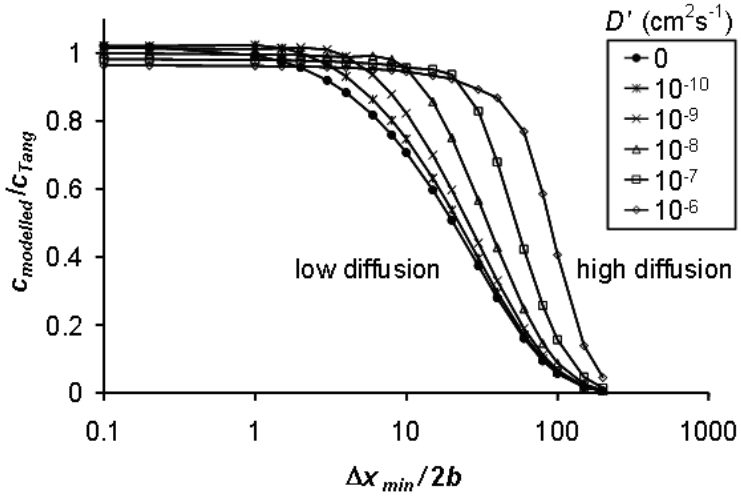

Figure 3.5 Ratio of modelled to analytical solute concentration (*t* = 4 days, *z* = 0.76 m) in the fracture as a function of $\Delta x_{min}/2b$.

It is apparent that the ability to match the analytical solution with coarser grids is strongly dependent on the magnitude of matrix diffusion. Highly diffusive cases are easily matched with coarser grids. However, as the magnitude of diffusion is reduced the discretisation at the FMI necessarily becomes finer. Previously mentioned studies have matched analytical solutions for solute transport in fractured rock without requiring the very fine discretisation identified in this study. Thus, it is useful to examine the quantitative disparity between numerical and analytical results as a function of the relative importance of matrix diffusion as a means of solute transport. Lever and Bradbury (1985) define the ratio of matrix diffusion to mechanical dispersion in the fracture by their associated timescales:

$$\beta = \frac{z^{3/2}}{4A^2 v\sqrt{\alpha}} \tag{3.6}$$

A β value greater than 1 indicates a diffusive scenario whereas a value less than 1 indicates a dispersive scenario. It should be noted that β is not an exact measure of the transport mode in a fracture-matrix system as it assumes matrix diffusion and mechanical dispersion are independent processes. However, it is very useful as an indicator of the relative strength of these two processes. Results for this study were obtained by altering A only whilst α, v and z were held constant. Figure 3.6 shows the maximum $\Delta x_{min}/2b$ required to simulate concentrations with an accuracy of 5, 10 and 20 % relative to the analytical solution as a function of β. Simulations were run at discrete values of Δx_{min} and as such the critical values are not exact. Clearly, scenarios where matrix diffusion is more significant (points on the right of this graph) can tolerate coarser discretisation. This is easily explained by the way a finite element model simulates reality. The concentration gradient is calculated as the difference in concentration between one node and the next divided by the distance between them. Any resultant transport occurs directly into the node down-gradient. In the case of the fracture-matrix system simulated here, a gradient exists from the fracture into the matrix. Thus a solute flux occurs from the common node in the fracture to the closest node that is purely a porous media node. If this node is located further into the matrix than the length scale associated with real matrix diffusion in a given timestep, the model will overestimate matrix diffusion. Since solute penetrates further into the matrix in more diffusive scenarios, these cases are less sensitive to the grid discretisation at the FMI, allowing the use of larger elements. Additionally, it can be inferred that scenarios with higher v or α will

require finer discretisation because transport along the fracture is more rapid, reducing solute contact time with the matrix. Reduced contact time results in a smaller length for diffusion into the matrix and subsequently finer discretisation is required in that direction to ensure solute is not spread to a distance greater into the matrix than it should be. For a given set of physical parameters, both the timescale of the model and timesteps used will also impact the discretisation requirements. Because the necessary discretisation at the FMI is related to the length scale for diffusion over a timestep, simulations that use longer timesteps will be able to utilise larger nodal spacings. Additionally, results generated after longer periods of simulation may be accurate even if early time results are not, because solute diffuses further into the matrix as time progresses.

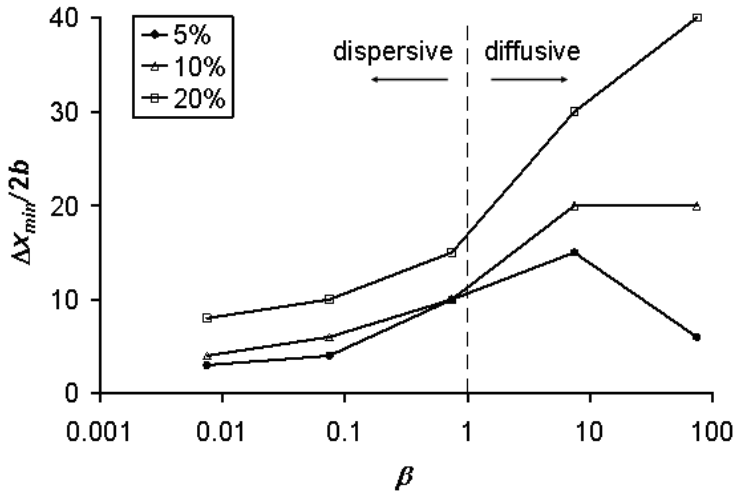

Figure 3.6 $\Delta x_{min}/2b$ required to reach 5, 10 and 20 % accuracy relative to the analytical solution (t = 4 days, z = 0.76 m) as a function of β.

In Figure 3.6 the point furthest to the right on the 5 % accuracy plot (corresponding to D' = 10^{-6} cm^2s^{-1}) requires finer discretisation than the less diffusive scenario to its left. Figure 3.6 shows that the D' = 10^{-6} cm^2s^{-1} does not

plateau at the analytical value. As mentioned earlier, this may be due to the approximation in the analytical solution of a diffusion gradient exactly perpendicular to the FMI. The D' = 10^{-6} cm^2s^{-1} scenario is the most diffusive case tested and thus differs most from this approximation.

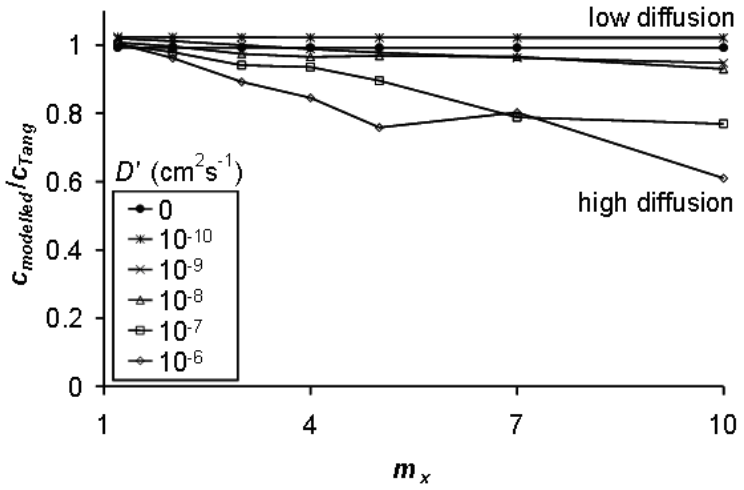

Figure 3.7 Ratio of modelled to analytical solute concentration (t = 4 days, z = 0.76 m) in the fracture as a function of m_x, where $\Delta x_{min} = 2b$ = 1.2 x 10^{-4} m.

We now consider the rate at which element size can increase into the matrix (m_x). Given the very fine discretisation required for the elements immediately adjacent to the fracture it is desirable that elements can rapidly increase away from the fracture to save CPU time and memory. Figure 3.7 shows the effect of the grid spacing multiplier, m_x, on simulated concentrations normalised by their analytical values. Increasing m_x leads to reduced simulated concentrations for D' = 10^{-6} and 10^{-7} cm^2s^{-1}, but has little effect on scenarios where diffusion is smaller even up to a large value of m_x = 10. This is because in less diffusive scenarios solutes do not reach very far into the matrix during the 4 day simulation, making fine grid discretisation away from the fracture unnecessary.

Therefore, whilst scenarios with low diffusion require very fine elements near the fracture, they can tolerate a very large grid multiplier, and thus fewer elements in the matrix. However, it should be noted that (for any given timestep size) to simulate transport over longer times when solute penetrates further into the matrix, such large increases in grid spacing may not be acceptable.

In summary, as expected, both the discretisation at the FMI (Δx_{min}) and the grid multiplier perpendicular to the FMI (m_x) affect simulation of solute transport in fractured rock. For the relatively short durations simulated in this study, low diffusion scenarios require very fine elements near the fracture (Δx_{min}), but can tolerate a very large grid multiplier (m_x), and thus fewer elements within the matrix. On the other hand, high diffusion scenarios can be simulated with bigger elements near the fracture (Δx_{min}), but with more matrix elements (m_x). These discretisation requirements are summarised in Table 3.2.

	$\beta < 1$ "dispersive scenario"	**$\beta > 1$ "diffusive scenario"**
Necessary discretisation at the FMI	smaller Δx_{min}	larger Δx_{min}
Necessary grid multiplier perpendicular to the FMI	larger m_x	smaller m_x

Table 3.2 Summary of grid requirements Δx_{min} and m_x for dispersive and diffusive scenarios.

Discussion

This study has shown by use of two different numerical models and several numerical methods that in some cases very fine spatial discretisation (on the order of the fracture aperture, 2*b*) perpendicular to the fracture-matrix interface is required in order to match analytical results. This requirement for such

extremely fine discretisation has not been reported by previous authors. The results indicate that scenarios where matrix diffusion is relatively high (i.e. slower water flow, higher porosity or diffusion coefficient, smaller aperture, longer times) do not require such small elements. On the other hand scenarios with low matrix diffusion require extremely fine grids (see Table 3.2). The aforementioned studies of Sudicky and McLaren (1992) and Cook et al. (2005) in which elements 250 times the fracture aperture were used to match the analytical solution of Sudicky and Frind (1982) were conducted using parameters which equate to β values of 0.143 and 885 respectively. These represent a slightly dispersive scenario and a highly diffusive scenario and combined with their long simulation periods of around 27.5 and 55 years in the case of Sudicky and McLaren (1992) and approximately 50 years for Cook et al. (2005), explain why they were able to use such large elements without encountering significant errors.

Thus, in many cases solute transport may be simulated accurately without discretisation on the order of the fracture aperture. However, when simulating scenarios involving high water velocity (e.g. forced gradient tracer tests), small diffusion coefficients (e.g. large compounds such as Uranium), low matrix porosity or very large fractures, simulations are prone to error and a rigorous sensitivity analysis of solutions to grid discretisation is warranted.

As a consequence of the inherent discretisation required for some practical scenarios, the use of discrete fracture network models in the simulation of catchment-scale phenomena may be severely limited by computing capacity.

With current computing capabilities, models requiring discretisation on the scale of the fracture aperture will be limited to incorporation of very few fractures and/or small scale model dimensions.

Conclusions

This study has examined the spatial discretisation required perpendicular to the fracture-matrix interface (FMI) in a discrete fracture model in order to demonstrate how simulation accuracy and required discretisation are influenced by the diffusive-dispersive nature of the problem being considered. Comparison with the analytical solution of Tang et al. (1981) has indicated:

1. Finite difference and element grids need to be designed according to the relative dominance of advection and dispersion in the fracture to diffusion in the matrix.
2. Diffusive scenarios ($\beta > 1$) tolerate larger elements close to the FMI (large Δx_{min}) but require the growth of matrix elements moving away from the fracture to be gradual (small m_x), a result not reported in previous literature.
3. Dispersive scenarios ($\beta < 1$) require small elements close to the FMI (small Δx_{min}), but are able to employ larger matrix elements (large m_x) for relatively short timescales, before solute penetrates far into the matrix, a result not reported in previous literature.
4. Results were compared from a wide range of numerical schemes and two different numerical codes. The requirement for fine discretisation at the FMI was found to be neither a phenomenon of the codes nor the numerical schemes used within them.

5. Minor discrepancies between numerical and analytical results were observed, especially for diffusive scenarios. These are assumed to be due to the assumption made in the analytical solution that matrix diffusion occurs only perpendicular to the FMI, but which is inherently 2-D in the numerical framework considered here.
6. Whilst it has previously been reported that fine discretisation is required to simulate solute transport in discretely fractured media, this study has quantified the relationship between Δx_{min} and β showing that the grid discretisation required for low matrix diffusion scenarios can be on the order of the size of the fracture aperture ($\Delta x_{min} \approx 2b$). This necessary grid spacing requirement is extremely fine and has not been reported previously in the literature.
7. Whilst the discretisation requirements at the FMI and in the adjacent matrix are related to the physical parameters of the system being modelled (eg *D'*, *v*, *z*), they are also tied to the timescales used for individual timesteps and overall model duration.

The results of this study clearly indicate that caution must be taken when modelling solute transport in discrete fracture systems using a numerical model. Careful attention must be given to the diffusive/dispersive ratio in the system under consideration. Critically, the results of this study provide guidance on the choice of Δx_{min} and m_x that should be employed for the varying cases of diffusive/dispersive effects in the physical system under consideration. These results are demonstrative and indicative only and we wish to exercise some caution in overgeneralising results here. However, it is abundantly clear that a

sensitivity analysis must be conducted to determine the precise spatial and temporal discretisation required in any given model of solute transport in fractured porous media.

Notation and Units

Subscript *f* denotes a fracture property.

Subscripts *i* and *j* denote a property of node *i* or *j* respectively.

Superscript *L* denotes the time level in a time-stepping procedure.

A	matrix diffusion term	$T^{1/2}$
a_i	area associated with fracture node	L^2
b	half fracture aperture	L
c	solute concentration	ML^{-3}
$\bar{c}$	solute concentration in the Laplace space	TML^{-3}
c'	solute concentration in the matrix	ML^{-3}
c_{max}	specified maximum concentration change per time-step	ML^{-3}
D	hydrodynamic dispersion coefficient	L^2T^{-1}
D^*	diffusion coefficient of solute in water	L^2T^{-1}
D'	diffusion coefficient of solute in matrix	L^2T^{-1}
h	hydraulic head	L
m_x	grid spacing multiplier in the *x* direction	-
n	integer element counter	-
p	Laplace space variable	T^{-1}
Pe_g	grid Peclet number	-
R	face retardation coefficient	-
R'	matrix retardation coefficient	-
t	time	T

v	water velocity	LT^{-1}
V_i	region or control volume associated with porous medium node i	L^3
x, y, z	spatial coordinates	L
$\Delta x, \Delta y, \Delta z$	grid spacing in x, y and z directions	-
X, Y, Z	model domain size in x, y and z directions	L
α	longitudinal dispersivity	L
β	ratio of diffusive to dispersive timescales	-
γ_{ij}	describes fluid flow between i and j	L^2T^{-1}
ε	finite difference time weighting factor	-
θ	matrix porosity	-
λ	radioactive decay constant	T^{-1}
τ	tortuosity	-
χ_{ij}	describes diffusive/dispersive solute flux between i and j	L^3T^{-1}
Ω	solute exchange rate between domains	T^{-1}

References

Anderson, M. P. and W. W. Woessner. 1992. *Applied Groundwater Modeling: Simulation of Flow and Advective Transport*, San Diego: Academic Press, Inc.

Chan, T., N. W. Scheier and V. Guvanasen. 1999a. MOTIF Version 3.2 Theory Manual, 06819-REP-01200-0091-R00. Toronto: Nuclear Waste Management Division, Ontario Power Generation Inc.

Chan, T., N. W. Scheier and F. W. Stanchell. 1999b. MOTIF Code Version 3.2 User's Manual, 06819-REP-01200-0090-R00. Toronto: Nuclear Waste Management Division, Ontario Power Generation Inc.

Clift, S. S., E. F. D'Azevedo, P. A. Forsyth and J. R. Knightly. 1996. WATSIT-1 and WATSIT-B Waterloo Sparse Iterative Matrix Solvers. User's Guide with Developer Notes for Version 2.0.0.

Cook, P. G., A. J. Love, N. I. Robinson and C. T. Simmons. 2005. Groundwater ages in fractured rock aquifers. *Journal of Hydrology* 308: 284-301.

Diodato, D. M. 1994. A Compendium of Fracture Flow Models, Argonne: Argonne National Laboratory.

England, R. L., N. W. Kline, K. J. Ekblad and R. G. Baca. 1986. MAGNUM-2D Computer Code: User's Guide, RHO-CR-143P. Rockwell Hanford Operations.

Graf, T. and R. Therrien. 2005. Variable-density groundwater flow and solute transport in porous media containing nonuniform discrete fractures. *Advances in Water Resources* 28, no. 12: 1351-1367.

Grisak, G. E. and J. F. Pickens. 1980. Solute transport through fractured media 1. the effect of matrix diffusion. *Water Resources Research* 16, no. 4: 719-730.

HSI-GeoTrans. 2000. Theory and Implementation for SWIFT for Windows: The Sandia Waste-Isolation Flow and Transport Model for Fractured Media, Sterling: HSI GeoTrans.

Huyakorn, P. S. and G. F. Pinder. 1983. *Computational Methods in Subsurface Flow*, Orlando: Academic Press, Inc.

Lever, D. A. and M. H. Bradbury. 1985. Rock-matrix diffusion and its implications for radionuclide migration. *Mineralogical Magazine* 49: 245-254.

Neuman, S. P. 2005. Trends, prospects and challenges in quantifying flow and transport through fractured rocks. *Hydrogeology Journal* 13, no. 1: 124-147.

Piessens, R. and R. Huysmans. 1984. Algorithm 619. Automatic numerical inversion of the Laplace transform. *Association of Computer Machinery Transactions on Mathematical Software* 10: 348-353.

Rausch, R., W. Schafer, R. Therrien and C. Wagner. 2005. *Solute Transport Modelling: An Introduction to Models and Solution Strategies*, Stuttgart: Borntraeger.

Reynolds, D. A. and B. H. Kueper. 2002. Numerical examination of the factors controlling DNAPL migration through a single fracture. *Ground Water* 40, no. 4: 368-377.

Robinson, N. I. and J. M. Sharp. 1997. Analytical solution for solute transport in a finite set of parallel fractures with matrix diffusion, CMIS C23/97. Adelaide: CSIRO.

Runchal, A. 2002. PORFLOW User's Manual, Version 5, Analytic & Computational Research, Inc.

Slough, K. J., E. A. Sudicky and P. A. Forsyth. 1999. Grid refinement for modeling multiphase flow in discretely fractured porous media. *Advances in Water Resources* 23, no. 3: 261-269.

Sudicky, E. A. and E. O. Frind. 1982. Contaminant transport in fractured porous media: analytical solutions for a system of parallel fractures. *Water Resources Research* 18, no. 6: 1634-1642.

Sudicky, E. A. and R. G. McLaren. 1992. The Laplace transform Galerkin technique for large-scale simulation of mass transport in discretely fractured porous formations. *Water Resources Research* 28, no. 2: 499-514.

Sudicky, E. A. and R. G. McLaren. 1998. FRACTRAN User's Guide. An Efficient Simulator for Two-Dimensional, Saturated Groundwater Flow and Solute Transport in Porous or Discretely-Fractured Porous Formations, Ontario: Groundwater Simulations Group, Waterloo Centre for Groundwater Research, University of Waterloo.

Tang, D. H., E. O. Frind and E. A. Sudicky. 1981. Contaminant transport in fractured porous media: analytical solution for a single fracture. *Water Resources Research* 17, no. 3: 555-564.

Therrien, R. and E. A. Sudicky. 1996. Three-dimensional analysis of variably-saturated flow and solute transport in discretely-fractured porous media. *Journal of Contaminant Hydrology* 23, no. 1-2: 1-44.

Therrien, R., E. A. Sudicky, R. G. McLaren and S. M. Panday. 2005. HydroGeoSphere: A three-dimensional numerical model describing fully-integrated subsurface and surface flow and solute transport. User's Guide, Waterloo, Canada: Groundwater Simulations Group.

Travis, B. J. and K. H. Birdsell. 1991. TRACR3D: A Model of Flow and Transport in Porous Media, Model Description and User's Manual, Los Alamos National Laboratory.

VanderKwaak, J. E. and E. A. Sudicky. 1996. Dissolution of non-aqueous-phase liquids and aqueous-phase contaminant transport in discretely-fractured porous media. *Journal of Contaminant Hydrology* 23, no. 1-2: 45-68.

Zheng, C. 1990. MT3D: A modular three-dimensional transport model for simulation of advection, dispersion and chemical reactions of contaminants in groundwater systems, Rockville, USA: S.S. Papadopulos and Associates Inc.

Chapter 4: Conceptual model choice for dipole tracer tests in fractured rock

Abstract

Applied tracer tests provide a means to estimate fracture and matrix parameters that determine solute transport in fractured rock. Dipole tracer tests utilise an injection-extraction well pair to create a forced hydraulic gradient, allowing tests to be conducted more rapidly than natural gradient tests. Tracer breakthrough is analysed using an analytical model to find the parameters that generate the best fit to the data. This study explores the differing interpretation that can be drawn from a tracer test when analysed with two different models; one assuming a dipole, the other a linear flow field. The analytical solution of Tang et al. (1981) is used to model a 1-D flow field and a multiple streamline summation of the same model is used to represent transport in a dipole flow field. The two models are able to produce almost identical breakthrough curves for a range of scenarios. Comparison of the parameters required to create matching breakthrough curves demonstrates the non-uniqueness of the 1-D and dipole interpretations, resulting in large parameter uncertainty. Considering that neither of the conceptual models incorporates the complexity of a real fracture network, it is expected that analytically interpreted parameters may be as different, or more different from reality as they are from those interpreted with a different analytical model. Given the complex nature of fractured rock systems and the many unknown fracture and matrix properties involved therein, this

study highlights the benefit of incorporating multiple conceptual models in the analyses of dipole tracer tests conducted in fractured rock.

Introduction

Dipole tracer tests are used as an in-situ means of characterising the solute transport properties of fractured rock systems. A dipole tracer test is conducted by applying tracer to the injection well of an injection-extraction well pair and monitoring its concentration in the extraction well. The resultant breakthrough curve is analysed with an analytical model to determine the parameters that generate the best fit to the observed data.

Grove and Beetem (1971) outlined a method for modelling a 2-D dipole of equal pole strength (as would occur in a fracture of infinite extent with smooth parallel walls). The approach is a summation of breakthrough curves from multiple streamlines. Each streamline has a path length and average flow velocity dependent on the angle of departure from the injection well. This method has been widely used to interpret dipole tracer tests conducted in single fractures (Novakowski, 1988; Novakowski et al., 2004; Novakowski et al., 1985) and in fracture networks (Himmelsbach et al., 1998; Himmelsbach and Maloszewski, 1992; Sanford et al., 2002; Webster et al., 1970).

Besides the usual experimental error, analyses of dipole tracer tests in fracture networks are inherently subject to potentially large errors due to the inability of analytical models to describe the unknown heterogeneity of complex fracture geometries at appropriate spatial scales. Consequently, the choice of model

used to analyse a tracer test is potentially the largest error in the analysis. Different approaches have been used to explain the long tailing typically observed in breakthrough curves from fractured rock. In many cases this is attributed to matrix diffusion. Tracers with differing diffusion coefficients have been found to produce different breakthrough curves (Jardine et al., 1999; Maloszewski et al., 1999; Sanford et al., 2002). The analytical models of Grisak and Pickens (1981), Tang et al. (1981) and Sudicky and Frind (1982) incorporate matrix diffusion and may be used to obtain transport parameters in such cases. Other authors (Becker and Shapiro, 2000; Tsang et al., 1991) attribute tracer tailing to complex transport pathways resulting in tracer channelling within and between fractures. Becker and Shapiro (2000) presented identical late-time breakthrough behaviour for tracers with different diffusion coefficients and claimed this proved that matrix diffusion was not responsible for the long tailing. Models such as those presented by Maloszewski et al. (1992), Neretnieks (1983), Rasmuson and Neretnieks (1986) and Tsang and Tsang (1987) may be used to interpret tracer tailing by channelling. In addition to these processes, tracer tests conducted in a dipole flow field are subject to long tailing due to the flow field geometry. With a range of models available for interpreting tracer tests in fractured rock a unique set of hydrogeologic parameters may be difficult to identify. As it is often not possible to know which model/s will best approximate a system, recent studies have begun to compare the analyses of tracer tests with different models (Akin, 2005; Pfingsten and Soler, 2003).

Typically dipole tracer tests are analysed assuming that a perfect dipole is attained in the fracture/s. However, laterally finite fractures and variable fracture

apertures may channel flow such that infinite dipole flow fields cannot develop and therefore a 1-D flow model may in fact better describe some systems. 1-D flow models have also previously been used to interpret dipole tracer tests where injection and extraction rates are not equal (Pfingsten and Soler, 2003). In order to demonstrate the potential non-uniqueness that may arise from the choice of conceptual model used to interpret dipole tracer tests, this study compares the parameters obtained by two models, one assuming a dipole flow field and the other a 1-D flow field. The models otherwise incorporate the same physical processes and parameters. These models are chosen as examples only in order to demonstrate the principle of non-uniqueness and consequences for parameter estimation. This study examines the degree of uncertainty in model parameters that can occur due to conceptual model choice when interpreting a dipole tracer test conducted in fractured rock. It is demonstrated that breakthrough curves can be easily fitted with both the dipole and 1-D analytical models. It is not easy to determine which fit, if any, is superior and more meaningful. Furthermore the values of the fitting parameters are seen to be vastly different and this has major implications for subsequent predictions that may be made using these parameters.

Methods

In order to compare the best-fit parameters yielded by fitting a breakthrough curve with two different flow models, a dipole flow model was used to create synthetic breakthrough curves which were subsequently analysed using a 1-D flow model. The roles of the two models could have been reversed, but the same conclusions would have been reached. The model used for the 1-D flow

case was that of Tang et al. (1981) whilst the dipole model followed the approach of Grove and Beetem (1971) which sums breakthrough curves from multiple streamlines, each representative of a flow line in a 2-D dipole flow field constrained to the fracture plane. Transport along each streamline was solved using the Tang et al. (1981) model and therefore flow geometry was the only difference between the two models. The two sets of model parameters were then compared to assess the parameter uncertainty arising from the choice of conceptual model.

The geometry and solution for the model presented by Tang et al. (1981) is outlined in Chapter 2 (see Figure 2.1 and equations 2.1, 2.2 and 2.3) and is not repeated here.

Grove and Beetem (1971) approximate a dipole breakthrough curve as the summation of breakthrough curves from multiple streamlines, each of which departs the injection well at an angle ϕ as illustrated in Figure 4.1. They present solutions for curved streamline length (z_ϕ) and travel time (t_ϕ) in a dipole. For a dipole between two wells separated by a distance z_0 within a fluid filled fracture of aperture 2b, these can be written as:

$$z_\phi = \frac{z_0 \phi}{\sin \phi} \qquad 0 < \phi < \pi \tag{4.1}$$

$$t_0 = \frac{2b\pi z_0^{\,2}}{3Q} \qquad \phi = 0 \tag{4.2a}$$

$$t_\phi = \frac{2b\pi z_0^{\,2}}{Q \sin^2 \phi}\left(1 - \phi \cot \phi\right) \qquad 0 < \phi < \pi \tag{4.2b}$$

where Q = volumetric injection/extraction rate of the wells (L^3T^{-1}). By assuming an average velocity along a streamline, v can be solved as z/t which yields:

$$v_0 = \frac{3Q}{2b\pi z_0} \qquad \phi = 0 \tag{4.3a}$$

$$v_\phi = \frac{Q\phi \sin\phi}{2\pi b z_0 (1 - \phi \cot\phi)} \qquad 0 < \phi < \pi \tag{4.3b}$$

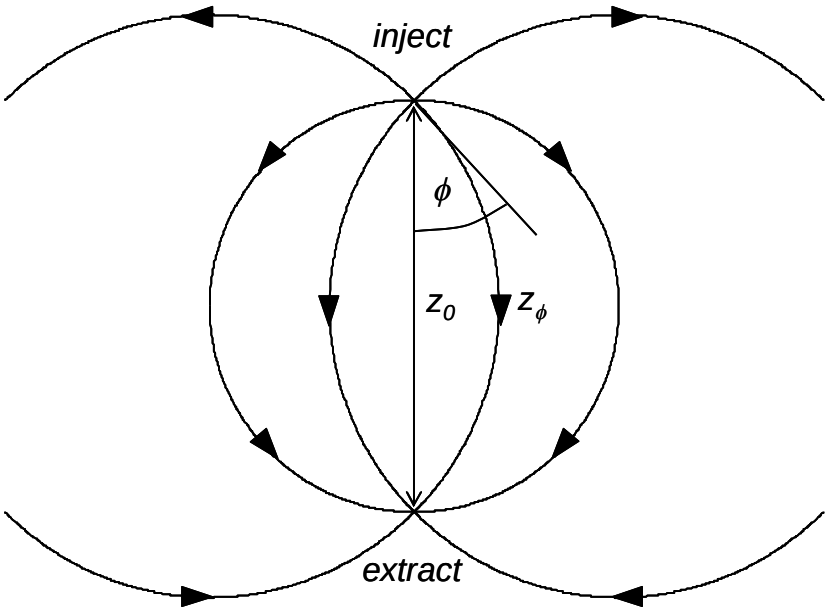

Figure 4.1 The dipole flow approximation presented by Grove and Beetem (1971). Flow occurs along streamlines of length (z_ϕ) and flow velocity (v_ϕ) that are dependent on the angle of departure/arrival (ϕ) from the wells.

Himmelsbach and Maloszewski (1992) used 120 streamlines to model dipole tracer breakthrough. Novakowski et al. (1985) found that as few as 12 streamlines were necessary when using a numerical approach to model unequal strength dipole flow whilst Novakowski et al. (2004) found that 45 streamlines were needed for convergence using the same numerical technique to model a dipole with an ambient ground water flow.

In order to ensure the results of this study would be appropriate for the typical parameters encountered in field studies, the tracer test parameters reported in several published natural gradient, monopole and dipole tracer tests conducted in fractured rock were examined. As a means of understanding and comparing the types of physical scenarios under which these tests were conducted, the dimensionless ratio of diffusive to dispersive time scales for the spreading of solute as defined by Lever and Bradbury (1985) was used.

$$\beta = \frac{z^{3/2}}{4A^2 v\sqrt{\alpha}} \tag{4.4}$$

A β value greater than 1 indicates diffusion dominated spreading of solute whilst a β value less than 1 indicates dispersion dominated spreading of solute. It should be noted that because β uses the independent time scales for diffusion and dispersion, that it is only an approximate measure of their relative importance in a coupled system. Additionally β_0 is used to denote a β value calculated along the direct streamline between the injection and extraction wells in a dipole configuration. Figure 4.2 shows the β_0 values of several previous tracer tests. Values lie in the range 10^{-7} to 200 with 13 out of 17 cases being more dispersive (β < 1) than diffusive. A β_0 range of 10^{-7} to 10^3 was therefore considered representative of tracer tests encountered in the current available literature.

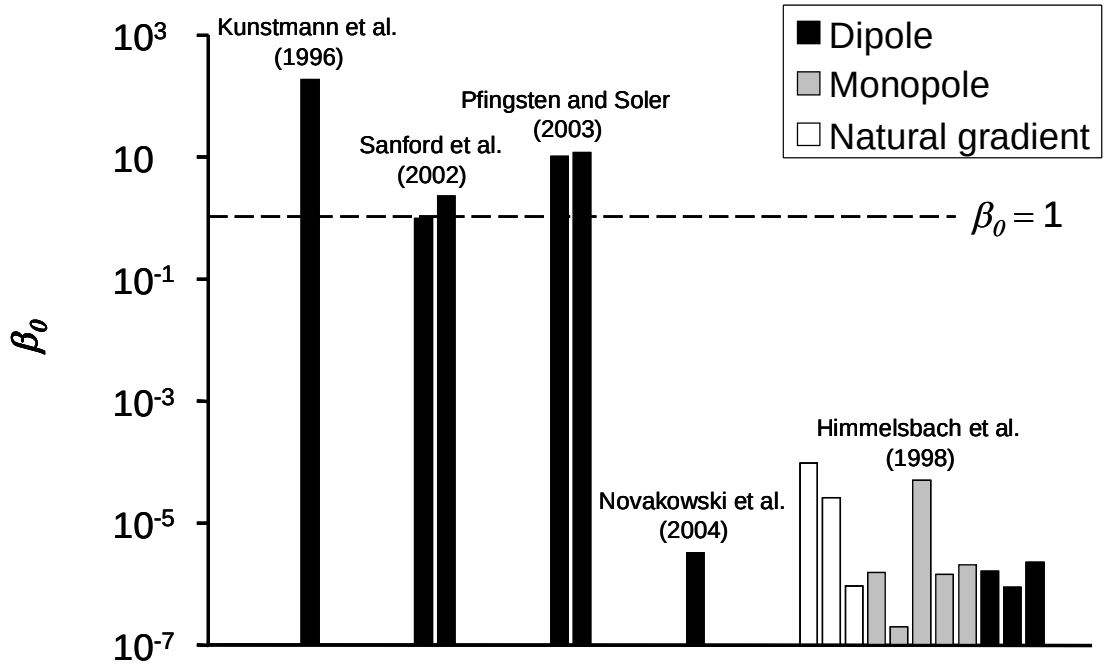

Figure 4.2 β_0 values for previous tracer tests conducted in fractured rock. Each column corresponds to a set of parameters related to a single tracer test.

Because of the large range of parameter values used in this study it was deemed necessary to perform an independent sensitivity analysis on the number of streamlines used. β_0 values (altered by changing v) spanning the entire range used in this study were tested in the sensitivity analysis. For each of the sensitivity runs the peak concentration, c_p was obtained from the highest concentration in a breakthrough curve composed of 96 data points, equally spaced in time, and was found to converge using approximately 45 streamlines for most cases. However, due to the small computational time required to evaluate breakthrough solutions at different times, 105 streamlines were used to model dipole transport and this was more than sufficient to ensure solution convergence.

β_0	α (m)	v_0 (md^{-1})	A (d$^{1/2}$)
10^{-7}	10^{14}	1.2649x10^{9}	790.57
10^{-6}	10^{12}	1.2649x10^{8}	250
10^{-5}	10^{10}	12 649 000	79.057
10^{-4}	10^{8}	1 264 900	25
10^{-3}	1 000 000	126 490	7.9057
10^{-2}	10 000	12 649	2.5
10^{-1}	100	1 264.9	0.79057
1	1	126.49	0.25
10^{1}	0.01	12.649	0.079057
10^{2}	0.0001	1.2649	0.025
10^{3}	0.000001	0.12649	0.0079057

Table 4.1 Parameters used to generate breakthrough curves at varied β_0 values. The β_0 = 1 values were used as the base case. Where β_0 was altered by a parameter the corresponding parameter value was substituted for the base case value.

For all simulations a dipole separation of 10 m, tracer pulse of duration 0.041667 d (1 hour) and fracture aperture of 100 μm were used. A base set of dipole model parameters was chosen such that β_0 = 1. These were a dispersivity of α = 1m, direct streamline water velocity of v_0 = 126.49 md^{-1} (corresponding to Q = 0.13246 m^{3}d^{-1}) and matrix diffusion term A of 0.25 d$^{1/2}$. In order to simulate dipole breakthrough curves for the β_0 range 10^{-7} to 10^{3} at order of magnitude intervals, each of α, v_0 and A were individually modified from their base case values whilst the other two parameters values remained fixed. The parameters used to create the dipole breakthrough curves for different β_0 values are presented in Table 4.1. Different parameter combinations result in

different time for tracer breakthrough. For each breakthrough curve, 96 data points equally spaced in time were calculated over durations ranging from 0.1 to 100,000 d. In each case the total time allowed for tracer breakthrough was chosen such that tracer concentration had peaked and dropped by at least 50 % of the peak concentration.

The generated dipole breakthrough curves were then each fitted by the 1-D flow model using the parameter estimation program PEST (Doherty, 2004). A range of initial parameter estimates were used in fitting each of the dipole breakthrough curves to ensure global best fit parameters were obtained.

Upon completing the fitting process, many initial parameter estimates yielded poor fits to the dipole breakthrough curves. In order to incorporate only the successful sets of parameters in the analysis, two fitting criteria were used. One was the r-squared value, or square of the Pearson product moment correlation coefficient

$$r^2 = \left(\frac{\sum_{i=1}^{n} \left(c_{i,\,fit} - \overline{c}_{fit}\right)\left(c_{i,tar} - \overline{c}_{tar}\right)}{\sqrt{\sum_{i=1}^{n} \left(c_{i,\,fit} - \overline{c}_{fit}\right)^2 \sum_{i=1}^{n} \left(c_{i,tar} - \overline{c}_{tar}\right)^2}} \right)^2 \qquad (4.5)$$

and the other the average normalised residual

$$E = \frac{1}{n} \sum_{i=1}^{n} \frac{\left| c_{i,\,fit} - c_{i,tar} \right|}{c_{p,tar}} \qquad (4.6)$$

where i = integer counter, n = number of data points in the breakthrough curve (96 in this study), *fit* indicates a fitted data value, *tar* represents a target data value and overscore indicates an average over the data set.

For each fit, r^2 and E were evaluated across the 96 data points. A minimum r^2 of 98.5% and a maximum average normalised residual of 10% were specified as an objective and consistent set of criteria for determining a 'good' fit. The parameters deemed to have generated a good fit were then used to calculate an average and standard deviation for each parameter.

Results

Figure 4.3 shows a breakthrough curve generated with the dipole model using α = 1 m, v_0 = 126.49 md^{-1} (Q = 0.13246 m^3d^{-1}) and A = 2.5 $d^{1/2}$, along with a 1-D breakthrough curve optimised to fit the dipole data with resulting parameters α = 0.1905 m, v = 289.95 md^{-1} and A = 0.073508 $d^{1/2}$. If these breakthrough curves were the result of optimisation to real field data it would be almost impossible to determine which model and associated parameter estimates best describe the system in the absence of additional information. It is now useful to explore the differences between parameter values for similar breakthrough curves generated with the two models.

Figure 4.4a shows the normalised (i.e. the fitted 1-D parameter value divided by the dipole parameter value used to generate the initial breakthrough curve) 1-D dispersivity values for the range of β_0 studied. It is worth noting that dipole and 1-D parameters are up to more than 7 orders of magnitude different. For $\alpha_{1D}(\alpha)$

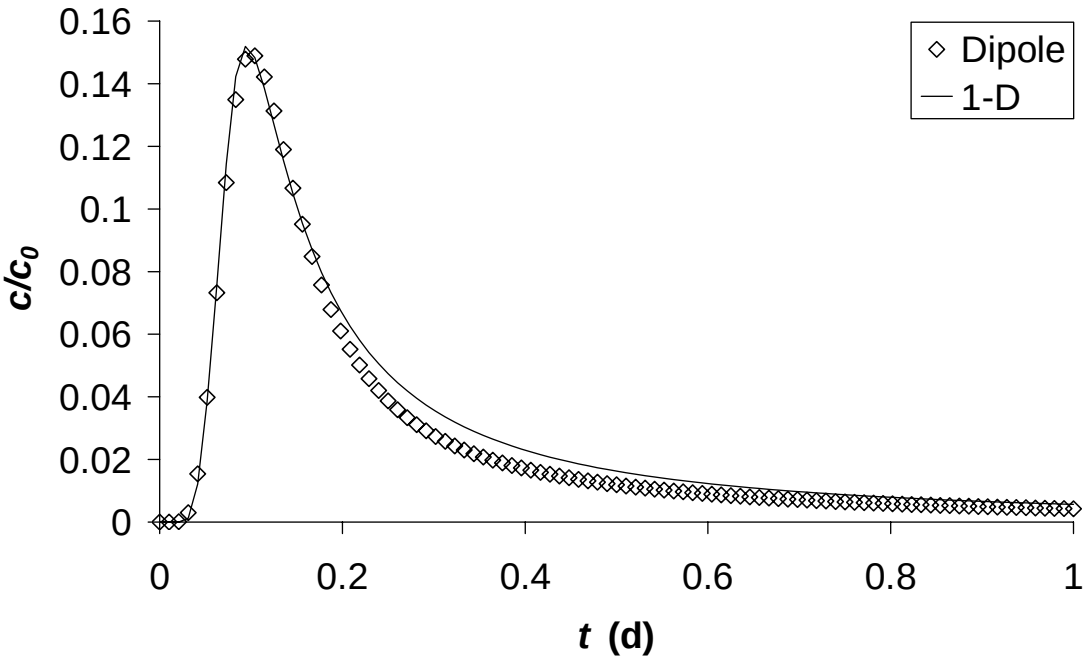

Figure 4.3 A dipole breakthrough curve generated with α = 1 m, v_0 = 126.49 md^{-1} (Q = 0.13246 m^{3}d^{-1}) and A = 2.5 d$^{1/2}$, fitted with a 1-D breakthrough curve with parameters α = 0.1905 m, v = 289.95 md^{-1} and A = 0.073508 d$^{1/2}$.

(i.e. β_0 is altered by α whilst holding v_0 and A constant) α_{1D} is underestimated for low β_0 (high α) and overestimated for high β_0 (low α). This is because $\alpha_{1D}(\alpha)$ values do not vary greatly, all falling between 10^4 and 10^6 m, compared with the span of dipole input α values ranging from 10^{-6} to 10^{14}. Regardless of the α value used in the dipole model to create the breakthrough curves, the 1-D model always requires a high dispersivity to account for the spreading of solute along multiple streamlines in the dipole model. $\alpha_{1D}(\alpha)$ is only underestimated by the 1-D model in β regions where the α value used to create the dipole breakthrough is so high that breakthrough is relatively insensitive to changes in dispersivity. This results from β not being an exact descriptor of tracer behaviour. Either doubling A or multiplying α by 16 from an initial set of

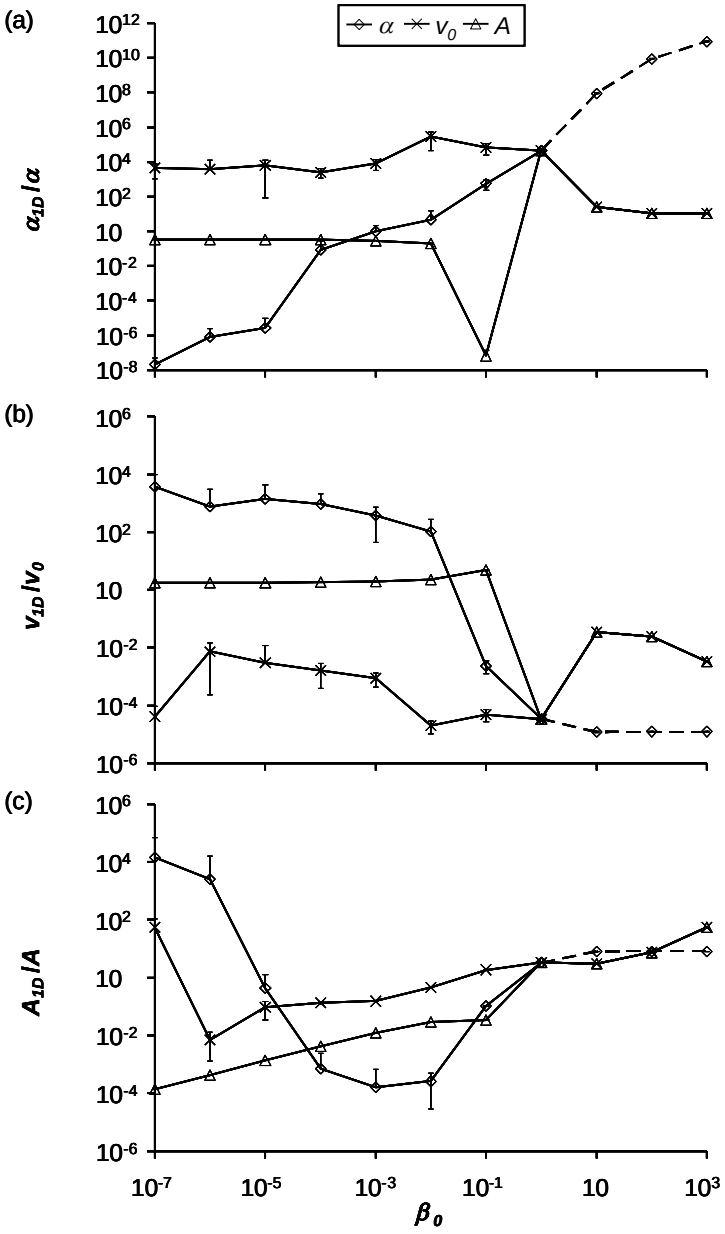

Figure 4.4 1-D parameter estimates normalised by dipole parameter values as a function of β_0 altered by α, v_0 and A for (a) dispersivity, (b) water velocity and (c) diffusion term. Dashed lines indicate parameter ranges where none of the attempts to fit the data yielded results that met the prescribed r^2 selection criterion deemed to indicate a good fit.

parameters would result in a β value 4 times smaller, however the breakthrough curves could be very different. For the range β_0 = 1 to 10^3 a dashed line for $\alpha_{1D}(\alpha)$ indicates that none of the attempts to fit the data yielded results that met

the r^2 selection criterion. Results shown are for those runs that met the *E* criterion alone. The dipole model, even with no dispersivity applied to individual streamlines, generates a tailed, smooth breakthrough curve with apparent dispersion due to the differing arrival times of each of the streamlines. In the high β_0 range, the dipole model has a very low input α value. The 1-D model is no longer able to match the dipole breakthrough simply by reducing the fitted α_{1D} value because, as for the low β_0 values, breakthrough is no longer sensitive to changes in α_{1D}. Hence very similar non-normalised α_{1D} values are returned for each breakthrough curve. In this same range $\alpha_{1D}(v)$ and $\alpha_{1D}(A)$ are able to match the dipole breakthrough by reducing the fitted α_{1D} values as breakthrough for these cases is still sensitive to α_{1D}. It is interesting to note the remarkable closeness of the normalised $\alpha_{1D}(v)$ and $\alpha_{1D}(A)$ curves from β_0 = 1 to 10^3. In this range, tracer breakthrough is dominated by spreading due to matrix diffusion. As the influence of dispersion reduces, the transport equation can be fitted using these two parameters (*v* and *A*) alone.

Results for normalised v_{1D} values are presented in Figure 4.4b. As with the α results, dipole breakthrough is relatively insensitive to changes in *v* for the lower values of β_0 resulting in similar large non-normalised v_{1D} values. Again the behaviour of $v_{1D}(v)$ and $v_{1D}(A)$ are remarkably alike for β_0 = 1 to 10^3. The 1-D solution (dashed) was not able to meet the good fit criteria for $v_{1D}(\alpha)$ for the range β_0 = 1 to 10^3 as previously mentioned.

Figure 4.4c shows normalised A_{1D} values. Normalised $A_{1D}(A)$ increases for the entire β_0 range, however the raw (non-normalised) $A_{1D}(A)$ values are approximately constant for $\beta_0 \leq 10^{-2}$ where diffusion has negligible impact on breakthrough. This results in a sloped straight line when parameter values are normalised. $A_{1D}(\alpha)$ and $A_{1D}(v)$ decrease and then increase again as β_0 increases. As in the other graphs, normalised $A_{1D}(v)$ and $A_{1D}(A)$ are very similar.

Normalised β_{1D} values obtained from the composite average parameters are plotted in Figure 4.5. All three means of altering β_0 yield a common trend for normalised β_{1D}. At low β_0, β_{1D} is greater than β_0 as diffusion is overestimated. This overestimation decreases as β_0 increases (and scenarios become more diffusive). This is because at low β_0 there is very little diffusion in the direct streamline of the dipole. However, the long streamlines of the dipole cause the combined breakthrough to appear as though greater matrix diffusion is occurring. At higher β_0 the dipole model undergoes greater diffusion. The 1D model interprets the presence of significant diffusion, but the effect of matrix diffusion is not so overestimated. At high β_0 the behaviour caused by modifying v and A is very similar, as was the case for the three individually tested parameters.

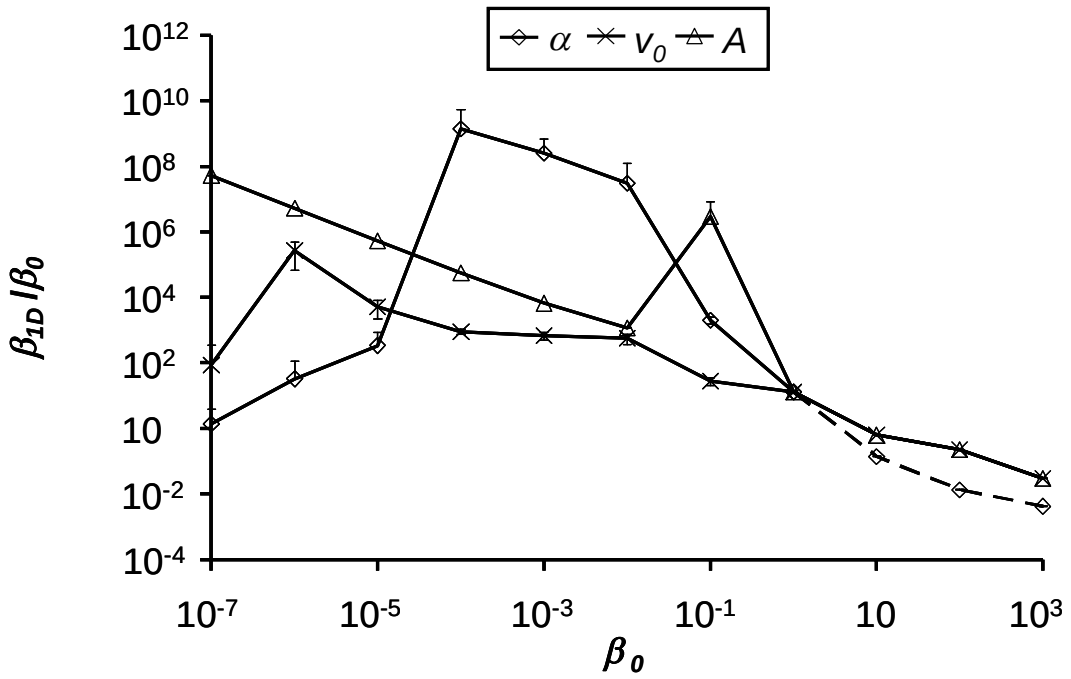

Figure 4.5 1-D β estimates normalised by dipole β_0 as a function of β_0 altered by α, v_0 and A.

Discussion

The results presented in Figures 4.4 and 4.5 show that for large ranges of α, v and A the dipole and 1-D models are able to produce almost identical breakthrough curves (see Figure 4.3) by using different parameter combinations. The consequence is that dipole tracer tests conducted in some fracture networks could be interpreted with either model by obtaining a good fit to measured data. Critically however, the parameter values obtained may be vastly different. If no other information is available to assist in the determination of which model best describes the system, the choice of which interpretative model is superior or preferred is difficult. Results demonstrate that there is no simple relationship between the best-fit parameters obtained using the two different conceptual models.

Possibly more important than the individual parameters obtained from the interpretation of a tracer test are the predictions of solute transport behaviour made in a system using these parameters. For example, a dipole tracer test may be conducted to determine hydraulic and solute transport parameters for an aquifer in which contamination has occurred, with the aim of ultimately predicting transport under the natural hydraulic gradient. Weatherill et al. (2006) showed that when using a single conceptual model, in some cases predictions of solute transport under lower hydraulic gradients can be better constrained than individual parameter values. However, if the initial interpretive model chosen poorly describes the system (even though it may fit the breakthrough data well), there is potential for large error in subsequent predictions under the natural hydraulic gradient. As an illustrative example, predictions of transport from a constant solute source were made for hydraulic gradients of 0.1, 0.01 and 0.001, which for a smooth-walled fracture of aperture 100 μm generates ground water velocities of 61.92, 6.192 and 0.6192 md^{-1} respectively. The parameter values from a dipole conceptual model (α = 1 m and A = 2.5 $d^{1/2}$) and 1-D conceptual model (α = 0.1905 m and A = 0.073508 $d^{1/2}$) that generated the breakthrough curves in Figure 4.3 were used. Figure 4.6 shows subsequent breakthrough 100 m downstream from the solute source using a 1-D transport solution with these different parameter values. Lower hydraulic gradients (with greatest difference from the forced gradient conditions) yield larger discrepancies between the two models, with the time for tracer arrival differing by up to three orders of magnitude. Thus, a good fit to measured data in a forced gradient tracer test used for parameter estimation may lead to poor

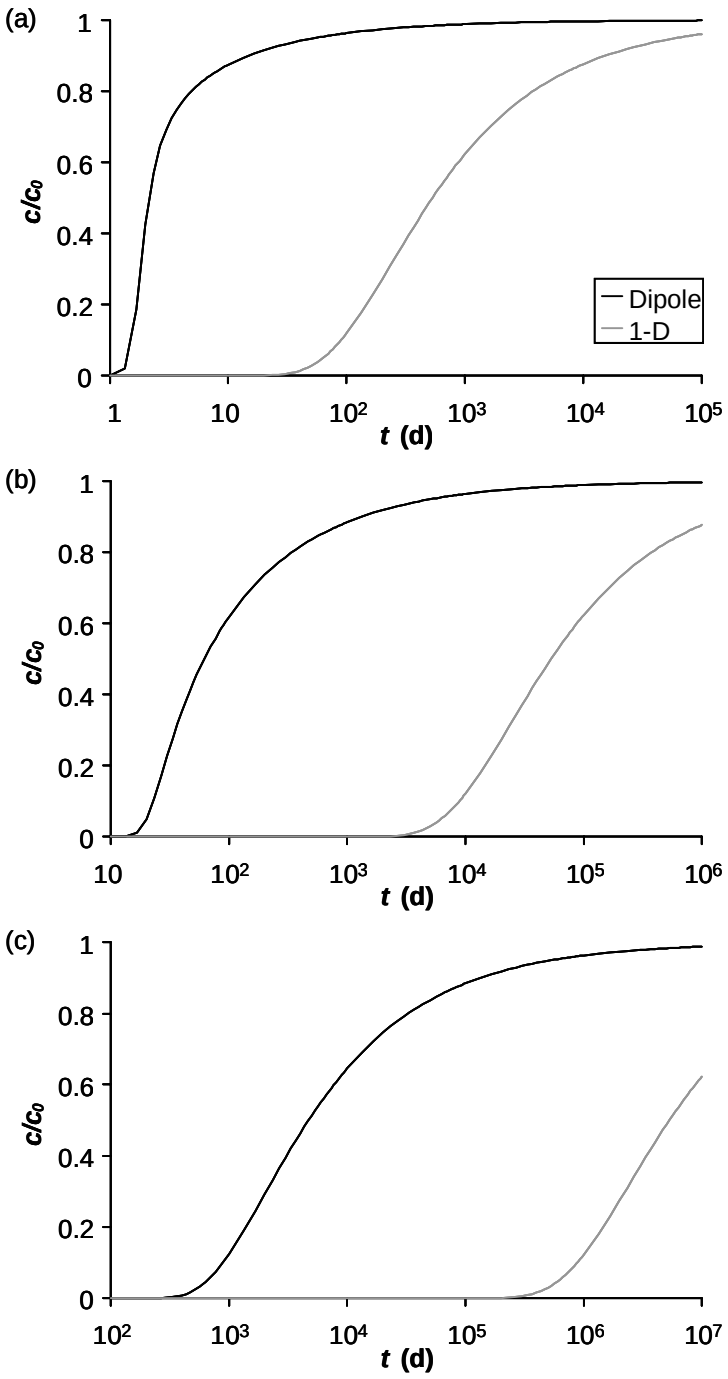

Figure 4.6 Predicted breakthrough 100 m downstream from a constant source of solute with parameters from both dipole (α = 1 m and A = 2.5 $d^{1/2}$) and 1-D (α = 0.1905 m and A = 0.073508 $d^{1/2}$) models under hydraulic gradients of (a) 0.1, (b) 0.01 and (c) 0.001.

predictions under natural (or other) conditions if the interpretative model does not adequately represent the system. This may seem obvious, but the point

regarding conceptual model choice is rarely demonstrated explicitly and quantitatively in ground water hydrology, although the philosophical principle is well understood.

Given the potentially large errors that can arise from a poor model choice (even if the model generates a good fit the measured data) any additional information about the system would assist both in further constraining parameters and determining which conceptual model may be more appropriate in the interpretation of field based observations. For this reason multiple tracers with different aqueous diffusion coefficients are often used in fractured rock tracer tests with the aim of isolating the effects of dispersion and diffusion on the resultant breakthrough curves. Similarly tests conducted under different forced gradients and over different well separations may be useful. Clearly, additional information on fracture geometry (e.g. orientations, spatial extent and connectedness) will also be beneficial.

Conclusions

This study has demonstrated the non-uniqueness that arises in the interpretation of dipole tracer tests conducted in fractured rock, when the appropriate interpretive model is not known. Breakthrough curves were generated for a wide range of parameter values using a dipole flow model and then fitted with a 1-D flow model. The parameter values required for each model to generate matching breakthrough curves were compared and found to be vastly (up to more than 7 orders of magnitude) different in many cases, having important implications for subsequent predictions based on these initial

parameter estimations. It is understood that conceptual model choice is a major issue in hydrogeology, but there are limited quantitative analyses that explicitly demonstrate the consequences of choosing different conceptual models over and above the general philosophical principle that it is a vital part of interpreting field data and making hydrologic predictions.

The key findings of this study are:

5. Dipole tracer test breakthrough curves can be easily fitted with different conceptual models yielding vastly different estimated parameter values. Given the similarity of the breakthrough curves it is quite surprising just how different the parameter values (α, *v* and *A*) can be. This is not necessarily intuitive. The potential impact of the choice of conceptual model can not be overstated. This reinforces that fact that a good model fit does not necessarily indicate a unique or correct interpretation of field based data.
6. Use of an incorrect interpretive model to determine aquifer parameters from a measured breakthrough curve can lead to very large errors in subsequent predictions (e.g. natural gradient solute transport), even if the fit to the original forced gradient breakthrough curve is excellent.
7. Additional information (such as the use of multiple tracers, multiple tests under different forcing conditions or prior knowledge of the extent and geometry of fractures) that can be used to identify the physical processes causing the spreading of tracer will assist in the interpretation of dipole tracer tests conducted in fractured rock.

8. For a more complex fractured rock setting, neither of the 1-D or dipole flow models assessed in this study is a ‘perfect’ representation of a real field scenario. Further work is required to elucidate where one is a better approximation than the other. What remains, however, is the potential disparity between the often simpler interpretative model chosen and the more complex processes occurring in the real world. This study has demonstrated differences between the 1-D and dipole interpretative parameters for a highly simplified and idealised test case. When interpreting transport in a more complex system, it is likely that both may be a poor conceptual model choice compared with the real system (which is rarely known). Further quantifying the disparity between a ‘real’ conceptual model and simplified interpretative models (e.g. 1-D or dipole) remains a subject for future inquiry.

Notation and Units

Subscript ϕ denotes a property of a streamline of departure angle ϕ.

A	matrix diffusion term	$T^{1/2}$
b	half fracture aperture	L
c	solute concentration	ML^{-3}
c'	solute concentration in the matrix	ML^{-3}
D	hydrodynamic dispersion coefficient	L^2T^{-1}
D^*	diffusion coefficient of solute in water	L^2T^{-1}
D'	diffusion coefficient of solute in matrix	L^2T^{-1}
E	average normalised error	-
Q	fluid injection/extraction rate	L^3T^{-1}
R	face retardation coefficient	-
R'	matrix retardation coefficient	-
r^2	square of Pearson product moment correlation coefficient	-
t	time	T
v	water velocity	LT^{-1}
x, z	spatial coordinates	L
α	longitudinal dispersivity	L
β	ratio of diffusive to dispersive time scales	-
θ	matrix porosity	-
λ	radioactive decay constant	T^{-1}
τ	tortuosity	-
ϕ	streamline departure angle	rad

References

Akin, S., 2005. Tracer model identification using artificial neural networks. Water Resources Research, 41: W10421, doi:10.1029/2004WR003838.

Becker, M.W. and Shapiro, A.M., 2000. Tracer transport in fractured crystalline rock: evidence of nondiffusive breakthrough tailing. Water Resources Research, 36(7): 1677-1686.

Doherty, J., 2004. PEST: Model-Independent Parameter Estimation. Watermark Numerical Computing, Brisbane, Australia.

Grisak, G.E. and Pickens, J.F., 1981. An analytical solution for solute transport through fractured media with matrix diffusion. Journal of Hydrology, 52: 47-57.

Grove, D.B. and Beetem, W.A., 1971. Porosity and dispersion constant calculations for a fractured carbonate aquifer using the two well tracer method. Water Resources Research, 7(1): 128-134.

Himmelsbach, T., Hotzl, H. and Maloszewski, P., 1998. Solute transport processes in a highly permeable fault zone of Lindau fractured rock test site (Germany). Ground Water, 36(5): 792-800.

Himmelsbach, T. and Maloszewski, P., 1992. Tracer tests and hydraulic investigations in the observation tunnel Lindau. Steirische Beitraege zur Hydrogeologie: 197-228.

Jardine, P.M. et al., 1999. Quantifying diffusive mass transfer in fractured shale bedrock. Water Resources Research, 35(7): 2015-2030.

Lever, D.A. and Bradbury, M.H., 1985. Rock-matrix diffusion and its implications for radionuclide migration. Mineralogical Magazine, 49(351): 245-254.

Maloszewski, P., Harum, T. and Benischke, R., 1992. Mathematical modelling of tracer experiments in the karst of Lurbach system, in Application of tracer models. Steirische Beitraege zur Hydrogeologie: 116-158.

Maloszewski, P., Herrmann, A. and Zuber, A., 1999. Interpretation of tracer tests performed in fractured rock of the Lange Bramke basin, Germany. Hydrogeology Journal, 7(2): 209-218.

Neretnieks, I., 1983. A note on fracture flow dispersion mechanisms in the ground. Water Resources Research, 19(2): 364-370.

Novakowski, K.S., 1988. Comparison of fracture aperture widths determined from hydraulic measurements and tracer experiments. In: B. Hitchon and S. Bachu (Editors), Proceedings: 4th Canadian/American Conference on Hydrogeology. National Water Well Association, Dublin, Ohio, pp. 68-80.

Novakowski, K.S., Bickerton, G. and Lapcevic, P., 2004. Interpretation of injection-withdrawal tracer experiments conducted between two wells in a large single fracture. Journal of Contaminant Hydrology, 73: 227-247.

Novakowski, K.S., Evans, G.V., Lever, D.A. and Raven, K.G., 1985. A field example of measuring hydrodynamic dispersion in a single fracture. Water Resources Research, 21(8): 1165-1174.

Pfingsten, W. and Soler, J.M., 2003. Modelling of nonreactive tracer dipole tests in a shear zone at the Grimsel test site. Journal of Contaminant Hydrology, 61: 387-403.

Piessens, R. and Huysmans, R., 1984. Algorithm 619. Automatic numerical inversion of the Laplace transform. Association of Computer Machinery Transactions on Mathematical Software, 10(3): 348-353.

Rasmuson, A. and Neretnieks, I., 1986. Radionuclide transport in fast channels in crystalline rock. Water Resources Research, 22(8): 1247-1256.

Robinson, N.I. and Sharp, J.M., 1997. Analytical solution for solute transport in a finite set of parallel fractures with matrix diffusion. CMIS C23/97, CSIRO, Adelaide.

Sanford, W.E., Cook, P.G. and Dighton, J.C., 2002. Analysis of a vertical dipole tracer test in highly fractured rock. Ground Water, 40(5): 535-542.

Sudicky, E.A. and Frind, E.O., 1982. Contaminant transport in fractured porous media: analytical solutions for a system of parallel fractures. Water Resources Research, 18(6): 1634-1642.

Tang, D.H., Frind, E.O. and Sudicky, E.A., 1981. Contaminant transport in fractured porous media: analytical solution for a single fracture. Water Resources Research, 17(3): 555-564.

Tsang, C.F., Tsang, Y.W. and Hale, F.V., 1991. Tracer transport in fractures: analysis of field data based on a variable-aperture channel model. Water Resources Research, 27(12): 3095-3106.

Tsang, Y.W. and Tsang, C.F., 1987. Channel model of flow through fractured media. Water Resources Research, 23(3): 467-479.

Weatherill, D., Cook, P.G., Simmons, C.T. and Robinson, N.I., 2006. Applied tracer tests in fractured rock: Can we predict natural gradient solute transport more accurately than fracture and matrix parameters? Journal of Contaminant Hydrology, 88: 289-305.

Webster, D.S., Proctor, J.F. and Marine, I.W., 1970. Two-well tracer test in fractured crystalline rock. US Geological Survey Water Supply Paper, 1544-I.

Chapter 5: Interpreting dipole tracer tests in fractured rock aquifers

Abstract

Dipole tracer tests, where transport of applied tracer is measured in a steady state injection-withdrawal dipole, provide a means to characterise in-situ solute transport parameters for fractured rock aquifers. Single fracture analytical models have been used in previous studies to analyse tracer tests conducted in single isolated fractures (Novakowski, 1988; Novakowski et al., 2004; Novakowski et al., 1985) and fracture networks (Himmelsbach et al., 1998; Himmelsbach and Maloszewski, 1992; Sanford et al., 2002). For tests conducted in a fracture network it is usually assumed that equivalent single fracture and matrix parameters can be used to represent the whole network. This study examines the performance of two single fracture analytical models when used to interpret simulated tracer tests conducted in hypothetical three-dimensional fracture networks and dipole tracer tests conducted in the Clare Valley, South Australia, both in terms of parameter estimation and subsequent solute transport predictions. The benefit of additional measured tracer data, either for a tracer with a different diffusion coefficient or for another test at a different injection and extraction rate is examined. The single fracture models could be calibrated to generate a good fit to a measured data set, but were not able to accurately predict solute transport under lower hydraulic gradients for the networks and field scenarios examined in this study. Simulations of transport in hypothetical fracture networks indicated that predictions could be

most improved by conducting an additional test at a lower injection and extraction rate.

Introduction

Dipole tracer tests have been used for decades to measure solute transport through in-situ aquifer material. A dipole tracer test uses an injection-extraction well pair to generate a steady state hydraulic dipole flow field in the aquifer. A tracer is introduced at the extraction well and the tracer breakthrough is measured at the extraction well. A dipole flow field allows sampling of a large volume of aquifer which can be controlled by the spacing of the wells. The forced gradient imposed by the dipole flow field enables rapid measurement of tracer transport. The measured tracer breakthrough curve is used to infer aquifer properties, usually using an analytical model. Single fracture analytical models have been used in previous studies to analyse tracer tests conducted in single isolated fractures (Novakowski, 1988; Novakowski et al., 2004; Novakowski et al., 1985) and fracture networks (Himmelsbach et al., 1998; Himmelsbach and Maloszewski, 1992; Sanford et al., 2002). For tests conducted in a fracture network it is usually assumed implicitly that equivalent single fracture and matrix parameters can be used to represent the whole network. The extent to which the complex geometry of a fracture network affects the interpretation of a dipole tracer test is not known.

Grove and Beetem (1971) outlined a method for modelling a 2-D dipole of equal pole strength (as would occur in a fracture of infinite extent with smooth parallel walls). The approach is a summation of breakthrough curves from multiple

streamlines. Each streamline has a path length and average flow velocity dependent on the angle of departure from the injection well. This method has been widely used to interpret dipole tracer tests conducted in single fractures (Novakowski, 1988; Novakowski et al., 2004; Novakowski et al., 1985) and in fracture networks (Himmelsbach et al., 1998; Himmelsbach and Maloszewski, 1992; Sanford et al., 2002; Webster et al., 1970).

Typically dipole tracer tests are analysed assuming that a perfect dipole is attained in the fracture(s). However, laterally finite fractures and variable fracture apertures channel flow such that infinite dipole flow fields cannot develop. In some cases a 1-D flow model may in fact better describe the flow field generated by an injection-extraction well pair. 1-D flow models have also previously been used to interpret dipole tracer tests where injection and extraction rates are not equal (Pfingsten and Soler, 2003). Thus a range of possible interpretative models exist and are subjectively applied. Systematic evaluation of their behaviour is warranted.

The first part of this study examines the performance of the two single fracture analytical models (1-D and dipole flow) when used to interpret simulated dipole tracer tests conducted in hypothetical three-dimensional fracture networks. The results are demonstrative only and the synthetic fracture networks are not moderated using real field data. Initially a single dipole tracer test is simulated numerically in a hypothetical fracture network. The analytical models are calibrated to the modelled tracer breakthrough curve and used to predict solute transport under a much lower hydraulic gradient. The predicted solute transport

is then compared to the ‘real’ simulated transport. In this way the consequences of the single fracture approximation and associated flow geometry of the two interpretative analytical models are identified. The study then examines how the predictive capability of the analytical models might be improved if additional information was available to calibrate them. The value of the following is examined: (a) an extra tracer test at either higher or lower hydraulic gradient, (b) an additional tracer with a different diffusion coefficient included in the initial tracer test and (c) knowledge of the length of the shortest fracture flow path between the injection and extraction wells (rather than an assumption of a straight line).

The second section of this study applies the methodology used in the hypothetical fracture networks to real dipole tracer tests conducted in the Clare Valley, South Australia. Application of the methodology to the field environment introduces additional variations between the assumptions of the analytical models and the reality of the field setting.

Generating Synthetic Fracture Networks

For this study three fracture networks were created, each consisting of ten orthogonal fractures in the x-y and y-z planes. The use of three networks was deemed sufficient to meet the demonstrative aim of this study. By generating fractures in two orthogonal orientations, tracer transport could be simulated in a three-dimensional network of interconnected fractures, rather than simply in parallel fractures that do not interact directly. Fracture apertures were chosen

from a negative exponential probability distribution with mean of 500 μm (see equation 1).

$$P(x) = \lambda e^{-\lambda x} \quad (5.1)$$

Where $P(x)$ = probability of a parameter value x in a distribution with both mean and standard deviation = $1/\lambda$.

A minimum fracture aperture cut-off of 100 μm was specified such that any apertures generated below this were subsequently regenerated from the distribution until they exceeded this threshold. Square fracture planes were generated with lengths chosen from the probability distribution outlined in Equation 1 with mean of 5 m and minimum cut-off of 1 m. The centre of each fracture was randomly located in the 10 x 10 x 10 m model domain with all locations having equal probability. Fractures protruding beyond the model domain were truncated at the boundary and thus not all fractures remained square. The three resulting fracture networks are shown in Figure 5.1.

Network	Av. *L* in *x-y* plane (m)	Av. *L* in *y-z* plane (m)	Av. *L* total (m)	Av. 2*b* in *x-y* plane (μm)	Av. 2*b* in *y-z* (μm)	Av. 2*b* total (μm)	Δ*h* (m)*
1	5.20	6.24	5.72	813	428	620	0.017
2	5.02	5.07	5.04	716	629	673	0.552
3	5.30	3.33	4.32	331	608	469	0.074

Table 5.1 Characteristics of the randomly generated fracture networks. * Head differences are those measured for $Q^+ = Q^- = 0.6$ L/min.

The three fracture networks were generated by sampling the same probability distributions for fracture aperture, length and location. However, the random

nature of the selection process leads to different statistical properties for each network. These are presented in Table 5.1. Statistical measures are based on fracture lengths within the model domain, accounting for fracture truncation.

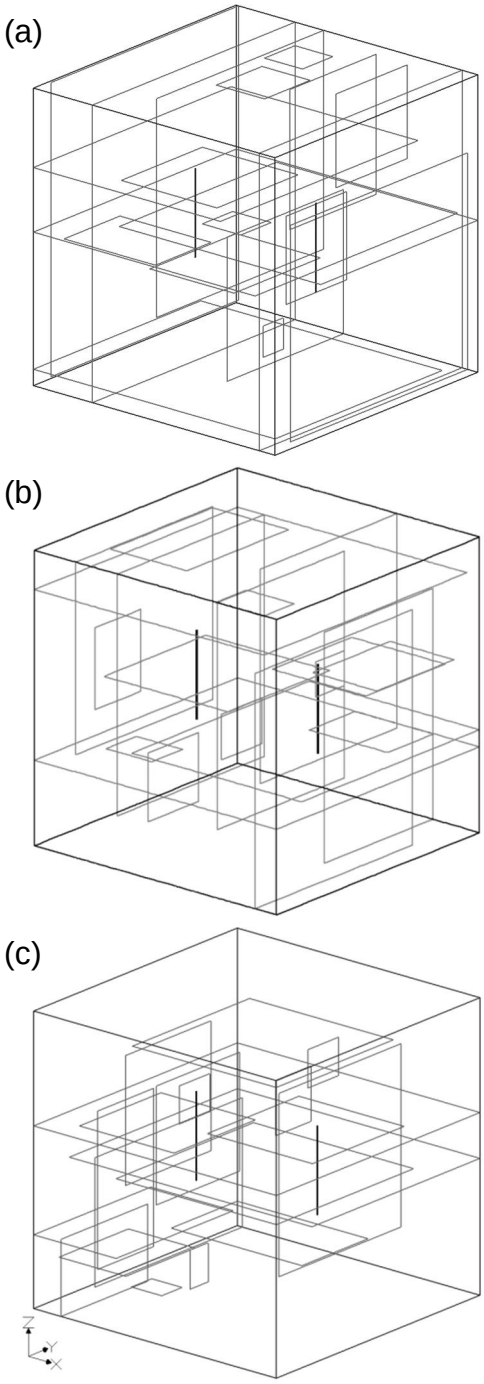

Figure 5.1 The three 10 x 10 m simulated fracture networks. Also shown are the 3 m injection and extraction well screens.

Numerical Modelling

Tracer tests were simulated in the 3 hypothetical networks using the discrete fracture fluid flow and solute transport model HydroGeoSphere (Therrien et al., 2005). HydroGeoSphere represents discrete fractures with 2-D planes of connected nodes that already form part of the 3-D porous medium finite element grid. The fracture and matrix domains are thus coupled by their co-location and by requiring that their corresponding hydraulic heads and concentrations be equal.

The discretised solute transport equations used by HydroGeoSphere can be simplified for a non-sorbing, non-decaying, non-reactive solute in fully saturated media. For the porous medium:

$$\left[\left(\theta c\right)_i^{L+1}-\left(\theta c\right)_i^{L}\right]\frac{V_i}{\Delta t}=\varepsilon\left(\sum_{j\in\eta_i}c_{(ij+1/2)}^{L+1}\gamma_{ij}\left(h_j^{L+1}-h_i^{L+1}\right)+\sum_{j\in\eta_i}\chi_{ij}\left(c_j^{L+1}-c_i^{L+1}\right)\right)+ \\ \left(1-\varepsilon\right)\left(\sum_{j\in\eta_i}c_{(ij+1/2)}^{L}\gamma_{ij}\left(h_j^{L+1}-h_i^{L+1}\right)+\sum_{j\in\eta_i}\chi_{ij}\left(c_j^{L}-c_i^{L}\right)\right)+\Omega_{ex}^{L+1}V_i \tag{5.2}$$

and for fractures:

$$\left[c_{fi}^{\,L+1}-c_{fi}^{\,L}\right]\frac{2ba_i}{\Delta t}=\varepsilon\left(2b\sum_{j\in\eta_{fi}}c_{f(ij+1/2)}^{\,L+1}\gamma_{fij}\left(h_{fj}^{\,L+1}-h_{fi}^{\,L+1}\right)+\sum_{j\in\eta_{fi}}\chi_{fij}\left(c_{fj}^{\,L+1}-c_{fi}^{\,L+1}\right)\right)+ \\ \left(1-\varepsilon\right)\left(2b\sum_{j\in\eta_{fi}}c_{f(ij+1/2)}^{\,L}\gamma_{fij}\left(h_{fj}^{\,L+1}-h_{fi}^{\,L+1}\right)+\sum_{j\in\eta_{fi}}\chi_{fij}\left(c_{fj}^{\,L}-c_{fi}^{\,L}\right)\right)+\Omega_f^{L+1}a_i$$

(5.3)

where: a_i = area associated with fracture node i (L^2), b = half fracture aperture (L), c = solute concentration (ML^{-3}), h = hydraulic head (L), t = time (T) V_i = region or control volume associated with porous medium node i (L^3), γ_{ij} = term arising from discretisation and describing fluid flow between i and j (L^2T^{-1}), η_i =

the set of nodes connected to node *i*, χ_{ij} = term arising from discretisation and describing diffusive/dispersive solute flux between *i* and *j* (L^3T^{-1}), ε = finite difference time weighting factor (-), θ - porosity (-) and Ω = solute exchange rate between fracture and porous medium domains (T^{-1}). Subscript *f* denotes a fracture property, subscripts *i* and *j* denote a property of node *i* or *j* respectively and superscript *L* denotes the time level, with *L*+1 corresponding to the time level for which the solution is sought.

The model domain measuring X = Y = Z = 10 m was discretised with a finite element grid. No flow was specified for all model domain walls. A 3 m injection well was located at x = -2.5 m (with the origin (0, 0, 0) positioned at the centre of the domain) and a 3 m extraction well at x = 2.5 m. Each well was screened over the 3 m interval from z = -1.5 to 1.5 m. A reference hydraulic head of 0 m was assigned to the centre of the injection well. Fracture planes and the centres and ends of the two wells were specified as required nodal locations. Discretisation was then conducted using variable grid spacing such that:

$$\Delta L = m_L^{(n-1)} \Delta L_{min} \tag{5.4}$$

where: ΔL = grid spacing in the *L* direction (L), m_L = grid spacing multiplier in the *L* direction (-), *n* = integer element counter where element number 1 borders the specified starting coordinate (-) and ΔL_{min} = the minimum element size occurring at *n* = 1 (L).

Weatherill et al. (2008) found that in cases where diffusion between the fracture and matrix is relatively small discretisation sometimes as fine as the fracture

aperture is required. This study simulates tracer migration under highly forced conditions where fluid velocities are high and the time available for diffusion into the matrix is reduced. Hence it was considered prudent to employ fine discretisation at the fracture-matrix interface. At each fracture plane ΔL_{min} was set to the size of the fracture aperture to ensure a sufficiently fine spatial discretisation. Following the recommendations of Weatherill et al. (2008) a sensitivity analysis to m_L over the range of forcing conditions was conducted and a value of 4 was adopted for discretisation moving away from fracture planes. At the wells ΔL_{min} = 0.05 m and m_L = 2 were used. A global maximum grid spacing of 0.5 m was enforced to avoid potential numerical problems associated with large elements. Because each network employed a different realisation of fracture locations and apertures, they necessarily employed different spatial discretisation.

Temporal discretisation was conducted using HydroGeoSphere's variable time-stepping procedure with a Crank-Nicolson implicit finite difference scheme in time, with ε = 0.5 in equations (2) and (3). Once a solution at time L is found, the next time-step is determined by:

$$\Delta t^{L+1} = \frac{c_{max}}{\max\left|c_i^{L+1} - c_i^{L}\right|}\Delta t^{L} \tag{5.5}$$

where c_{max} = specified maximum change in concentration desired in a time-step and c_i = calculated concentration at node i. This procedure allows the model to increase time-step size when there are only small changes in concentration and reduce it when rapid changes occur. Computation time is reduced without decreasing numerical accuracy. This study used a very small initial time-step of

0.01 s and a target concentration change per time-step of c_{max} = 0.01. A maximum time-step multiplier of 2 was imposed.

Other than the fracture locations, lengths and apertures, the networks employed the same parameter values. These are listed in Table 5.2. Matrix hydraulic conductivity was set extremely low to simulate an essentially impermeable matrix, forcing all significant fluid flow to occur in the fracture network.

Parameter	Value
Model domain size X, Y, Z	10 m
Matrix porosity θ	0.02
Matrix hydraulic conductivity K	10^{-50} ms^{-1}
Longitudinal dispersivity α_L	1 m
Transverse dispersivity α_T	0.1 m
Vertical transverse dispersivity α_{VT}	0.1 m
Tortuosity τ	1
Fracture longitudinal dispersivity α_{Lf}	1 m
Fracture transverse dispersivity α_{Tf}	0.1 m
Well screen length L_w	3 m
Well radius r_w	0.025 m
Injection and extraction rate Q^+, Q^-	10^{-5} m^{3}s^{-1}

Table 5.2 Numerical model parameters for the fracture network simulations.

In each of the 3 networks 6 tracer tests were simulated under steady state flow with transient solute transport. The base case simulations were for a dipole of $Q^+ = Q^-$ = 0.6 L/min with a tracer pulse of 1 hour. Tracer was injected at a nominal concentration of 1 kgm^{-3}. Density effects were not simulated and therefore the chosen injectant concentration is immaterial. Tracer transport was

simulated for 1 day. Additional tracer tests were simulated at factors of 10, 0.1, 0.01, 0.001 and 0.0001 of the base case pumping rates. All simulations were for 1 hour of tracer input, but recovery periods were modified in order to obtain tracer breakthrough curves which had peaked and begun decreasing. Tracer aqueous diffusion coefficients of 2.01×10^{-9} m^2/s and 1.27×10^{-9} m^2/s were used to simulate bromide (Br^-) and sulphur hexafluoride (SF_6) respectively. Initial tracer concentration was set to zero throughout the domain.

Analytical Modelling

The breakthrough curves generated by HydroGeoSphere were fitted using two single-fracture analytical models, first to obtain interpreted aquifer parameters and then to make predictions of the other tests. The least-squares parameter estimation program PEST (Doherty, 2004) was used to fit the analytical models to the numerical data. Weights were assigned to data values, calculated as $1/c_p$, so that when fitting multiple breakthrough curves those with higher concentrations would not dominate the fitting process. The analytical models were those for 1-D flow in a single 'parallel plate' fracture (Tang et al., 1981) and one using the approach of Grove and Beetem (1971) to sum breakthrough curves from multiple streamlines, each representative of a flow line in a 2-D dipole flow field constrained to the fracture plane. Transport along each streamline was solved using the Tang et al. (1981) model. Therefore the only difference between the two analytical models was the flow geometry.

The geometry and solution for the model presented by Tang et al. (1981) is outlined in Chapter 2 (see Figure 2.1 and equations 2.1, 2.2 and 2.3) and is not repeated here.

The geometry and solution for the model presented by Grove and Beetem (1971) is outlined in Chapter 4 (see Figure 4.1 and equations 4.1 to 4.3b) and is not repeated here.

Himmelsbach and Maloszewski (1992) used 120 streamlines to model dipole tracer breakthrough. Novakowski et al. (1985) found that as few as 12 streamlines were necessary to model unequal strength dipole flow when using a numerical approach whilst Novakowski et al. (2004) found that 45 streamlines were needed for convergence using the same numerical technique to model a dipole with an ambient ground water flow. We conducted an independent sensitivity analysis and found that approximately 45 streamlines were sufficient for solution convergence for most parameter combinations. However, due to the short computational time required, 105 streamlines were used to model dipole transport and this was more than sufficient to ensure solution convergence.

Initially the analytical models were calibrated using data from the base case (Q^+ = Q^- = 0.6 L/min) Br^- breakthrough curves only. Predicted breakthrough curves were then generated with both analytical models using the calibrated parameters, but now with scaled pumping rates and corresponding changes to v. Now knowing the predictive capabilities of the calibrated models for each of

the three networks we assessed how additional calibration information might affect the predictions. The information tested was:

1) An additional tracer test at 10 x base case *Q*
2) An additional tracer test at 0.1 x base case *Q*
3) An additional tracer (SF_6) with a different diffusion coefficient
4) Knowledge of the length *z* of the shortest path between the two wells (rather than an assumption of a straight line)

As would be expected, predictions worsen as the difference between the hydraulic gradients of the prediction and test (calibration) scenarios increases. Fitted and predicted breakthrough curves for network 1 in Figure 5.2 clearly illustrate this effect. We use in v_{pr}, defined as the ratio of the water velocity in the prediction to that of the calibration tracer test, to quantify the difference between predictive scenarios. At v_{pr} = 1 both analytical models fit the simulated data well, with the 1-D flow model providing the best fit. At v_{pr} = 0.01 both predictions fit the data less well and at v_{pr} = 0.0001 they are very poor. Although not shown here, the same trend is observed for all three networks. Interestingly, for all networks the dipole model predicts peak concentrations higher than those simulated and conversely the 1-D flow model under-predicts peak concentrations. This can be explained by the assumed flow geometry of the two

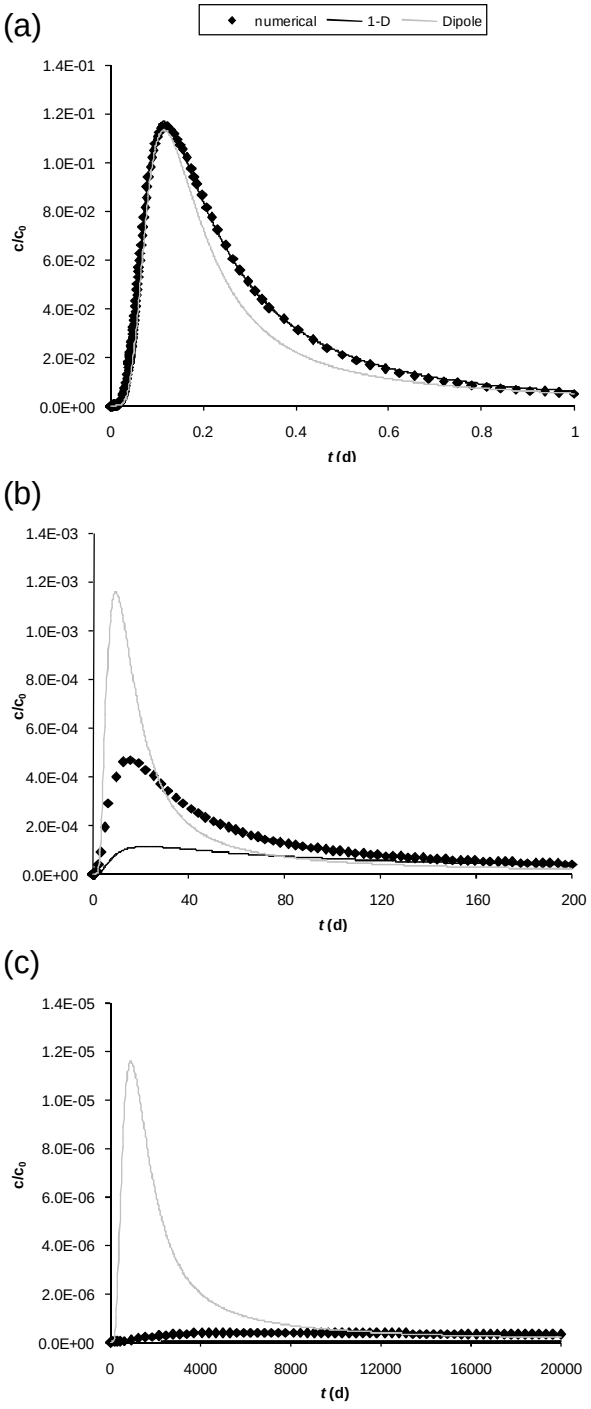

Figure 5.2 (a) Simulated tracer breakthrough for the network 1 base case (v_{pr} =1) along with fitted curves for the 1-D and dipole models. (b and c) Simulated tracer breakthrough along with analytical predictions at v_{pr} = 0.01 and 0.0001 respectively.

models. In reality, flow in each connected fracture will not follow a purely 1-D or purely dipole geometry. Rather, it is likely to be somewhere between the two. Even for a hypothetical case where a single fracture connects the wells, its finite extent bounds flow, and a perfect dipole cannot form. Therefore neither model would work perfectly for such a simple case, and could not be expected to perform any better for a network of connected fractures. Despite the geometrical simplifications employed by the analytical models, the fitting process may obtain a good fit to the measured data by over- or under-estimating one or more of the three fitting parameters; v, α, and A. For all three networks A is greatly overestimated (by eight to nine orders of magnitude) by the dipole model, effectively underestimating the diffusive capability of the system. The dipole model is able to replicate the long tailing of the breakthrough curve without matrix diffusion because of the prolonged solute travel time along the long, slow streamlines that depart at large ϕ. However, as v_{pr} is decreased in the predictions, the impact of matrix diffusion increases at a greater than linear rate in the simulated network transport, but the time taken for advection along the long streamlines increases linearly. Therefore whilst the dipole model can be 'forced' to match measured data for a single tracer test, it does not provide good predictions at lower flow speeds.

Having established base case standards for predictive ability by using a single test with one tracer, additional information was added to the fitting process to assess how it improved subsequent predictions, if at all. Figure 5.3 shows, for the range of v_{pr} covered in the study, normalised predictions of three characteristics of the network 1 breakthrough curves; the time to the first

inflection point t_{i1}, the time to the peak t_p and the peak concentration c_p. Normalisation is performed by dividing the characteristics predicted by the calibrated analytical models by those measured in the simulated tracer transport in the fracture networks. The predicted values for all characteristics are within

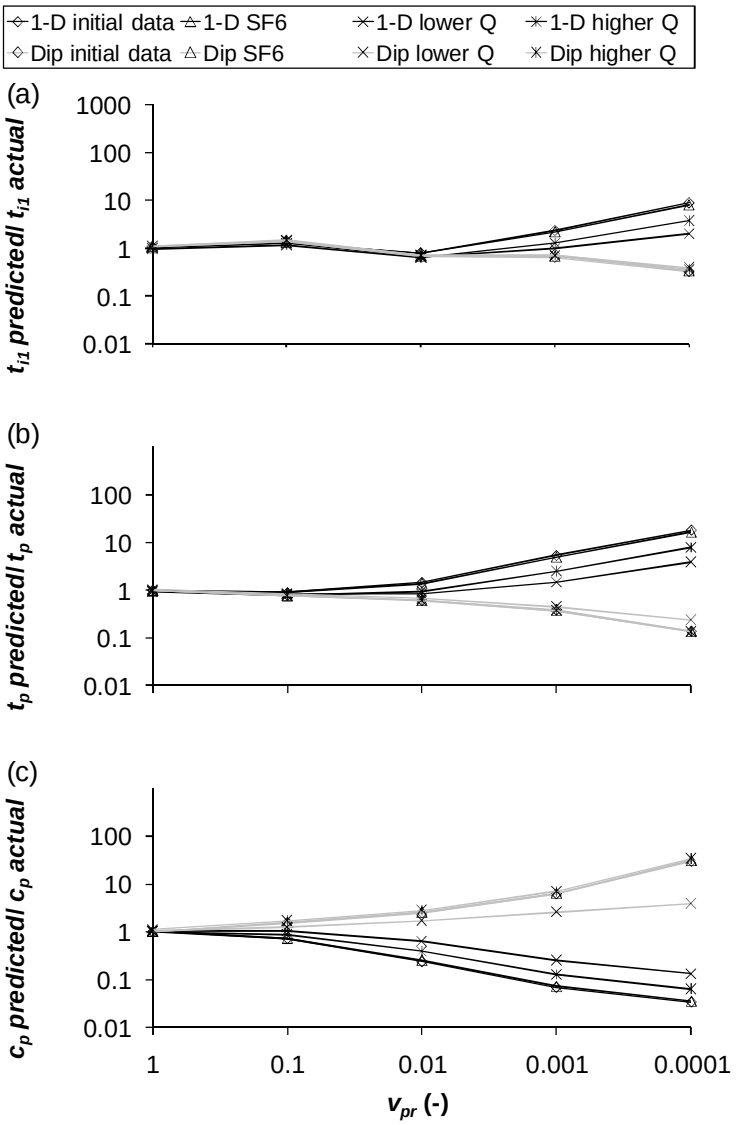

Figure 5.3 Normalised predictions of (a) time to the first inflection point, (b) time to the peak and (c) peak concentration for the base case and when additional information is included in the calibration for network 1.

an order of magnitude of the actual values for v_{pr} down to 0.01, but beyond that predictions begin to deteriorate rapidly. For the 1-D flow model an additional tracer makes negligible difference to the predictions. An additional test at higher velocity makes a significant improvement and a test at a lower velocity makes a large improvement. The only significant improvement to the dipole model predictions is made by adding an additional test at a lower forced gradient. Results were similar for all three networks.

Figure 5.4 shows Pearson product moment correlation coefficients, r plotted against normalised peak concentrations. Normalised peak concentration indicates accuracy of the magnitude of the predicted breakthrough curve whilst r is an indicator of phase or timing of concentration increase and decrease across the entirety of a breakthrough curve. Plotting r against normalised c_p allows non-biased comparison of the goodness of fit of all breakthrough curves regardless of their respective durations and magnitudes. Figure 5.4a shows that the fitted breakthrough curves for both models plot very closely to the measured data (i.e. c_p = 1, r = 1). However, many of the predicted breakthrough curves summarised in Figure 5.6b are seen to be highly inaccurate. Generally, the 1-D model predictions plot between c_p = 0.001 and 1 (i.e. under-predicting peak concentration) and between r = 0 and 1 (positive correlation). Conversely, the dipole model predictions generally over-predict peak concentrations and are negatively correlated with the measured breakthrough curves. Generally, it can be seen that the 1-D model predictions are better than the dipole model predictions. This indicates that the structure of the fracture networks has constrained flow to a geometry that is better approximated as 1-D than a dipole.

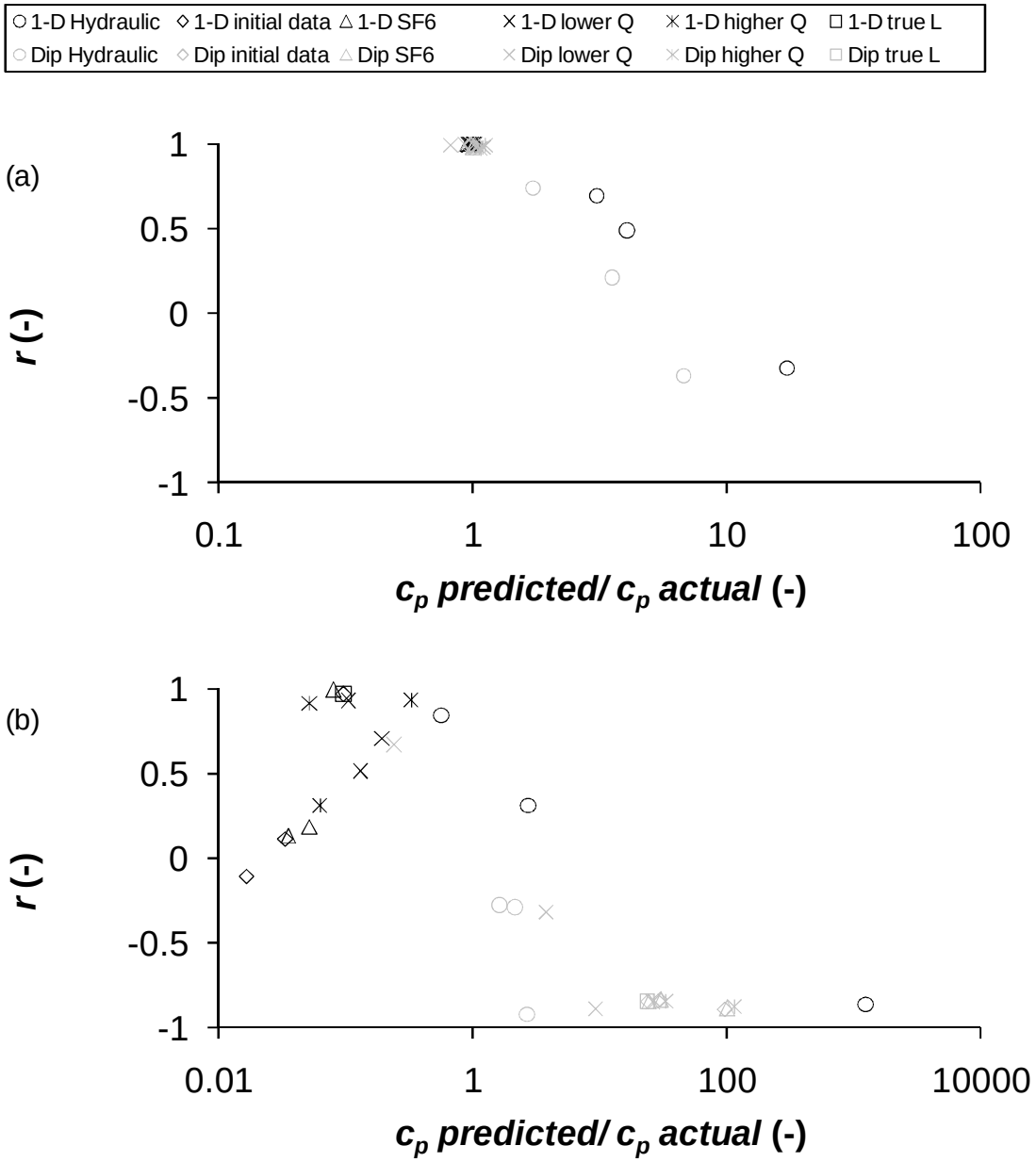

Figure 5.4 Pearson product moment correlation coefficient versus normalised predicted peak concentration for the range of fitting scenarios in all three fracture networks (a) at the fitting speed and (b) at v_{pr} = 0.0001.

This is an important finding and is not intuitively obvious. A range of fracture properties (e.g. length, spacing, orientation and connectedness) as well as the model domain size are likely to affect the relative performance of the two

models, an analysis of which is beyond the scope of this study. Of the scenarios where additional data was included in the calibration process, the best performing across the three networks as a whole is when a slower test is added when using the 1-D model. For this scenario, predictions for all three networks plot relatively close to (1,1).

Also shown in Figure 5.4 are the performances of the two models when populated with composite data based on hydraulic and fracture data alone (i.e. not fitted to measurement of tracer transport). The average of the fracture apertures present in each network was used to calculate the average fracture hydraulic conductivity for each network. Combined with the computed head differences between the wells, and assuming that all fluid flow occurs within the fractures (as was the case for the simulations) this allowed calculation of an average Darcy velocity for each network. The dispersivity used in the simulations was known (specified) as were the molecular diffusion coefficient and matrix porosity, allowing calculation of *A*. The hydraulically based *v*, α, and *A* were then used to generate breakthrough curves at the test and prediction hydraulic gradients for comparison with the breakthrough curves based on calibration to measured tracer data. Of the input parameters, the only one that could not be calculated purely from hydraulic data was the dispersivity of the fractures. In this study the inputs to the numerical model were known. In an applied field scenario, if predictions were to be based on measured hydraulic data and fracture mapping data alone, estimates of porosity and dispersivity would be required to enable prediction of solute transport. The results shown in Figure 5.4 show that at the test speed and for the predictions, the purely

hydraulic approach performs very poorly. Clearly, when predicting solute transport it is best to use measurements of solute transport to inform prediction models.

Field Tracer Tests

Following the results obtained with the hypothetical fracture networks, the methodology was implemented in real dipole tracer tests to examine whether similar outcomes were obtained in a real field setting. A series of equal strength ($Q^+ = Q^-$) dipole tracer tests were conducted to examine the predictive performance of the two analytical models and how additional calibration information altered predictions of solute transport. The imposed hydraulic gradient between the well pair was varied between tests by altering the injection and extraction pumping rates. Following the methodology outlined for the synthetic fracture networks, a base case tracer test was carried out with two tracers (bromide and helium) at 2.3 L/min. A slower tracer test was conducted at 0.7 L/min using sulphur hexafluoride (SF_6). This slow tracer test provided the measured data against which predictions could be compared. Two additional tests were carried out at pumping rates of 6 L/min and 4 L/min using bromide. Data from this suite of tracer tests enabled (1) initial predictions based on calibration to the 2.3 L/min bromide data only, (2) analysis of the impact of including another tracer (helium) and (3) analysis of the impact of an additional tracer test at a different pumping rate (the 6 L/min and 4 L/min data).

The tracer tests were conducted in the Clare Valley, approximately 120 km north of Adelaide, South Australia. The tests were performed between two wells

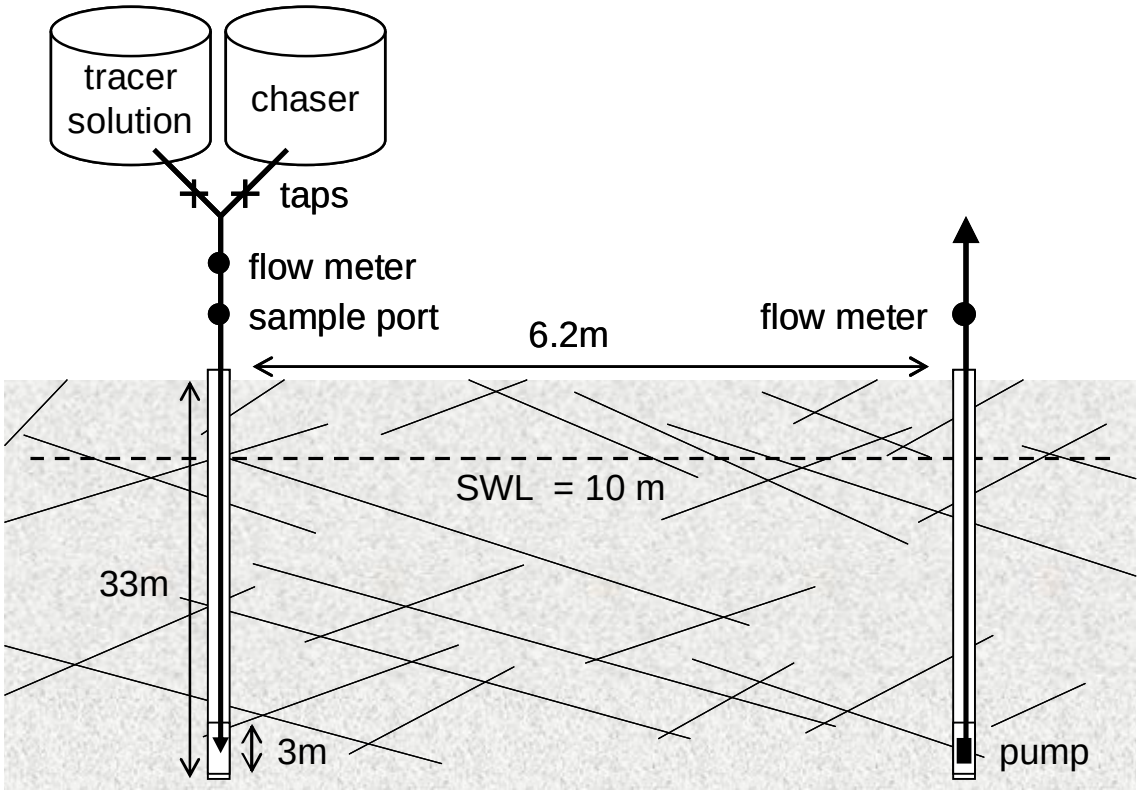

Figure 5.5 Equipment and geometry for the dipole tracer tests at the Clare Valley field site.

completed in the fractured Undalya Quartzite, which constitutes the water table aquifer. The wells were separated by 6.2 m, each with piezometers screened over a 3 m interval between 30 and 33 m below ground level. The arrangement of equipment used to implement the tracer tests is illustrated in Figure 5.5. Two tanks were used, one for tracer solution and one for tracer-free water. Copper pipe and gas-tight fittings were used to plumb the system to avoid diffusive loss of dissolved gas tracers. Gravity injection rates were controlled by placing narrower pipe of various diameters and lengths on the end of the injection piping to constrict flow. A variable speed submersible pump was used to extract groundwater. A flow meter and rubber septum sample port were plumbed in-line

at the injection well head an in-line flow meter was used at the head of the extraction well.

Injectant samples were taken during injection of tracer and afterwards during injection of chaser. Effluent samples were taken initially at 10 minute intervals which were allowed to increase once the tracer peak had passed and the rate of change in tracer concentration was seen to be decreasing. Gas-tight syringes were used to take samples for dissolved gas tracer analysis. Samples for bromide analysis were collected in plastic bottles. On-site bromide analysis was conducted using an ion-selective electrode. Field measurements were later verified by ion chromatography. All dissolved gas samples were analysed on site using a gas chromatograph. Details of the tracer tests, conducted at four different equal strength dipole flow rates, are provided in Table 5.3. Head differences between the two wells before and during application of the dipole flow demonstrate that the gradients applied during the tests were much greater than those present under ambient aquifer conditions.

$Q^+ = Q^-$ (L/min)	6	4	2.3	0.7
Tracers	Br	Br	Br & He	SF_6
Source Br concentration (mg/L)	700	1740	2530	-
Tracer source (min)	60	60	49	60
Injection well drawdown (m)	-0.81	-0.51	-0.26	-0.11
Extraction well drawdown (m)	7.64	4.41	1.49	0.45
Δh pre-test (m)	-0.124	-0.124	0.01	-0.04
Δh forced (m)	8.32	4.80	1.76	0.51
Mass recovery (%)	55	59	59 & 39	36

Table 5.3 Details of dipole tracer tests conducted in the Clare Valley.

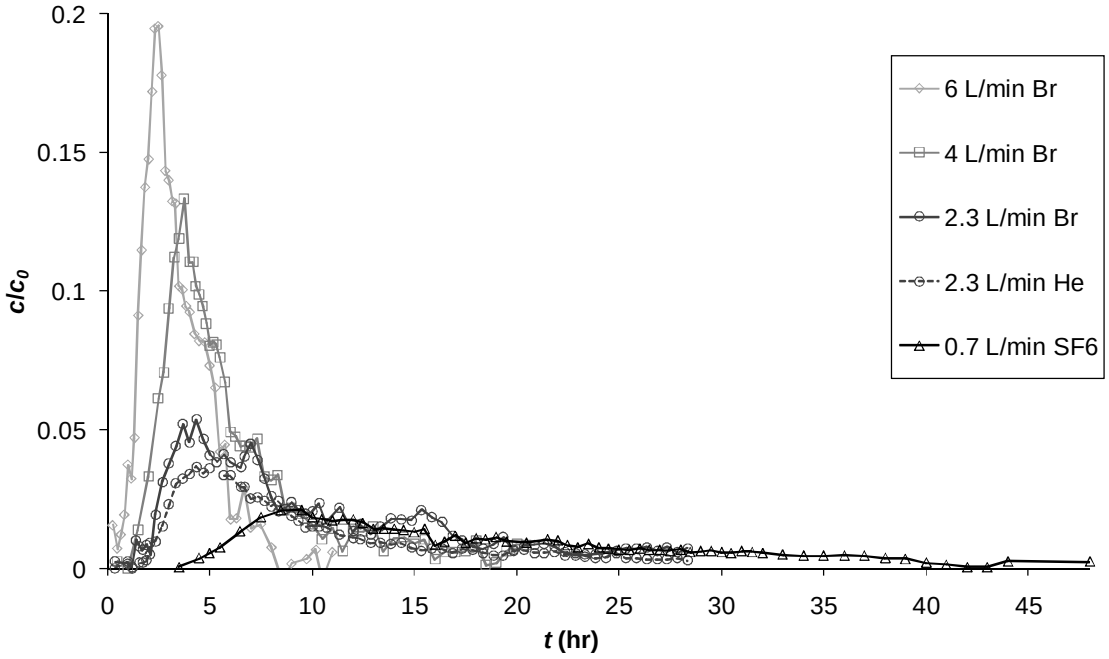

Figure 5.6 Normalised measured peak tracer concentration for dipole tracer tests conducted in the fractured Undalya Quartzite of the Clare Valley.

Normalised breakthrough curves for the tracer tests are presented in Figure 5.6. Comparison of the three bromide breakthrough curves shows that peak tracer concentration and velocity decreases from the 6 L/min to the 4 L/min test and again to the 2.3 L/min test. This behaviour is expected in fractured rock aquifers where solute diffuses from the fast flowing water in the fractures into the relatively immobile water in the rock matrix. A decreased pumping rate causes water to flow slower in the fractures, allowing more time for solute to diffuse into the matrix, thereby reducing tracer concentration in the fractures. Further evidence of matrix diffusion is seen in the comparison of the breakthrough curves for bromide and helium in the same 2.3 L/min test. The helium breakthrough curve has a lower peak concentration and is retarded relative to the bromide. The higher molecular diffusion coefficient of helium causes it to

diffuse more rapidly and further into the rock matrix than the bromide, thereby experiencing greater effects of matrix diffusion.

Sanford et al. (2006) outline a methodology, based on hydraulic measurements, for estimating the maximum tracer mass recovery that can be expected for a tracer test between a well pair. The approach is based on apportioning flow that goes into the injection well to fractures connecting the wells and fractures that are connected to 'elsewhere' by their relative conductances. Using this methodology conductances were determined to be 8.7×10^{-6} m^2s^{-1} between the well pair, 5.2×10^{-5} m^2s^{-1} between the injection well and 'elsewhere' and 7.0×10^{-6} m^2s^{-1} between the extraction well and 'elsewhere'. A maximum expected mass recovery of 58 % was calculated. Two factors dictate that all tracer sent along fracture pathways connecting the two wells will never be recovered in a real field setting. A dipole flow field creates some long flow paths along which water and tracer movement is very slow and therefore it is not likely that this tracer will be recovered within the duration of a tracer test. In addition, solute that diffuses into the rock matrix is never fully recovered. Therefore the theoretical maximum mass recovery is obtainable at infinite time, not within the duration of an applied tracer test. Actual tracer mass recoveries for the tests were 55 % of bromide at 6 L/min, 59 % of bromide at 4 L/min, 59 % of bromide and 39 % of helium at 2.3 L/min and 36 % of SF_6 at 0.7 L/min. The measured values are generally consistent with the theoretically expected 58 %. Recovery of helium was considerably lower than bromide in the 2.3 L/min test, as would be expected in a system where matrix diffusion retards solute transport. Had the

2.3 and 0.7 L/min tests been continued longer it is expected the recovery of helium and SF_6 would have approached the theoretical 58 %.

The tracer tests were fitted using PEST to optimise parameters for both the 1-D and dipole flow implementations of the Tang et al. (1981) solution. The 2.3 L/min bromide data set was used as a base case and the optimised parameters were then used to predict the 0.7 L/min SF_6 breakthrough. Additional data sets were included in the calibration process to investigate how different information affected the predictions. The helium dataset was included to examine the impact of an additional tracer (in the same test) with a different diffusion coefficient. Two additional tests using bromide under higher flow rates were included, separately and together, to assess the benefit of performing multiple tests under different hydraulic gradients. Measured tracer concentrations were scaled by the expected maximum mass recovery prior to calibration. The data were assigned weights ($1/c_p$ and 1/data points in breakthrough) to avoid biasing of the calibration to a particular data set with more data points or higher concentrations.

Figure 5.7 is analogous to Figure 5.2 for the hypothetical fracture networks. For the 4 L/min measured data the 1-D model is seen to provide a better fit than the dipole model which is poorly calibrated. The two models generate predictions of peak arrival time that lag slightly behind the measured data from the 2.3 L/min tracer test. Predictions of the 0.7 L/min SF_6 tracer test are poor. Both models predict around double the actual time for peak arrival and peak concentration is under-predicted. The trend of decreasing predictive capability as the difference

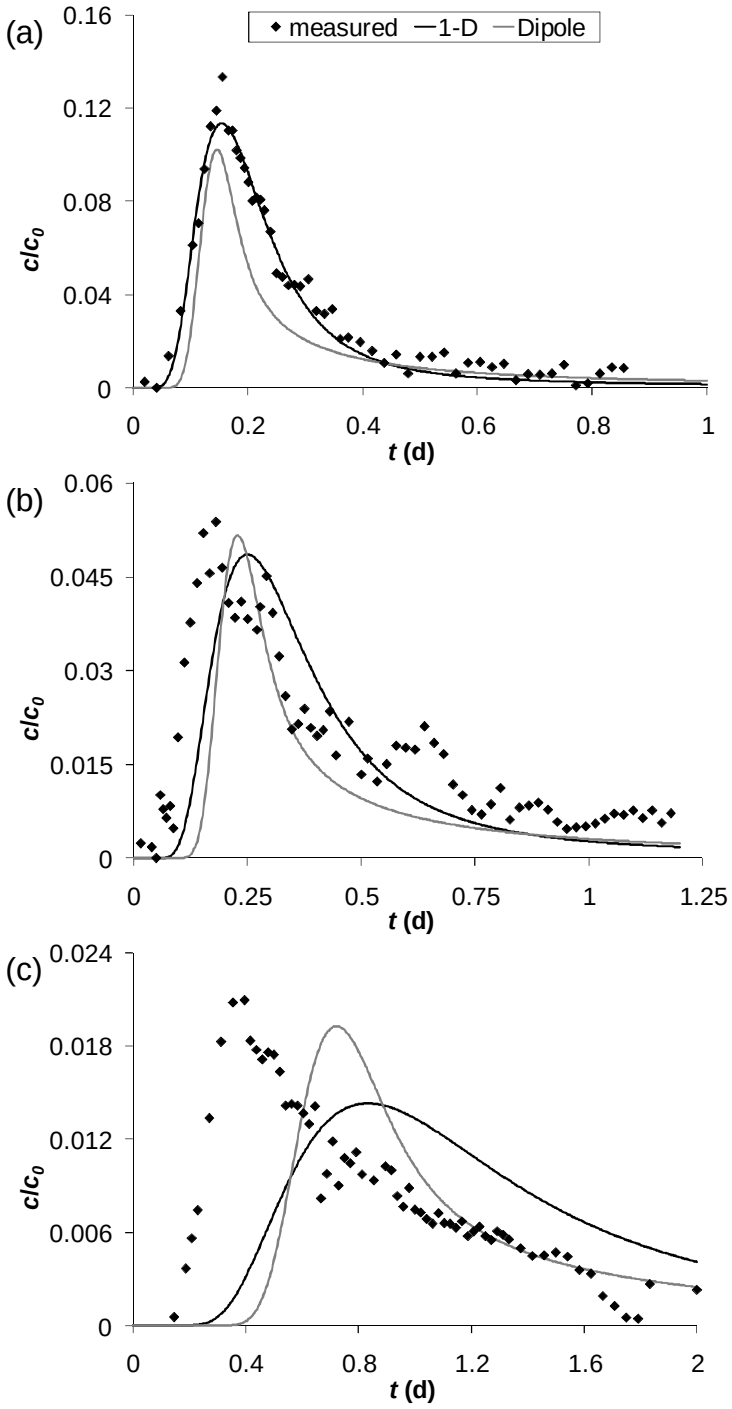

Figure 5.7 (a) Measured 4 L/min Br^- data and fitted analytical models, (b) measured 2.3 L/min Br^- data and predictions using analytical models calibrated to the 4L/min test and (c) measured 0.7 L/min SF_6 data and predictions using analytical models calibrated to the 4L/min test.

between the pumping rates of the calibration and prediction tests increases is consistent with that observed in the synthetic fracture networks.

Q (L/min)	2.3	2.3	2.3 & 6	2.3 & 4	2.3, 4 & 6
Tracer(s)	Br	Br & He	Br	Br	Br
1-D flow model parameters					
α (m)	2.4	1.2	1.1	0.59	0.95
v (m/d)*	4.1	6.9	6.0	6.7	6.1
A ($d^{1/2}$)	2.4×10^{8}	1.5	3.9	1.5	3.0
Dipole flow model parameters					
α (m)	0.48	0.57	0.15	0.12	0.17
v (m/d)*	22	20	22	17	20
A ($d^{1/2}$)	3.6×10^{9}	4.0×10^{9}	3.7×10^{9}	4.5×10^{9}	3.9×10^{9}

Table 5.4 Interpreted parameters for the Clare Valley dipole tracer tests using the two analytical models. * Scaled for Q = 0.7 L/min

The predictive performance of the range of calibrations of the two models is presented in Figure 5.8 using r and normalised (predicted/actual) c_p. Optimised parameter values for each of the calibrations are presented in Table 5.4. Nine of the ten calibrations result in under-prediction of peak concentration. The dipole model predicts higher (and more accurate) peak concentrations for four of the five calibration data sets than the 1-D flow model and has better correlation in all five predictions. The 1-D solution requires more matrix diffusion to attain the same solute retardation and concentration reduction as the dipole model. Matrix diffusion has a greater effect on predictions at lower flow rates and therefore peak concentrations are lower than those for the dipole flow model, even though they may have been very similar for the calibration flow rate. The best

predictions with each model are considerably different to the measured data. Of the two analytical solutions, the dipole model appears to better describe flow and transport in this particular field setting, however there are other processes or different flow geometry impacting the transport of tracer between the two wells.

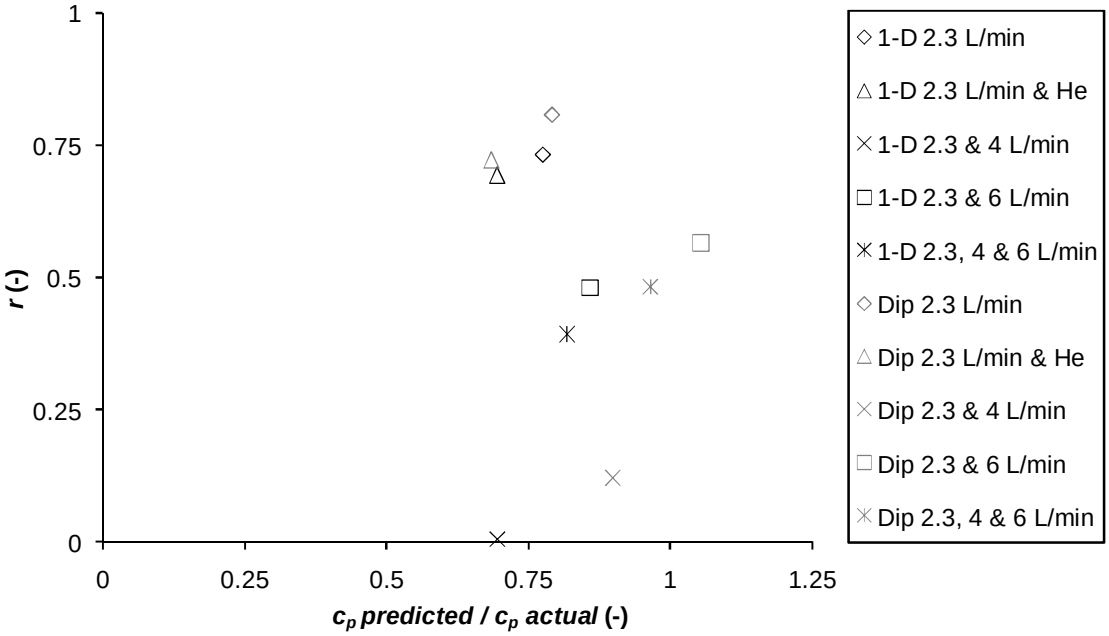

Figure 5.8 Pearson product moment correlation coefficient versus normalised predicted peak concentration for the range of tested calibration data sets when predicting SF_6 breakthrough at 0.7 L/min.

The best predictions are obtained when the models are calibrated with the initial data set using only one tracer at a single flow rate. Given the results from the synthetic fracture networks, this is an unexpected result. There are a range of factors that were not simulated in the hypothetical fracture networks that may have impacted tracer transport in the field. These include, but are not limited to,

mixing in the plumbing and the wells, ambient groundwater flow in the aquifer, density effects, dilation and contraction of fractures with hydraulic pressure, residual tracer from previous tracer tests and saturation and desaturation of fractures with the applied hydraulic gradients.

Discussion

Results from the hypothetical fracture networks indicated that including additional information in the calibration of the two analytical models improved predictions of solute transport under a reduced hydraulic gradient. However, the predictions based on calibration to measured field data did not improve with additional calibration data. The best predictions were obtained using only one dataset, that with the lowest hydraulic gradient and therefore the most similar to the predictive scenario. Of the wide range of factors that may have caused variation between the theoretical and field observations, two were identified as potentially significant; desaturation of fractures and residual tracer from previous tests at the site.

The field tracer tests were conducted in an unconfined aquifer with approximately 20 m of saturated aquifer above the well screens prior to inducing the dipole flow fields. Injection and extraction at the two wells induced hydraulic gradients between the wells that were different for each of the tests. Data presented in Table 5.3 indicates that the hydraulic head difference between the two wells varied between 0.51 and 8.32 m for the five tests. The majority of the head differences was generated by drawdown at the extraction well. Drawdown of 7.64 m was observed for the 6 L/min test, reducing the

saturated thickness of the aquifer near the well by almost 40 %. Whilst it isn't known what proportion of the previously active fracture pathways between the wells were desaturated by the imposed dipole flow field, it is likely that it was significant. The relationship between drawdown and pumping rate was greater than linear, indicating that conductive fractures were being desaturated. Given the hydraulic results, it is evident that tests conducted at different pumping rates were each sampling a different network of active fractures. Therefore the addition of tracer data for tests at higher pumping rates may bias the calibration process to a different interpretation of aquifer parameters that is not representative of the active fracture network for the 0.7 L/min test being predicted. In this scenario it is quite conceivable that the inclusion of tracer data for higher pumping rates in the calibration process could lead to a decrease in predictive performance. This helps explain why the addition of data from the 6 L/min and 4L/min tests to that of the 2.3 L/min lead to worse predictions of the 0.7 L/min SF_6 tracer breakthrough. However, addition of the 4 L/min data worsened predictions more than when the 6 L/min data was included, even though the network of active fractures would have been more similar to that in the predicted test.

It is likely that each of the tests was impacted to a varying degree by residual tracer in the aquifer from previous tests. Two tests using bromide were conducted prior to any of the tests presented in this study and then each of the bromide tests presented here left tracer in the aquifer. In order to account for any background bromide in the aquifer, samples of the ambient groundwater were taken before each of the tests and this concentration was subtracted from

those measured at the extraction well during the test. This was deemed the best approach to account for the residual tracer, but it is a simplification as the bromide concentration will not have been uniform throughout the aquifer prior to each test. The build-up of background bromide was the reason for using SF_6 in the final, lowest gradient test. The SF_6 and helium data sets were not impacted by any previous tracer tests at the site. Of the tests using bromide presented in this study, the 6 L/min test was carried out first, followed by the 4 L/min and 2.3 L/min tests. The background bromide concentration at the site prior to carrying out any tests was around 2 mg/L. Prior to the 6 L/min test it had increased to 35 mg/L then further to 40.5 mg/L before the 4 L/min test. Background bromide had decreased considerably to 19 mg/L by the time the 2.3 L/min test was conducted. Based on this information it is expected that the simple process used to account for background tracer would have the greatest consequences in interpreting the 4 L/min test, followed by the 6 L/min test then the 2.3 L/min test. Therefore the residual bromide present in the aquifer may explain why the predictions made using the 6 L/min data were superior to those using the 4 L/min data, despite the latter inducing a hydraulic gradient (and associated active fractures) more similar to that of the 0.7 L/min prediction. It is not clear why the inclusion of the helium data did not improve predictions.

Conclusions

This study has examined the ability of two analytical models to predict solute transport in fracture networks when calibrated to tracer test data. Dipole tracer tests were simulated in three hypothetical fracture networks and a series of field

tracer tests were conducted in the Clare Valley, South Australia. Key findings can be summarised as follows:

1) Whilst not being exact descriptions of flow in a fracture network, the 1-D flow and dipole flow models could each be calibrated to generate a good fit to the measured data. The suitability of the analytical models could only be determined when they were calibrated to one data set and used to predict another data set under different conditions. Multiple tracer data sets should be obtained when characterising a field site to enable identification of a suitable interpretive model.
2) Predictions of solute transport were more accurate when calibrated to measured tracer data than when parameters were assigned values based on hydraulic data and averaged fracture properties.
3) For the hypothetical fracture networks, inclusion of additional data sets in the calibration process resulted in better predictions. The most useful additional data was that obtained at a lower hydraulic gradient, closer to that of the prediction. Field confirmation of these results in a confined fractured rock aquifer would be useful.
4) Predictions of the field dipole tracer test conducted at the lowest pumping rate were not improved by including additional data sets in the calibration process.
5) In shallow unconfined aquifers the desaturation of the fracture pathways between a well pair with increased dipole strength can result in poor characterisation of solute transport under lower hydraulic gradients. If hydraulic testing indicates significant dewatering of the aquifer near the

extraction well tests should be conducted at the lowest practical dipole strengths.

Notation and Units

Subscript *f* denotes a fracture property.

a_i	area associated with fracture node	L^2
b	half fracture aperture	L
c	solute concentration	ML^{-3}
$\bar{c}$	solute concentration in the Laplace space	TML^{-3}
c'	solute concentration in the matrix	ML^{-3}
c_{max}	specified maximum concentration change per time-step	ML^{-3}
c_p	peak concentration	ML^{-3}
D	hydrodynamic dispersion coefficient	L^2T^{-1}
D^*	diffusion coefficient of solute in water	L^2T^{-1}
D'	diffusion coefficient of solute in matrix	L^2T^{-1}
h	hydraulic head	L
K	hydraulic conductivity	LT^{-1}
L_w	well screen length	L
m_x	grid spacing multiplier in the *x* direction	-
n	integer element counter	-
p	Laplace space variable	T^{-1}
Q	injection or extraction rate	L^3T^{-1}
r_w	well radius	L
r	Pearson product moment correlation coefficient	-
R	face retardation coefficient	-

R'	matrix retardation coefficient	-
t	time	T
v	water velocity	LT^{-1}
V_i	region or control volume associated with porous medium node i	L^3
v_{pr}	prediction water velocity / test water velocity	-
x, y, z	spatial coordinates	L
X, Y, Z	model domain size in x, y and z directions	L
α_L	longitudinal dispersivity	L
α_T	transverse dispersivity	L
α_{VT}	vertical transverse dispersivity	L
γ_{ij}	describes fluid flow between i and j	L^2T^{-1}
ε	finite difference time weighting factor	-
θ	porosity	-
λ	radioactive decay constant	T^{-1}
τ	tortuosity	-
χ_{ij}	describes diffusive/dispersive solute flux between i and j	L^3T^{-1}
Ω	solute exchange rate between domains	T^{-1}

References

Doherty, J., 2004. PEST: Model-Independent Parameter Estimation. Watermark Numerical Computing, Brisbane, Australia.

Grove, D.B. and Beetem, W.A., 1971. Porosity and dispersion constant calculations for a fractured carbonate aquifer using the two well tracer method. Water Resources Research, 7(1): 128-134.

Himmelsbach, T., Hotzl, H. and Maloszewski, P., 1998. Solute transport processes in a highly permeable fault zone of Lindau fractured rock test site (Germany). Ground Water, 36(5): 792-800.

Himmelsbach, T. and Maloszewski, P., 1992. Tracer tests and hydraulic investigations in the observation tunnel Lindau. Steirische Beitraege zur Hydrogeologie: 197-228.

Novakowski, K.S., 1988. Comparison of fracture aperture widths determined from hydraulic measurements and tracer experiments. In: B. Hitchon and S. Bachu (Editors), Proceedings: 4th Canadian/American Conference on Hydrogeology. National Water Well Association, Dublin, Ohio, pp. 68-80.

Novakowski, K.S., Bickerton, G. and Lapcevic, P., 2004. Interpretation of injection-withdrawal tracer experiments conducted between two wells in a large single fracture. Journal of Contaminant Hydrology, 73: 227-247.

Novakowski, K.S., Evans, G.V., Lever, D.A. and Raven, K.G., 1985. A field example of measuring hydrodynamic dispersion in a single fracture. Water Resources Research, 21(8): 1165-1174.

Pfingsten, W. and Soler, J.M., 2003. Modelling of nonreactive tracer dipole tests in a shear zone at the Grimsel test site. Journal of Contaminant Hydrology, 61: 387-403.

Piessens, R. and Huysmans, R., 1984. Algorithm 619. Automatic numerical inversion of the Laplace transform. Association of Computer Machinery Transactions on Mathematical Software, 10(3): 348-353.

Robinson, N.I. and Sharp, J.M., 1997. Analytical solution for solute transport in a finite set of parallel fractures with matrix diffusion. CMIS C23/97, CSIRO, Adelaide.

Sanford, W.E., Cook, P.G. and Dighton, J.C., 2002. Analysis of a vertical dipole tracer test in highly fractured rock. Ground Water, 40(5): 535-542.

Sanford, W.E., Cook, P.G., Robinson, N.I. and Weatherill, D., 2006. Tracer mass recovery in fractured aquifers estimated from multiple well tests. Ground Water.

Tang, D.H., Frind, E.O. and Sudicky, E.A., 1981. Contaminant transport in fractured porous media: analytical solution for a single fracture. Water Resources Research, 17(3): 555-564.

Therrien, R., Sudicky, E.A., McLaren, R.G. and Panday, S.M., 2005. HydroGeoSphere: A three-dimensional numerical model describing fully-integrated subsurface and surface flow and solute transport. User's Guide, Groundwater Simulations Group, Waterloo, Canada.

Weatherill, D. et al., 2008. Discretizing the fracture-matrix interface to simulate solute transport. Ground Water, 46(4): 606-615.

Webster, D.S., Proctor, J.F. and Marine, I.W., 1970. Two-well tracer test in fractured crystalline rock. US Geological Survey Water Supply Paper, 1544-I.

Chapter 6: Concluding Remarks

Summary of Findings

Through a combination of analytical modelling, numerical modelling and implementation of field tracer tests, the research carried out in this thesis has delivered new scientific knowledge regarding the use of applied tracer tests to predict solute transport in fractured rock. In so doing, the thesis has met its stated objectives which are to:

1) evaluate how accurately aquifer parameters can be determined from tracer test data, given the inability of analytical models to completely describe the complex nature of fractured rock and associated tracer breakthrough curves;
2) quantify the impact of parameter and interpretative model uncertainty on predictions of solute transport under lower hydraulic gradients;
3) identify the most effective ways to improve the accuracy of predictions of solute transport in fractured rock aquifers made using tracer test data;

Chapter 2 demonstrates that, when 'accepting' a number of analytical interpretations of a breakthrough curve (all using the same model) non-uniqueness associated with individual parameters can become significant. However, results show that predictions of breakthrough curve characteristics (first inflection point time, peak arrival time and peak concentration) for groundwater flow speeds orders of magnitude smaller than that at which a test

is conducted can sometimes be determined even more accurately than the fracture and matrix parameters.

Chapter 4 takes the ideas behind Chapter 2 a step further to examine the non-uniqueness introduced when two different analytical flow models are considered in the interpretation of a dipole tracer test. Results demonstrate that the two models can produce almost identical breakthrough curves for a range of scenarios. However, in order to do so, sometimes very different and conflicting interpreted aquifer parameter values are required in order to produce the same tracer breakthrough. The study demonstrates the importance of incorporating multiple conceptual models in the analyses of dipole tracer tests conducted in fractured rock, where the actual flow geometry may be poorly understood.

Chapter 5 builds on the outcomes of Chapter 4, using two different analytical models to interpret breakthrough curves and then subsequently predict transport under lower hydraulic gradients. This is done firstly with breakthrough curves generated by simulating dipole tracer tests in hypothetical 3-D fracture networks for which the characteristics were known, and secondly, with breakthrough curves obtained by carrying out dipole tracer tests in the field. Several approaches to reducing predictive uncertainty are tested. The most effective method is to carry out an additional test at a lower injection and extraction rate. In practice this suggests that, when the aim of a tracer test is to enable prediction of transport under ambient flow conditions, the test should be carried out under the lowest feasible imposed hydraulic gradient.

Chapter 3 is a by-product of some of the work carried out in Chapter 5, which involved simulating tracer transport in fractured networks between a dipole well pair. The study examines the required spatial discretisation perpendicular to the FMI for numerical simulation of solute transport in discretely-fractured porous media. To match analytical results on the relatively short timescales simulated in the study, very fine grid spacing perpendicular to the FMI, of the scale of the fracture aperture, is necessary if advection and/or dispersion in the fracture are high compared to diffusion in the matrix. The requirement of such extremely fine spatial discretisation has not been previously reported in the literature. In cases of high matrix diffusion, matching the analytical results is achieved with larger grid spacing at the FMI. Cases where matrix diffusion is lower can employ a larger grid multiplier moving away from the FMI.

Further Research

This thesis has tackled some of the issues associated with using applied tracer tests to predict solute transport in fractured rock, but other aspects remain to be addressed. The following section outlines areas where further research is warranted.

The up-scaling of interpreted aquifer properties from an applied tracer test, sampling a particular portion of aquifer, to the aquifer more generally is an issue that warrants further attention. Whilst applied tracer tests can be designed to sample differing volumes of aquifer, the reality is that most tests will be conducted over shorter intervals, and sample lesser volumes of aquifer, than that over which predictions are made. The act of applying test-scale results to

the broader aquifer, necessarily assumes that the test has been carried out over a sample of aquifer greater than the representative elementary volume (REV). A combination of field-based and modelling studies could be used to investigate this issue. Activities might include carrying out/simulating tests at different locations and over different scales within a fractured rock aquifer.

A similar issue concerns the anisotropy inherent in most fractured rock aquifers. Generally, the fracturing in the rock will create anisotropy in bulk hydraulic conductivity. A study could focus on the use of applied tracer tests to investigate anisotropy and how it varies with spatial scale.

This study examined the uncertainties associated with parameters and predictions when using single fracture models to investigate both field derived and numerically simulated breakthrough curves. The numerical simulations of transport in 3-D fracture networks were numerically cumbersome which limited the number of networks that were simulated. However, with ever-increasing computational capabilities, particularly recent advances in parallel and could computing, the time and memory demands for simulating solute transport in 3-D fracture networks are becoming less burdensome. This opens the door to the use of stochastic modelling approaches for investigating tracer behaviour in 3-D fracture networks. Stochastic modelling, through its ability to deliver probabilistic outcomes, has the potential to provide insights into the characteristics of networks in which tracer transport can be reasonably approximated by single fracture analytical solutions and those that require representation of discrete fracture sets or fractures.

Similarly, the use of stochastic modelling techniques could allow investigation of the linkages between network geometry and the most appropriate analytical solution for describing flow geometry. This thesis has made initial comparisons between interpretations with 1-D and dipole flow analytical models. The applicability of these, and additional flow geometries, could be investigated for appropriately chosen network geometry classifications.

Appendix A: Published Papers

Available online at www.sciencedirect.com
ScienceDirect
Journal of Contaminant Hydrology 88 (2006) 289–305
JOURNAL OF Contaminant Hydrology
www.elsevier.com/locate/jconhyd

Applied tracer tests in fractured rock: Can we predict natural gradient solute transport more accurately than fracture and matrix parameters?

Douglas Weatherill [a,*], Peter G. Cook [b], Craig T. Simmons [a], Neville I. Robinson [a]

[a] *School of Chemistry, Physics and Earth Sciences, Flinders University, GPO Box 2100 Adelaide, SA 5001, Australia*
[b] *CSIRO Land and Water, Private Bag 2, Glen Osmond, SA 5064, Australia*

Received 30 May 2005; received in revised form 18 July 2006; accepted 21 July 2006
Available online 7 September 2006

Abstract

Applied tracer tests provide a means to estimate aquifer parameters in fractured rock. The traditional approach to analysing these tests has been using a single fracture model to find the parameter values that generate the best fit to the measured breakthrough curve. In many cases, the ultimate aim is to predict solute transport under the natural gradient. Usually, no confidence limits are placed on parameter values and the impact of parameter errors on predictions of solute transport is not discussed. The assumption inherent in this approach is that the parameters determined under forced conditions will enable prediction of solute transport under the natural gradient. This paper considers the parameter and prediction uncertainty that might arise from analysis of breakthrough curves obtained from forced gradient applied tracer tests. By adding noise to an exact solution for transport in a single fracture in a porous matrix we create multiple realisations of an initial breakthrough curve. A least squares fitting routine is used to obtain a fit to each realisation, yielding a range of parameter values rather than a single set of absolute values. The suite of parameters is then used to make predictions of solute transport under lower hydraulic gradients and the uncertainty of estimated parameters and subsequent predictions of solute transport is compared. The results of this study show that predictions of breakthrough curve characteristics (first inflection point time, peak arrival time and peak concentration) for groundwater flow speeds with orders of magnitude smaller than that at which a test is conducted can sometimes be determined even more accurately than the fracture and matrix parameters.

Keywords: Fractures; Tracer test; Parameter estimation; Prediction; Uncertainty

* Corresponding author. Tel.: +61 8 82012724; fax: +61 8 82012905.
E-mail address: douglas.weatherill@flinders.edu.au (D. Weatherill).

0169-7722/$ - see front matter.
doi:10.1016/j.jconhyd.2006.07.004

1. Introduction

Applied tracer tests provide a means to estimate aquifer parameters in fractured rock. Tests conducted under a forced hydraulic gradient, for example Novakowski et al. (1985) and Sanford et al. (2002), enable more rapid measurement of tracer breakthrough than could be achieved under ambient flow conditions and so these types of tests are usually preferred.

Many fractured rock tracer tests are analysed with a single fracture model, regardless of whether they were conducted in a single fracture or through a network of fractures. The model may be optimised to fit the breakthrough curve but the parameters, and indeed the model itself, may not be a good representation of reality. An extreme case is when multiple peaks are observed such as those reported by Abelin et al. (1991) and Jakob and Hadermann (1994). A single flow path model can never describe such a system correctly, although a best-fit model could be obtained. Similarly, the choice of whether to model variable apertures, ambient flow and other processes will impact upon the integrity of the interpretation.

Complex models incorporating many processes and therefore many parameters have greater potential to generate non-unique solutions, whereas simpler models may not be able to adequately match the data. Thus due to the complex nature of fractured rock, analysis of tracer tests conducted in fracture networks is subject to the potential for large errors in the analysis phase, as well as the measurement errors associated with any experimental procedure. Maloszewski and Zuber (1983) go as far as saying *"The great number of non-disposable parameters make a correct interpretation of tracer experiments impossible."* Knowing that our models are always a simplification of reality, it is probably optimistic to place exact values on the parameters obtained from them. There may be many parameter sets that will generate an approximation to a breakthrough curve, but a conventional best-fit inversion approach yields a single set of parameters. For example, for a dipole tracer test in an isolated fracture Novakowski et al. (1985) present parameter values of effective fracture aperture and dispersivity based on a single fracture model with no matrix diffusion. The authors state that due to the goodness of the fit over the entire data range and the sensitivity of the model to dispersivity that their fit is unique, but they do not quantify the errors on the parameters. Similarly, for a dipole tracer test in a fracture network Sanford et al. (2002) present best-fit parameter values for fracture path length, fracture aperture, maximum water velocity and dispersivity for a single fracture model with dispersion and matrix diffusion. Whilst these authors show that different parameter values do not match the measured breakthrough curves quite as well as the best fit parameters do, they do not quantify the errors on the parameter values. Numerous examples of analyses of tracer tests can be found in the literature in which the absolute parameter values that optimise the fit between a modelled breakthrough curve and the measured one are found. Whilst some authors make comparisons between these parameter values and those obtained using other means or at other sites, errors are rarely quantified. With many assumptions made in analysing tracer test data, it is valuable to obtain a range of parameter sets that fit the data within a prescribed tolerance level and to ascertain the uncertainty on these estimations. This is likely to be more useful than a set of absolute parameter values where error or uncertainty is not known at all.

There is an additional factor that warrants attention. Typically, forced gradient tracer tests are conducted to enable prediction of solute transport under the natural gradient (such as leakage from a waste disposal site). The fracture and matrix parameters obtained from the inversion process are usually a step towards prediction at lower velocities. Yet we have been unable to find any previous studies which have considered the effect that the errors on these parameters may have for prediction. If prediction is the ultimate aim then the errors on the predictions are important.

This paper considers the uncertainty on parameters and predictions that might arise from analysis of breakthrough curves obtained from forced gradient applied tracer tests. In order to simulate the complexity observed in field data, we add noise to an exact solution to create multiple realisations of an initial breakthrough curve simulated using the analytical solution of Tang et al. (1981). The best fit for each realisation is found using a least squares fitting routine, yielding a range of parameter values rather than a single set of absolute values. The suite of parameters is then used to make a range of predictions of solute transport under lower hydraulic gradients. The uncertainty of estimated parameters from tracer test breakthrough curves and subsequent predictions of solute transport at lower groundwater velocities are compared.

Although this study interprets data generated with a particular single fracture model, the same process is applicable to other models. The purpose of this study is not to provide an absolute description of the behaviour of solute transport in fractured rock, but rather to demonstrate that the uncertainty associated with solute transport predictions under natural gradients may, in some cases, be smaller than the uncertainty of parameters estimated from breakthrough curves. This paradigm/philosophy has not been explored in previous literature.

The objectives of this study are to identify:

1) How accurately individual parameters can be determined from a breakthrough curve;
2) How accurately can predictions be made of solute transport under lower hydraulic gradients using parameters obtained from fitting a forced gradient breakthrough curve;
3) How the uncertainties on parameters compare to those on predicted solute transport.

2. Theory

Tang et al. (1981) present a solution for solute transport in a single fracture with geometry as outlined in Fig. 1. Fluid flow occurs within the fracture only whilst solute transport occurs both within the fracture and the porous matrix. The solution incorporates solute transport via advection, longitudinal mechanical dispersion and molecular diffusion in the fracture, adsorption

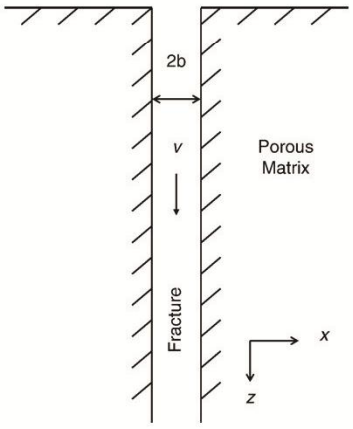

Fig. 1. The fracture–matrix system after Tang et al. (1981) showing fracture aperture ($2b$) and water flow (v).

onto the face of the matrix, diffusion and adsorption within the matrix and radioactive decay. Tang et al. (1981) describe transport in the fracture as:

$$\frac{\partial c}{\partial t}+\frac{v}{R}\frac{\partial c}{\partial z}-\frac{D}{R}\frac{\partial^2 c}{\partial z^2}+\lambda c-\left.\frac{\theta D'}{bR}\frac{\partial c'}{\partial x}\right|_{x=b}=0 \qquad 0 \le z \le \infty \tag{1}$$

where c=solute concentration (M L ^{3}), t=time (T), v=water velocity (L T ^{1}), R=face retardation coefficient, z=spatial coordinate along the fracture (L), D=hydrodynamic dispersion coefficient in the fracture (L^2 T ^{1}), λ=radioactive decay constant (T ^{1}), θ=matrix porosity (–), b=half fracture aperture (L), D'=diffusion coefficient of solute in the matrix (L^2 T ^{1}) and x=spatial coordinate perpendicular to the fracture axis (L). D is defined to be $\alpha v+D^*$ where α=dispersivity and D^*=diffusion coefficient of solute in water and D' is defined as τD^*.

The Laplace transformed solution to the problem as presented by Tang et al. (1981) is:

$$\frac{\mathrm{d}^2\bar{c}}{\mathrm{d}z^2}-\frac{v}{D}\frac{\mathrm{d}\bar{c}}{\mathrm{d}z}-\frac{R}{D}\left\{p+\lambda+\frac{\sqrt{p+\lambda}}{A}\right\}\bar{c}=0 \tag{2}$$

where

$$A=\frac{bR}{\theta\sqrt{R'D'}} \tag{3}$$

and R'=matrix retardation coefficient.

We solved the Tang et al. (1981) expression by numerical Laplace transform inversion using the accurate and robust routine of Piessens and Huysmans (1984). The solution method was verified by reproducing the analytical results presented in Figs. 9 and 10 of Tang et al. (1981) and checking with a series solution for finite length fractures of Robinson and Sharp (1997).

It can be seen from Eq. (2) that for a solute that does not decay or sorb (λ=0, R=1, R'=1) the only parameters affecting the solute concentration in the fracture are v, D and A. These represent the three processes of advection, dispersion and matrix diffusion, respectively. By assuming that hydrodynamic dispersion within the fracture is dominated by the mechanical dispersion component (i.e. $\alpha v >> D^*$) the 6 parameters (v, α, D^*, θ, τ and b) can be reduced to v, α and A, where A is now simplified to $A=b/\theta D'^{1/2}$.

3. Methods

3.1. Forward model

The Tang et al. (1981) analytical solution for solute transport in a single fracture was used to generate breakthrough curves for seven initial parameter sets (see Table 1 for parameter values). Parameters for the base case were chosen to be similar to results presented in the literature. The other six parameter sets were chosen by increasing and decreasing the three variable parameters, v, α and A. In all cases, an input tracer pulse duration of 1 h was used, breakthrough curves were measured at a distance z=10 m along the fracture, retardation constants were set to 1 and radioactive decay was set to zero. The breakthrough curves were defined by 16 equally (temporally) spaced data points over 1 day.

Table 1
Initial parameters used for each of the parameter sets

Parameter set	$2b$ (m)	D' (m^2/day)	θ (–)	α (m)	v (m/day)	z (m)	A ($days^{1/2}$)	β (–)
Base case	10^{-4}	10^{-4}	0.02	1	100	10	0.25	1.26
Low α	10^{-4}	10^{-4}	0.02	0.001	100	10	0.25	40.00
High α	10^{-4}	10^{-4}	0.02	2	100	10	0.25	0.89
Low A	10^{-4}	10^{-4}	0.04	1	100	10	0.125	5.06
High A	10^{-4}	10^{-4}	0.01	1	100	10	0.5	0.32
Low v	10^{-4}	10^{-4}	0.02	1	50	10	0.25	2.53
High v	10^{-4}	10^{-4}	0.02	1	200	10	0.25	0.63

3.2. Adding noise to the breakthrough curve

In order to determine the sensitivity of the breakthrough curves to different hydrogeologic parameters, 100 realisations were generated from each parameter set, each with different added random noise of a specified level (ranging from 5% to 20%) added to each data point. The effect of the applied noise level is examined in this study. By progressively increasing the number of realisations employed, it was found that 100 realisations were more than sufficient to achieve converged average fitted parameters.

We first attempted to understand how such noise might appear in field tracer experiments. Clearly, the interpreted differences between a real breakthrough curve and any mathematical fit (herein after called "noise") are a function of numerous factors including (1) measurement error in instruments, field data collection and subsequent analyses, (2) the choice of conceptual and hence mathematical model used to fit the field data, (3) the inherent complexity (at many spatial and temporal scales) in heterogeneous geologic field settings that is not captured by the mathematical model employed, and (4) the fitting algorithms and convergence criteria used to define when an optimised fit to the data has been obtained. An analysis of typical tracer test results presented by Sanford et al. (2002) reveals an average residual of 19% (with residual mode=2% to 4%) for bromide and 18% (with residual mode=6% to 8%) for helium, where the residual is defined as the absolute value of $(c_{measured}-c_{modelled})/c_{measured}$. In comparing these average and modes, it is clear that the average is somewhat larger owing to a small number of data points which have large associated residuals. This comparison with field data is fairly crude and is based upon one case only. However, it suggests that the level of noise applied in this study is indeed likely in a field-based scenario. It was difficult to determine what distribution these residuals followed due to the limited number of points in the breakthrough curves. This problem is expected to arise in the analysis of most, if not all, previously published breakthrough curves due to the typically limited number of measurement points and a resultant inability to construct the precise statistical distribution of residuals. To the authors best knowledge the nature of such residuals (i.e., discrepancies between measured and modelled data) are rarely, if ever, known and have not been the subject of previous investigation. Therefore, the choice of noise type used in this study (white noise) might be arbitrary, but the aim of this study is intended to be demonstrative rather than absolutely quantitative. Therefore, the key trends and outcomes of the study are expected to be qualitatively similar regardless of the choice of noise distribution employed.

Random numbers were obtained using a random number generator in which each random number had an equal probability of falling anywhere between 0 and 1 (white noise). The level of

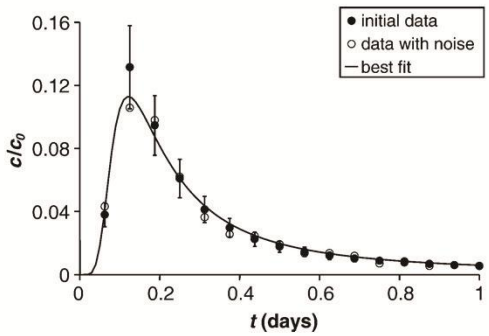

Fig. 2. Initial data for the base case (with 20% error bars) and a realisation of the data with 20% noise added. The best fit to the realisation is shown as the solid line.

noise was specified such that the maximum deviation from the initial data was a chosen percentage of the initial data value itself. This process is illustrated in Fig. 2, where the initial data for the base case is shown as well as a realisation of the data with 20% noise added. The best-fit breakthrough curve for the realisation does not pass directly through the initial data points, but is similar to the initial curve. Adding noise creates a fit that is not the absolute best fit to the initial data, but that still approximates it. Repeating this process creates a range of similar breakthrough curves that approximate the initial data.

It should be noted that the number of data points and the noise applied to them affects the parameter estimation process. As the number of data points increases, the range of fits to the data decreases and the realisations more closely approximate the forward model. Also the higher the noise level, the greater the range of fits to the data.

3.3. Parameter estimation with PEST

PEST (Doherty, 2004) is a model-independent parameter estimation program. PEST finds the parameters that minimise the squared sum of weighted residuals between the target and fitted data values. In our study, equal weighting was assigned to all data values. PEST has a number of ways of determining when it has found optimal parameter values (or done the best it can). The ideal termination criterion is that the objective function (squared sum of weighted residuals) reaches zero. This means that the parameters have been found such that the modelled values exactly match the measured values. This cannot always be achieved, so other termination criteria are required. In our study, if 4 iterations pass since the lowest objective function value, or if the lowest 4 objective function values are within 0.005, relative to the minimum objective function, of each other, PEST stops. Otherwise if 4 iterations pass in which the largest relative parameter value change has been less than or equal to 0.01, PEST terminates execution. As a final criterion for ending execution, PEST will stop after 30 iterations. For further detail on PEST, the reader is referred to Doherty (2004).

During the fitting process, bounds must be placed on the parameters. In order to find a representative range of possible fits to the data, large bounds were placed on the parameters so that they would not interfere with the parameter estimation process, except in cases where parameters must be logically bounded (i.e. α, v, $A \geq 0$).

3.4. Breakthrough curve characteristics

In order to quantify the differences between breakthrough curves, properties that would describe the shape and behaviour of a breakthrough curve were required. Three characteristics were used; time to the first inflection point (t_{i1}), time to the peak concentration (t_p) and the peak concentration (c_p). These three characteristics are the most basic descriptors of a breakthrough curve and can most easily be obtained from tracer test data. Other indicators such as mass recovery may be more difficult to quantify accurately and harder to interpret due to mass losses that result from non-recovered tracer, long breakthrough curve tails resulting from the flow geometry induced by the forced gradient and/or matrix diffusion. Thus, mass recovery, whilst theoretically determinable was not used here due to the complications associated with quantifying it under field conditions.

In order to quantify the spread of parameter values and subsequent predictions of the breakthrough characteristics, the coefficients of variation (CV=standard deviation/mean) of parameter values and predicted characteristics were found for each set of realisations. This enables uniform and consistent comparison of the confidence in different estimated parameters/predictions regardless of their numerical values.

In order to determine the accuracy of predictions based on parameters obtained under a forced gradient (high water velocity), breakthrough curves were generated using parameters from each of the best-fit realisations at several slower groundwater flow velocities. It is assumed here that the hydraulic pressures associated with the different hydraulic gradients have no effect on the fracture apertures or other physical properties of the system other than to change the flow velocity of water in the fracture. Characteristics t_{i1}, t_p and c_p were determined at v_{pr}=1, 0.3, 0.1, 0.03, 0.01, 0.003, 0.001, 0.0003 and 0.0001 where:

$$v_{pr} = \frac{v_{prediction}}{v_{test\ (fitted)}} \tag{4}$$

where $v_{prediction}$=prediction water velocity (L T $^{-1}$) and $v_{test\ (fitted)}$=fitted water velocity under the forced gradient (L T $^{-1}$).

Scaling down to v_{pr}=0.0001 is sufficient to cover the scaling required for most current forced gradient tracer tests. Love et al. (2002) quote hydraulic gradients ranging from 0.005 to 0.1 for a fractured rock catchment. Consider a tracer test conducted between two wells 10 m apart in such a system. In order to require a scaling factor of v_{pr}=0.0001, a head difference of 500 m to 10 000 m between the two wells would need to be imposed. This head difference is unrealistically large and therefore suggests that the range of v_{pr} employed in this study more than adequately covers the range likely to be encountered in realistic field settings.

4. Results

Fig. 3 shows the breakthrough curves for the seven initial parameter sets outlined in Table 1. In fractured rock systems, particularly where the porosity of the matrix is greater than the fracture porosity, solute transport over long time scales is dominated by matrix diffusion. By applying a forced gradient, tracer tests increase the impact of dispersion and are less sensitive to diffusion. In order to assess the predictive capability of parameters obtained under forced conditions it was necessary to cover a range of diffusive to dispersive scenarios under the forced gradient. Lever and Bradbury (1985) quantify the relative

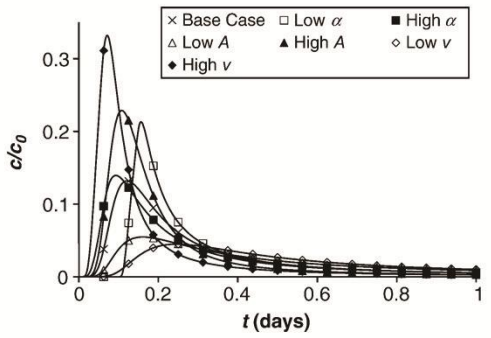

Fig. 3. Initial breakthrough curves for the parameter sets, each consisting of 16 data points over 1 day. Parameter values are given in Table 1.

importance of diffusion and dispersion by the ratio of time scales over which each spreads solute, defined as:

$$\beta = \frac{z^{3/2}}{4A^2 v\sqrt{\alpha}} \tag{5}$$

Values less than 1 indicate that dispersion dominates whilst values greater than one indicate the dominance of diffusion. Whilst the Lever and Bradbury (1985) approach treats diffusion and dispersion as independent processes, in contrast to the coupled solution of Tang et al. (1981), it gives an indication of the relative dominance of the processes. The parameters chosen for this study cover a range of diffusive versus dispersive scenarios, with β ranging from 0.316 to 40, with the base case close to unity at 1.26. A complete set of values for β is presented in Table 1.

4.1. Best-fit parameters

Fig. 4 shows the range in optimised parameter values obtained for the base case with noise levels of 5%, 10%, 15% and 20%. As would be expected, increased noise broadens the range of possible parameter values for α, v and A. For the case of dispersivity, it can be seen that at a 20% noise level one standard deviation (0.472 m) is almost half as large as the average parameter value (1.07 m) itself. The average values for α, v and A remain close to the initial values despite the range of values increasing. However, if sufficient noise was applied, the parameter bounds may be reached (i.e. α, v, $A \geq 0$) causing parameter biasing.

4.2. Predictions

Predictions of solute transport under slower groundwater velocities were made using the same solute source duration and the best-fit parameters for each realisation (with water velocity scaled by v_{pr}). Fig. 5 (a) shows the initial data points for the base case and best-fit breakthrough curves for the first ten realisations with a noise level of 20%. All breakthrough curves could be considered to fit the initial data. The noise bounds are shown to indicate the maximum possible variability for the realisations, all of which lie within this range. Fig. 5 (b), (c), (d) and (e) show the predicted breakthrough curves for the same ten realisations at v_{pr}=0.1, 0.01, 0.001 and

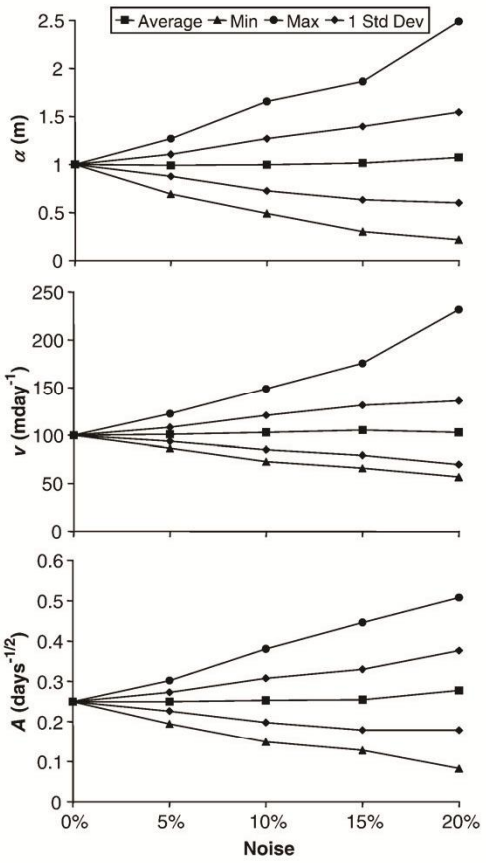

Fig. 4. Best-fit parameters for 100 realisations of the base case with noise of 5%, 10%, 15% and 20% for (a) dispersivity, (b) water velocity and (c) matrix diffusion term. Averages, minimum, maximum and average ± 1 S.D. are shown.

0.0001, respectively. As velocity decreases, solute arrives at later times (increased t_{i1} and t_p) and at lower concentrations (c_p). As would be expected, the breakthrough curves are less similar as the prediction velocity differs more from the test velocity (i.e. v_{pr} gets smaller). However, the rate at which the overall shape of the breakthrough curves differs appears to decrease at low v_{pr}. This observation is confirmed by examination of the predicted breakthrough curve characteristics t_{i1}, t_p and c_p.

Coefficients of variation of predicted values of t_{i1}, t_p and c_p as a function of v_{pr} are presented in Fig. 6. All three characteristics behave in a similar manner. Greater noise increases the uncertainty of all predictions. Also, CV increases as v_{pr} decreases from 100%, but plateaus at lower values of v_{pr}. It should be pointed out that the data is plotted on a log scale and $\partial CV/\partial v_{pr}$ is non-zero, but very small and constant at low v_{pr}. As mentioned earlier, the range of v_{pr} values covered in this study is greater than that which would be used in current practice. The plots cannot be extrapolated back to $v_{pr}=0$ as this is meaningless. The plateauing is explained by the lessening impact of dispersivity on the solution at lower velocity. The behaviour asymptotes towards one in which only v and A have

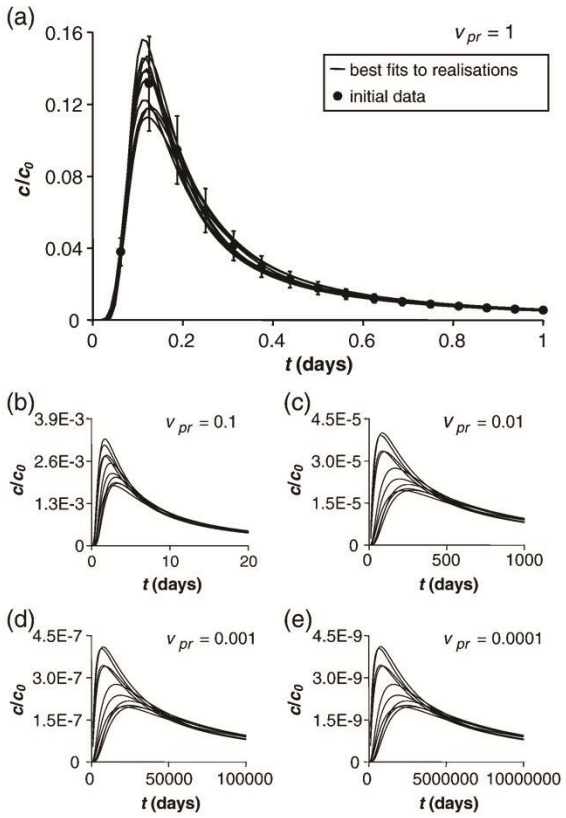

Fig. 5. (a) Initial data points (with 20% error bars) for the base case and the best-fit breakthrough curves for realisations 1–10 (of 100) with 20% noise. Predictions for realisations 1–10 for v_{pr}=(b) 0.1, (c) 0.01, (d) 0.001 and (e) 0.0001.

an impact. For example, in the 20% noise case, the CV values are 44% for α, 32% for v and 36% for A. With the dispersion coefficient dominated by αv, as velocity decreases, so does the dispersion coefficient. In addition, slower water flow allows greater matrix diffusion, increasing the dominance of A on the solution. Overall at lower water velocity (and lower v_{pr}) the solution is governed more by the better constrained parameters (A and v) and less by the poorest defined (α).

In order to demonstrate the range of predicted values around the actual values, Fig. 7 shows the average predicted characteristic values normalised by the actual values with error bounds of ± 1 S.D. The range of predictions is best constrained at the test speed and broadens with decreasing v_{pr}. Minor biasing of average predictions is evident. Both averages and ranges of predictions plateau for lower v_{pr}.

To test whether the results obtained for the base case apply more generally, a further 6 parameter sets were tested using the same procedure used for the base case, but with decreased and increased α, A and v (Table 1). Fig. 8 shows the behaviour of the predicted transport characteristics. As with the base case, breakthrough curve characteristics for all parameter sets display a decrease in certainty with decreasing v_{pr} and then a levelling at the lowest values of v_{pr}.

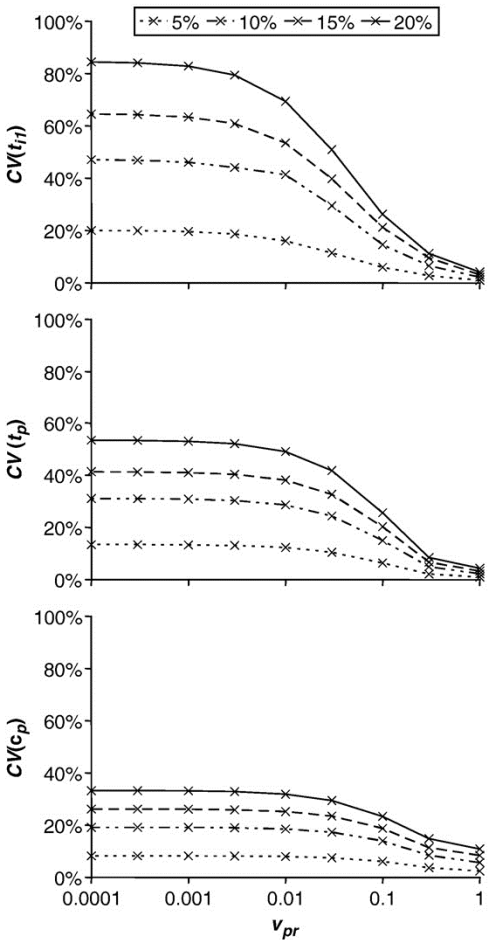

Fig. 6. Base case coefficient of variation of (a) t_{f1}, (b) t_p and (c) c_p as a function of v_{pr} with noise of 5%, 10%, 15% and 20%. After an initially rapid increase CV levels off at low v_{pr} for all characteristics and noise levels.

Each of the parameter sets reaches a different level of uncertainty. It should be pointed out that as v_{pr} is a function of the water velocity at the test speed, identical values of v_{pr} for the altered v cases do not correspond to the same prediction velocities.

The level of uncertainty on the predictions of solute transport under slower velocities depends on the uncertainty in the parameters themselves and on the dominance of the individual parameters at the different prediction velocities. It may be possible to constrain a particular parameter very well at the test speed, but that parameter may have less impact on transport at the prediction speed. The relative contributions of dispersion in the fracture and diffusion in the matrix at the test and prediction velocities and the degree to which they can be identified determine the accuracy of the predictions.

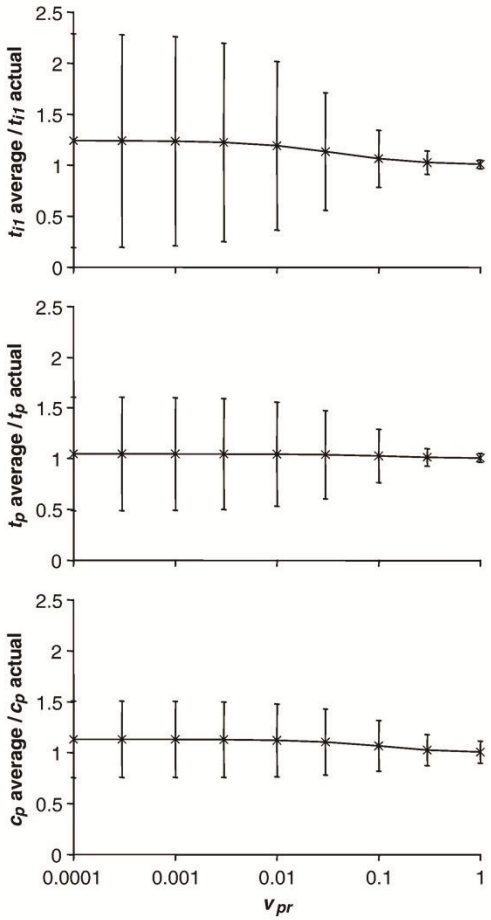

Fig. 7. Base case (noise=20%) average values for (a) t_{i1}, (b) t_p and (c) c_p, normalised by the actual values, as a function of v_{pr}. Therefore 1 represents the correct value for a characteristic. Error bars indicate ±1 S.D. from the average.

4.3. Uncertainty comparison: parameter estimation vs. prediction

Having determined the uncertainty on the parameters and the predicted breakthrough curve characteristics under different flow velocities, we can now compare the two. Fig. 9 shows CV for parameters α, v and A and the predicted breakthrough curve characteristics t_{i1}, t_p and c_p (at $v_{pr}=0.0001$) for all the parameter sets with 20% noise as well as 5%, 10% and 15% noise levels for the base case. For each of the base case scenarios t_{i1} is the least well constrained predicted characteristic and is less constrained than the parameters. t_p is better constrained and almost as well defined as the parameters. c_p is the most constrained predicted characteristic and even better constrained than α and A and almost as constrained as v. Whilst the individual values vary, many of the other parameter sets display better constrained predicted characteristics than estimated parameter values.

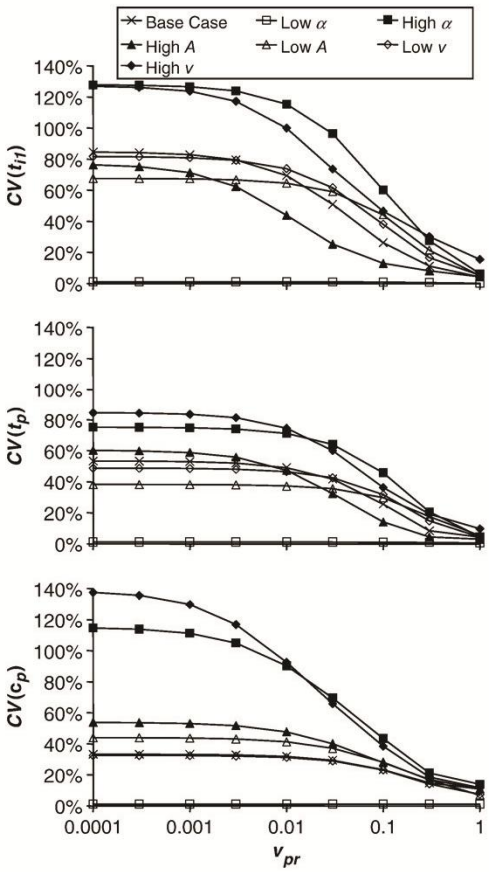

Fig. 8. Coefficient of variation (noise=20%) of (a) t_{i1}, (b) t_p and (c) c_p as a function of v_{pr} for all parameter sets. After an initial increase CV of all characteristics for all parameter sets levels off at low v_{pr}.

In the low A case all three characteristics can be predicted with greater certainty than the individual parameters themselves can be determined. However, in the high A case the opposite is observed. The β parameter used by Lever and Bradbury (1985) can be used to explain this. A comparison of the uncertainty on predicted characteristics relative to parameters with respect to β shows a trend. By counting the number of predicted characteristics that are better constrained than all the corresponding parameters (Fig. 9) we see that the low A case (β=5.06) has 3, the low v case (β=2.53) has 1 but all other scenarios have at least 1 parameter better constrained than the predicted characteristics. According to their β values, the low A and low v scenarios are relatively diffusive. Generally the degree to which the predictions of characteristics can be constrained relative to the parameters seems to be controlled by β. Scenarios with high β values (more diffusive) tend to yield better constrained predictions of characteristics than parameters and scenarios with low β values (more dispersive) yield less constrained predictions of characteristics than parameters. Furthermore, as natural gradient predictions are dominated by diffusion, tests

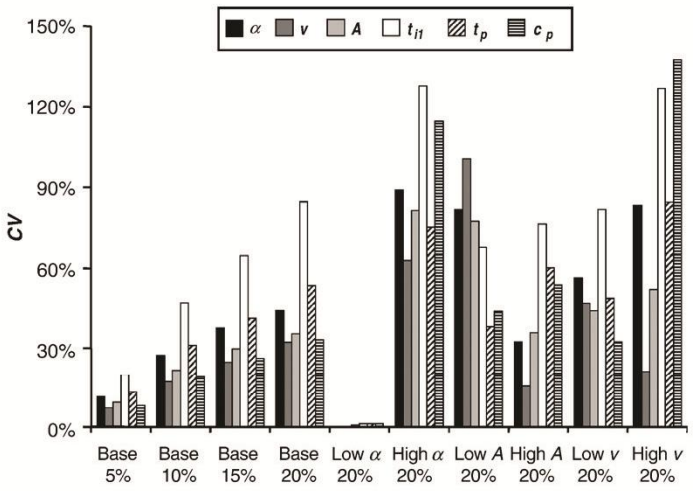

Fig. 9. Coefficient of variation of parameters α, v and A and predictions (at v_{pr}=0.0001) of t_{i1}, t_p and c_p for all parameter sets (noise=20%) and at noise=5%, 10% and 15% for the base case.

conducted under more diffusive conditions will yield greater constrained predictions of breakthrough characteristics. This can be seen in Fig. 8, where the least constrained predictions of characteristics occur for the high α and high v cases.

5. Discussion

This study has demonstrated that by accepting a range of fits to a simulated forced gradient breakthrough curve, not only can bounds be placed on the parameters themselves, but also on predicted solute transport under the natural gradient. Furthermore the uncertainty on the predicted transport characteristics can be lower than that on the individual parameters. This has important implications for our ability to predict solute transport in fractured rock. Essentially, the results suggest that we are able to conduct a tracer test under a forced gradient 4 orders of magnitude larger than the natural gradient and use the results to predict transport under the natural gradient with errors on peak arrival time of typically CV(t_p)=40% to 60%.

Results have shown that tracer tests in which β is large give the best predictions of solute transport under low gradients (where diffusion dominates). In the field, the only parameter in β that can be controlled is v. Therefore as would be expected, the lower the velocity of a test is, the better the predictions of solute transport under the natural gradient will be.

Besides the physical test conditions, a number of factors affect the uncertainty on estimated parameters and subsequent predictions of solute transport. The convergence criteria used in the optimisation process determine the accuracy of the fit to each realisation. The number of data points and the noise level applied to them affect the range of estimated parameters and predictions. Whilst the absolute uncertainties are determined by these choices, we are interested in the relative uncertainties and general trends of parameters and predictions and have shown that they are of a similar magnitude and that in some cases, resultant predictions have less uncertainty than the individual constituent parameters.

This previously unreported behaviour provides positive support for the use of forced gradient tests to predict transport under natural gradient conditions. It was necessary to determine whether this behaviour was real and not a numerical artifact of the solution procedure used in the modelling process. To do this we compare our numerical implementation of the Tang et al. (1981) solution with the zero-dispersivity solution presented by Lever and Bradbury (1985). The dispersivity for the low dispersion case in this study was chosen to be very low to enable comparison with the Lever and Bradbury (1985) analytical solution. The solution for t_p presented in Eq. (5.1) of Lever and Bradbury (1985) is:

$$t_p = \frac{z^2}{6}\left(\frac{1}{A^2v^2}\right) + \frac{z}{v} \tag{6}$$

By applying the formula for variance of a linear function:

$$\mathrm{Var}\left(U = \sum_i a_i P_i\right) = \sum_i a_i^2 \mathrm{Var}(P_i) + \sum_i \sum_{\neq j} a_i a_j \mathrm{Cov}(P_i P_j) \tag{7}$$

letting $a_1P_1 = z^2/6A^2v^2$, $a_2P_2 = z/v$ and assuming z is accurately known, variance of the peak arrival time is:

$$\mathrm{Var}(t_p) = \frac{z^4}{36}\mathrm{Var}\left(\frac{1}{A^2v^2}\right) + z^2\mathrm{Var}\left(\frac{1}{v}\right) + \frac{z^3}{3}\mathrm{Cov}\left(\frac{1}{A^2v^2}, \frac{1}{v}\right) \tag{8}$$

where Var = variance and Cov = covariance.

In the low dispersivity case, a comparison of the actual $\mathrm{Var}(t_p)$ at $v_{pr} = 0.0001$ with that calculated from the variances of the fracture and matrix parameters using Eq. (8) provides a means to check the validity of the CVs generated by the model. To four significant figures, the variances are identical ($\mathrm{Var}(t_p) = 6.109 \times 10^9$ days). Thus, the results of the Tang et al. (1981) and Lever and Bradbury (1985) solutions are in excellent agreement and this provides further evidence in support of not only the Tang et al. (1981) numerical solution employed here but also the findings of this study more generally.

This study is a demonstration of a paradigm. As such, it is limited in that both the initial breakthrough curves and fits were generated using a particular model, the single fracture solution of Tang et al. (1981). However, the philosophy behind this work can be extended to all conceptual models of solute transport in fractured rock systems. Indeed, given that the choice of model itself may be the biggest source of error, multiple models could be incorporated into the process. In a field scenario, tracer may travel in complicated flow geometries through channels in multiple fractures with different properties. Whilst tracer tests are usually analysed using single flow-path models (with various flow geometries incorporated), there has been no definitive study to determine the validity and errors associated with this approach for tracer tests conducted on fracture networks. This should form the subject of future investigations.

6. Conclusions

The key findings of this study are:

1. As the hydraulic gradient decreases, the uncertainty of solute transport predictions does not increase significantly. In particular, this study has shown that a 4 order of

magnitude scaling reduction in v results in no worse than an 85% CV on t_p but that CVs on the order of 40%–60% are typical. This result is not intuitively obvious and is an important finding that has consequences for scaling forced gradient tracer tests in hydrogeology.

2. The uncertainty of solute transport predictions under a natural gradient is typically similar to the uncertainty of the parameters estimated from forced gradient breakthrough curves, and importantly, it is occasionally better. This result suggests that an uncertainty analysis may be more useful than is commonplace in the interpretation of field based tracer tests. Whilst it is typical to only determine the best fit to observed data, these findings suggest that determining the range of acceptable fits is important in understanding the range of both acceptable fitting parameters and hence subsequent predictions of solute transport that are likely.
3. Tracer tests conducted under more diffusive conditions (high β) yield better predictions of solute transport under the natural gradient. In practical terms, v is usually the most easily controllable parameter in β. Therefore, to maximise β to improve predictability necessarily involves conducting tracer tests at the lowest forced gradients that are practically feasible.
4. Therefore, forced gradient applied tracer tests may be a valuable means of estimating solute transport under natural gradients in fractured rock providing that an appropriate choice of interpretational conceptual model is made.

Further work is required to explore how uncertainties on parameter estimation and subsequent predictions at lower velocities are affected by the choice of interpretative conceptual model. This may be a fundamental limitation and clearly warrants further investigation.

Notation and units

A	matrix diffusion term	$T^{1/2}$
b	half fracture aperture	L
c	solute concentration	$M L^{-3}$
c'	solute concentration in the matrix	$M L^{-3}$
Cov	covariance	–
CV	coefficient of variation	–
D	hydrodynamic dispersion coefficient	$L^2 T^{-1}$
D^*	diffusion coefficient of solute in water	$L^2 T^{-1}$
D'	diffusion coefficient of solute in matrix	$L^2 T^{-1}$
R	face retardation coefficient	–
R'	matrix retardation coefficient	–
t	time	T
t_p	peak arrival time	T
v	water velocity	$L T^{-1}$
Var	variance	–
v_{pr}	prediction water velocity / test water velocity	–
$v_{prediction}$	prediction water velocity	$(L T^{-1})$
$v_{test\ (fitted)}$	fitted water velocity under the forced gradient	$(L T^{-1})$
x	spatial coordinate perpendicular to the fracture axis	L
z	spatial coordinate along a fracture	L
α	longitudinal dispersivity	L
β	ratio of diffusive to dispersive time scales	–
θ	matrix porosity	–
λ	radioactive decay constant	T^{-1}
τ	tortuosity	–

Acknowledgements

The authors gratefully acknowledge project funding from Land and Water Australia. Douglas Weatherill thanks the Centre for Groundwater Studies for research stipend support.

References

Abelin, H., Birgersson, L., Moreno, L., Widen, H., Agren, T., Neretnieks, I., 1991. A large-scale flow and tracer experiment in granite: 2. Results and interpretation. Water Resources Research 27 (12), 3119–3135.

Doherty, J., 2004. PEST: Model-Independent Parameter Estimation. Watermark Numerical Computing, Brisbane, Australia.

Jakob, A., Hadermann, J., 1994. INTRAVAL Finnsjon Test – modelling results for some tracer experiments. PSI-Bericht No. 94-12, PSI (Paul Scherrer Institut), Wurenlingen.

Lever, D.A., Bradbury, M.H., 1985. Rock-matrix diffusion and its implications for radionuclide migration. Mineralogical Magazine 49, 245–254.

Love, A.J., Cook, P.G., Harrington, G.A., Simmons, C.T., 2002. Groundwater Flow in the Clare Valley. DWR02.03.0002. Department for Water Resources, Adelaide.

Maloszewski, P., Zuber, A., 1983. Interpretation of artificial and environmental tracers in fissured rocks with a porous matrix. In: Isotope Hydrology: proceedings of an International Symposium on Isotope Hydrology in Water Resources Development, I.A.E.A., Vienna, Austria, pp. 635–651.

Novakowski, K.S., Evans, G.V., Lever, D.A., Raven, K.G., 1985. A field example of measuring hydrodynamic dispersion in a single fracture. Water Resources Research 21 (8), 1165–1174.

Piessens, R., Huysmans, R., 1984. Algorithm 619. Automatic numerical inversion of the Laplace transform. Association of Computer Machinery Transactions on Mathematical Software 10, 348–353.

Robinson, N.I., Sharp, J.M., 1997. Analytical solution for solute transport in a finite set of parallel fractures with matrix diffusion. CMIS C23/97. CSIRO, Adelaide.

Sanford, W.E., Cook, P.G., Dighton, J.C., 2002. Analysis of a vertical dipole tracer test in highly fractured rock. Ground Water 40 (5), 535–542.

Tang, D.H., Frind, E.O., Sudicky, E.A., 1981. Contaminant transport in fractured porous media: analytical solution for a single fracture. Water Resources Research 17 (3), 555–564.

ground water

Discretizing the Fracture-Matrix Interface to Simulate Solute Transport

by Douglas Weatherill[1], Thomas Graf[2,3], Craig T. Simmons[4], Peter G. Cook[5], Rene Therrien[6], and David A. Reynolds[7]

Abstract

This article examines the required spatial discretization perpendicular to the fracture-matrix interface (FMI) for numerical simulation of solute transport in discretely fractured porous media. The discrete-fracture, finite-element model HydroGeoSphere (Therrien et al. 2005) and a discrete-fracture implementation of MT3DMS (Zheng 1990) were used to model solute transport in a single fracture, and the results were compared to the analytical solution of Tang et al. (1981). To match analytical results on the relatively short timescales simulated in this study, very fine grid spacing perpendicular to the FMI of the scale of the fracture aperture is necessary if advection and/or dispersion in the fracture is high compared to diffusion in the matrix. The requirement of such extremely fine spatial discretization has not been previously reported in the literature. In cases of high matrix diffusion, matching the analytical results is achieved with larger grid spacing at the FMI. Cases where matrix diffusion is lower can employ a larger grid multiplier moving away from the FMI. The very fine spatial discretization identified in this study for cases of low matrix diffusion may limit the applicability of numerical discrete-fracture models in such cases.

Introduction

Recent computational and theoretical advances have allowed the development of numerical codes for simulating solute transport in fractured rock. A range of models have been suggested that encompass differing complexity in fracture geometry and the interaction of solutes between fractures and the rock matrix. In a review article, Neuman (2005) summarized a range of conceptual models for flow and transport in fractured rock. Diodato (1994) presented a compendium of the available numerical models for flow in fractured media. Equivalent porous media (EPM) and multiple-continuum approaches allow solutions that are relatively rapid computationally but are not always suitable on smaller spatial and temporal scales due to the conceptual simplifications they employ. Neuman (2005) stated that a single continuum model of flow and transport in fractured rock is usually inadequate. Discrete-fracture models, while more demanding computationally, allow simulation of complex fracture networks where the interaction between fractures and the matrix cannot be simplified to an EPM multiple-continuum approach. A range of discrete-fracture models exists, incorporating a variety of physical and chemical processes. While current computing capabilities can limit the application of such models to small-scale simulations, they are of benefit in studying system processes and phenomena that occur on the smaller scale. Examples of discrete-fracture models capable of simulating solute transport include FRACTRAN (Sudicky and McLaren

[1]Corresponding author: School of Chemistry, Physics and Earth Sciences, Flinders University, GPO Box 2100, Adelaide, South Australia 5001, Australia; 61-8-82012724; fax 61-8-82012905; douglas.weatherill@flinders.edu.au

[2]Département de Géologie et Génie Géologique, Université Laval, Quebec, Canada G1K 7P4; thomas.graf@geo.uni-goettingen.de and thomas.graf.1@ulaval.ca

[3]Currently at Centre of Geosciences, Goldschmidtstrasse 3, Georg-August-University Göttingen, 37077 Göttingen, Germany.

[4]School of Chemistry, Physics and Earth Sciences, Flinders University, South Australia, Australia; craig.simmons@flinders.edu.au

[5]CSIRO Land and Water, Private Bag 2, Glen Osmond, South Australia 5064, Australia; peter.g.cook@csiro.au

[6]Département de Géologie et Génie Géologique, Université Laval, Quebec, Canada; rene.therrien@ggl.ulaval.ca

[7]School of Environmental Systems Engineering, University of Western Australia, M015, 35 Stirling Highway, Crawley, Western Australia 6009, Australia; david.reynolds@uwa.edu.au

Received June 2007, accepted December 2007.

doi: 10.1111/j.1745-6584.2007.00430.x

1998), HydroGeoSphere (Therrien et al. 2005), MAGNUM-2D (England et al. 1986), MOTIF (Chan et al. 1999a, 1999b), PORFLOW (Runchal 2002), SWIFT (HSI-GeoTrans 2000), and TRACR3D (Travis and Birdsell 1991). Examples of numerical simulations of solute transport in discretely fractured porous media with matrix diffusion are found in Grisak and Pickens (1980), Sudicky and McLaren (1992), Therrien and Sudicky (1996), VanderKwaak and Sudicky (1996), Reynolds and Kueper (2002), and Graf and Therrien (2005).

Solute transport in fractured rock is typically characterized by rapid advection within the fractures and minimal advection in the matrix. Much slower solute transport can occur by diffusion into porous matrix material, thereby complicating the simulation of mass transport by introducing an additional timescale. Slough et al. (1999) found that longitudinal grid discretization of fracture elements, particularly at fracture intersections, can have a significant impact on simulated DNAPL transport paths and rates in fracture networks. Additionally, when matrix diffusion is modeled, grid discretization in the matrix must be fine to correctly simulate the high-concentration gradients that develop between fractures and the matrix (Sudicky and McLaren 1992). Previous numerical studies have matched analytical solutions for solute transport in fractured rock, despite using grid spacing at the fracture-matrix interface (FMI) that is much larger than the fracture aperture. For example, Sudicky and McLaren (1992) used a grid spacing of 25 mm perpendicular to fractures of aperture 0.1 mm when matching the analytical solution of Sudicky and Frind (1982), equating to elements 250 times the size of the fracture aperture. Cook et al. (2005) matched chlorofluorocarbon-12 (CFC-12) concentrations modeled with the analytical solution of Sudicky and Frind (1982) in a 0.1-mm fracture using a grid spacing of 25 mm (250 times the fracture aperture). In contrast, Reynolds and Kueper (2002) used a much finer discretization of 100 μm when modeling DNAPL migration in fractures of apertures from 15 to 50 μm (two to seven times the fracture aperture). To date, there has been no systematic study of the spatial discretization required for accurate simulation of solute transport in fractured rock as a function of the parameter values employed in the model domain, in particular the relative strength of longitudinal advection and dispersion in the fracture to transverse diffusion in the matrix.

This study compares concentrations simulated with the discrete-fracture model HydroGeoSphere (Therrien et al. 2005) and a discrete-fracture implementation of MT3DMS (Zheng 1990) to those computed with the analytical solution of Tang et al. (1981) for transport in a single fracture embedded in a porous rock matrix. Two aspects of spatial discretization were investigated: (1) the discretization of the elements closest to the fracture (Δx_{min}) and (2) the grid multiplier perpendicular to the fracture (m_x). The work of Sudicky and McLaren (1992) and Cook et al. (2005) focused on scenarios where diffusion is higher than that in this study and demonstrated that over long simulation times, relatively coarse discretization is adequate when advection and mechanical dispersion within the fracture are small compared to diffusion in the adjacent matrix. In contrast, this study examines a scenario with relatively fast fluid flow in the fracture that reduces potential for matrix diffusion. Such conditions can occur when simulating transport on a small spatiotemporal scale and/or under high hydraulic gradients such as those encountered in some tracer tests. Quantitative relationships are developed between β (a ratio of the timescales for dispersion and advection in the fracture to diffusion in the matrix) and Δx_{min} and m_x to guide discretization principles. This study demonstrates that when both fracture and matrix domains are modeled with a discrete-fracture model, not only do spatial grids have to be fine at the FMI, but in cases of low matrix diffusion, they need to be on the scale of the fracture aperture to accurately simulate solute transport, not only within the matrix but also within the fracture. Even where matrix diffusion is deemed to be physically unimportant over relevant timescales, inappropriate discretization will lead to an overprediction of matrix diffusion and subsequently to an underestimation of advective/dispersive transport within the fracture. This required level of spatial discretization has not been previously reported in the literature. Another result reported here is that dispersive scenarios can employ a larger grid multiplier moving away from the FMI than diffusive scenarios.

Analytical Modeling

The geometry of the analytical solution presented by Tang et al. (1981) is outlined in Figure 1. Fluid flow occurs within the fracture only while solute transport occurs both within the fracture and the porous matrix. The

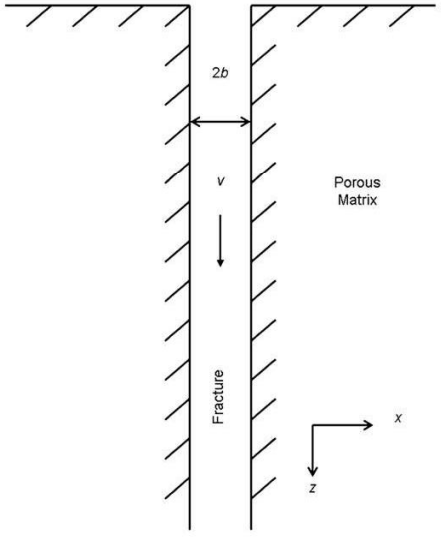

Figure 1. The fracture-matrix system of the model of Tang et al. (1981) showing fracture aperture (2*b*) and water flow (*v*).

solution incorporates solute transport via advection, longitudinal mechanical dispersion and molecular diffusion in the fracture, adsorption onto the face of the matrix, diffusion and adsorption within the matrix, and radioactive decay. Tang et al. (1981) described transport in the fracture as:

$$\frac{\partial c}{\partial t} + \frac{v}{R}\frac{\partial c}{\partial z} - \frac{D}{R}\frac{\partial^2 c}{\partial z^2} + \lambda c - \frac{\theta D'}{bR}\frac{\partial c'}{\partial x}\bigg|_{x=b} = 0 \qquad 0 \le z \le \infty, \quad (1a)$$

and transport in the matrix as:

$$\frac{\partial c'}{\partial t} - \frac{D'}{R'}\frac{\partial^2 c'}{\partial x^2} + \lambda c' = 0 \qquad b \le x \le \infty, \quad (1b)$$

where b = half fracture aperture (L), c = fracture solute concentration (ML $^{-3}$), c' = matrix solute concentration (ML $^{-3}$), D = hydrodynamic dispersion coefficient (L^{2}T $^{-1}$), D' = diffusion coefficient of solute in the matrix (L^{2}T $^{-1}$), R = face retardation coefficient (–), R' = matrix retardation coefficient (–), t = time (T), v = water velocity (LT $^{-1}$), x = spatial coordinate perpendicular to the fracture axis (L), z = spatial coordinate along the fracture (L), θ = matrix porosity (–), and λ = radioactive decay constant (T $^{-1}$). D is defined to be $\alpha v + D^*$, where α = dispersivity (L) and D^* = diffusion coefficient of solute in water (L^{2}T $^{-1}$), and D' is defined as τD^*, where τ = tortuosity (–).

The Laplace-transformed solution to the problem as presented by Tang et al. (1981) is:

$$\frac{d^2\bar{c}}{dz^2} - \frac{v}{D}\frac{d\bar{c}}{dz} - \frac{R}{D}\left\{p + \lambda + \sqrt{\frac{p+\lambda}{A}}\right\}\bar{c} = 0, \quad (2)$$

where

$$A = \frac{bR}{\theta\sqrt{R'D'}}, \quad (3)$$

and $\bar{c}$ = solute concentration in the Laplace space (TML $^{-3}$) and p = Laplace space variable (T $^{-1}$).

We solved the analytical expression for concentration by numerical Laplace transform inversion using the accurate and robust routine of Piessens and Huysmans (1984). The solution method was verified by reproducing the analytical results presented in figures 9 and 10 of Tang et al. (1981) and checking with a series solution for finite-length fractures (Robinson and Sharp 1997).

Numerical Modeling

The discrete-fracture fluid flow and solute transport model HydroGeoSphere (Therrien et al. 2005) was used to simulate solute transport in the fracture-matrix system presented by Tang et al. (1981). The control volume finite-element (CVFE) method was used to discretize both the flow and the transport equations with full upstream weighting of advective flux terms. The discretized equations are solved using the WATSIT iterative solver package of general sparse matrices (Clift et al. 1996) and a conjugate gradient stabilized (CGSTAB) acceleration technique (Rausch et al. 2005). HydroGeoSphere represents discrete fractures with two-dimensional (2D) planes of connected nodes that already form part of the three-dimensional (3D) grid for the porous medium. The fracture and matrix domains are thus coupled by their colocation and by requiring that their corresponding hydraulic heads and concentrations be equal.

The discretized solute transport equations used by HydroGeoSphere can be simplified for a nonsorbing, nondecaying, nonreactive solute in fully saturated media. For the porous medium:

$$\left[(\theta c)_i^{L+1} - (\theta c)_i^L\right]\frac{V_i}{\Delta t} = \varepsilon\left(\sum_{j\in\eta_i} c_{(ij+1/2)}^{L+1}\gamma_{ij}\left(h_j^{L+1} - h_i^{L+1}\right) + \sum_{j\in\eta_i}\chi_{ij}\left(c_j^{L+1} - c_i^{L+1}\right)\right) + (1-\varepsilon)\left(\sum_{j\in\eta_i} c_{(ij+1/2)}^{L+1}\gamma_{ij} \times \left(h_j^{L+1} - h_i^{L+1}\right) + \sum_{j\in\eta_i}\chi_{ij}\left(c_j^L - c_i^L\right)\right) + \Omega_{ex}^{L+1}V_i, \quad (4)$$

and for fractures:

$$\left[c_{fi}^{L+1} - c_{fi}^L\right]\frac{2ba_i}{\Delta t} = \varepsilon\left(2b\sum_{j\in\eta_{fi}} c_{f(ij+1/2)}^{L+1}\gamma_{fij}\left(h_{fj}^{L+1} - h_{fi}^{L+1}\right) + \sum_{j\in\eta_{fi}}\chi_{fij}\left(c_{fj}^{L+1} - c_{fi}^{L+1}\right)\right) + (1-\varepsilon)\left(2b\sum_{j\in\eta_{fi}} c_{f(ij+1/2)}^{L}\gamma_{fij} \times \left(h_{fj}^{L+1} - h_{fi}^{L+1}\right) + \sum_{j\in\eta_{fi}}\chi_{fij}\left(c_{fj}^L - c_{fi}^L\right)\right) + \Omega_f^{L+1}a_i, \quad (5)$$

where a_i = area associated with fracture node i (L^2), h = hydraulic head (L), V_i = region or control volume associated with porous medium node i (L^3), γ_{ij} = term arising from discretization and describing fluid flow between i and j (L^{2}T $^{-1}$), η_i = the set of nodes connected to node i, χ_{ij} = term arising from discretization and describing diffusive/dispersive solute flux between i and j (L^{3}T $^{-1}$), Ω = solute exchange rate between fracture and porous medium domains (T $^{-1}$), and ε = finite-difference time weighting factor (–). Subscript f denotes a fracture property; subscripts i and j denote a property of node i or j, respectively; and superscript L denotes the time level, with $L + 1$ corresponding to the time level for which the solution is sought.

The first term on the right-hand side (RHS) of Equations 4 and 5 describes solute transport due to advection. The second term on the RHS describes the flux that results from dispersive and diffusive processes. The last term incorporates mass exchange fluxes between porous medium and fracture domains due to the requirement for

their concentrations at common nodes to be equal. In Equations 4 and 5, the concentration terms $c_{(ij+1/2)}$ and $c_{f(ij+1/2)}$ depend on the type of spatial weighting used for the advective term between nodes i and j. For example, $c_{(ij+1/2)}$ and $c_{f(ij+1/2)}$ are equal to the average concentration between nodes i and j for the central weighting scheme. Prior to solving the transport equations, HydroGeoSphere first solves the fluid flow equation for the two domains, and simulation errors that result from inadequate spatial discretization of the FMI are generated in the second term of the RHS. When simulating solute transport in a coupled system where transport rates have the potential to vary by orders of magnitude between the two domains (fracture and matrix), it is obvious that inadequate discretization in the matrix could lead to simulation errors in the fractures.

Figure 2 illustrates the model domain used to simulate the fracture-matrix system. A finite-element grid was used to discretize the model domain measuring $X = 0.1$ m, $Y = 0.2$ m, and $Z = 2$ m. A single fracture of aperture $2b = 1.2 \times 10^{-4}$ m was located at $x = 0$. No flow (or solute flux) boundary conditions were imposed on all boundaries, except the upper and lower faces ($z = 0$ and 2 m) where specified heads were applied such that the flow rate in the fracture was 0.75 m/d. A specified concentration of 1 was applied to the fracture nodes at $z = 0$ m. A regular grid spacing of $\Delta z = 0.01$ m was used parallel to flow in the fracture, and two 0.1 m elements were used in the y dimension (although the problem is essentially 2D). In the x dimension, perpendicular to the FMI, symmetrical variable grid spacing was used such that:

$$\Delta x = m_x^{(n-1)} \Delta x_{min}, \tag{6}$$

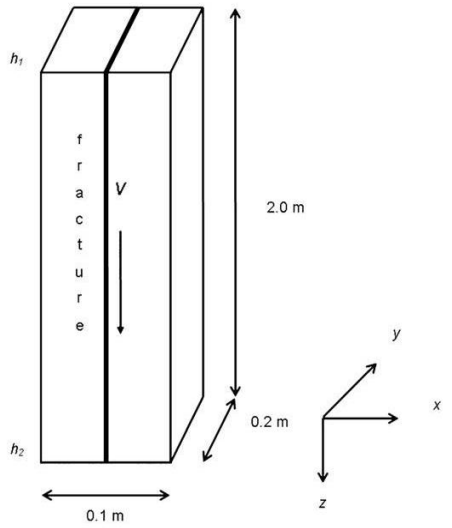

Figure 2. Geometry of the numerical model.

where Δx = grid spacing in the x direction (L), m_x = grid spacing multiplier in the x direction (–), n = integer element counter where element number 1 borders the fracture center (–), and $\Delta x_{\min}$ = the minimum element size occurring at $n = 1$ (L).

Spatial discretization is often conducted in accordance with the grid Peclet number:

$$\mathrm{Pe}_g = \frac{|v|\Delta z}{D' + \alpha|v|}. \tag{7}$$

As diffusion is typically much smaller than mechanical dispersion ($D' << \alpha\,|v|$), Pe_g can be simplified to $\Delta z/\alpha$. Depending on the numerical scheme used, the necessary Peclet criterion will vary. However, for numerical stability, it is usually recommended that Pe_g be less than around 4 (Anderson and Woessner 1992) up to as high as 10 (Huyakorn and Pinder 1983) when central weighting of the advective term is used, which is the case for the simulations presented here. For the chosen grid, Pe_g is 0.0132 along the fracture. Because flow occurs only in the z direction, Pe_g is not applicable for the other dimensions.

Temporal discretization was conducted using HydroGeoSphere's variable time-stepping procedure with a Crank-Nicolson implicit finite-difference scheme in time, with $\varepsilon = 0.5$ in Equations 4 and 5. Once a solution at time L is found, the next time step is determined by:

$$\Delta t^{L+1} = \frac{c_{\max}}{\max|c_i^{L+1} - c_i^L|} \Delta t^L, \tag{8}$$

where $c_{\max}$ = specified maximum change in concentration desired in a time step and c_i = calculated concentration at node i. This procedure allows the model to increase time steps when there are only small changes in concentration and similarly reduce them when rapid changes occur. Thus, computation time is reduced without decreasing numerical accuracy. This study used a very small initial time step of 0.01 s and a target concentration change per time step of $c_{\max} = 0.01$. A maximum time step of 1000 s and maximum time step multiplier of 2 were imposed. Model output was generated every 0.4 d for a total duration of 4 d.

To provide a check on the performance and accuracy of HydroGeoSphere, the solute transport model MT3DMS (Zheng 1990) was also used to simulate the system depicted in Figure 2. The linked combination of MT3DMS and the USGS flow code MODFLOW is one of the most commonly used and widely accepted approaches for modeling flow and solute transport in the subsurface. In the majority of cases, this combination of models is used to simulate flow and transport in fractured media using the EPM approach; however, it is fully capable of simulating a discrete-fracture formulation at very fine grid spacings. The problem was solved using a third-order accurate total variation diminishing (TVD) scheme. An identical model domain was used for the MT3DMS simulations. Discretization in the y and z directions was identical to that used in HydroGeoSphere. Discretization perpendicular to the fracture was slightly different because MT3DMS uses a block-centered grid rather than

Table 1
Parameter and Base Grid Specifications for HydroGeoSphere

$2b$ (m)	0.00012
D' (cm^2/s)	10^{-6} to 10^{-10} and 0
v (m/d)	0.75
α (m)	0.76
θ (–)	0.35
Δh (m)	0.001658219
z (m)	0.76
t (d)	4.0
X (m)	0.1
Y (m)	0.2
Z (m)	2.0
Δx_{min} (m)	0.00012
Δy (m)	0.1
Δz (m)	0.01
m_x (–)	2

Note: Δh is measured across the entire model length Z, not the distance over which transport is measured, z.

point-centered grid. In all cases, elements of width $2b = 1.2 \times 10^{-4}$ m and 100% porosity were used for the fracture. The minimum discretization in the matrix (Δx_{min}) was varied and a grid multiplier of 1.5 used. An initial time step of 0.001 s and a time step multiplier of 1.1 were used with a maximum time step of 100 s.

Model parameters for HydroGeoSphere and MT3DMS simulations were chosen to match those used by Tang et al. (1981), who in turn successfully replicated the earlier numerical results of Grisak and Pickens (1980). Those were $2b = 1.2 \times 10^{-4}$ m; $D' = 10^{-6}$, 10^{-7}, 10^{-8}, 10^{-9}, 10^{-10}, and 0 cm^2/s; $v = 0.75$ m/d; $\alpha = 0.76$ m; and $\theta = 0.35$. The range of diffusion coefficients covers typical values for free diffusion in water (10^{-6} cm^2/s) through to diffusion in tortuous rock (10^{-11} cm^2/s). In addition, a matrix hydraulic conductivity of 10^{-50} m/s was used to ensure that water flow in the matrix was negligible. Model parameters, grid, and time-stepping specifications are summarized in Table 1. Grids employing different spatial discretization were used to model the problem of Tang et al. (1981). Unless otherwise stated, $\Delta x_{min} = 2b = 1.2 \times 10^{-4}$ m and $m_x = 2$.

Results

HydroGeoSphere results are now presented for a range of grid discretizations. They are compared with results obtained using the commonly used MT3DMS model.

Figure 3 illustrates the effect of spatial discretization perpendicular to the FMI (Δx_{min}). Concentration contours of 0.2, 0.4, 0.6, and 0.8 are shown after 4 d for a solute with a high matrix diffusion coefficient of 10^{-8} cm^2/s. The elements closest to the fracture were of size $\Delta x_{min} =$ (a) $200b$, (b) $20b$, and (c) $2b$. In most ground water models, even the coarsest grid in case (a) would be considered extremely fine. The results shown in case (c) were found

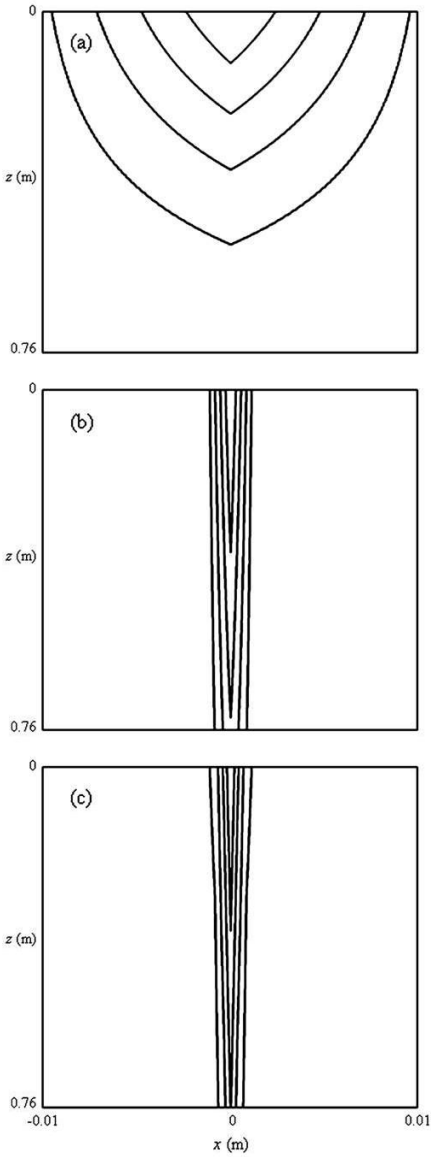

Figure 3. Concentration contours (0.2, 0.4, 0.6, and 0.8) after 4 d for $D' = 10^{-8}$ cm^2/s, with Δx_{min} = (a) $200b$, (b) $20b$, and (c) $2b$ where $2b$ = 120 µm.

to match the analytical solution, while the larger elements used in cases (a) and (b) are clearly not fine enough to correctly model the system.

Figure 4 compares the analytical solution of Tang et al. (1981) with corresponding numerical results both (1)

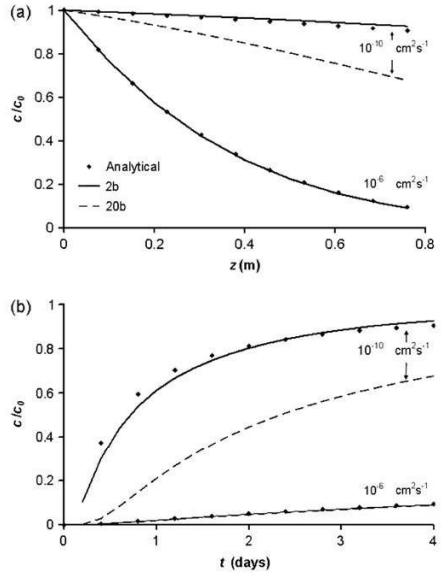

Figure 4. Comparison of HydroGeoSphere concentrations for $\Delta x_{min} = 20b$ and $2b$ with the analytical solution for $D' = 10^{-10}$ and 10^{-6} cm²/s: (a) along the fracture at $t = 4$ d and (b) with time at $z = 0.76$ m.

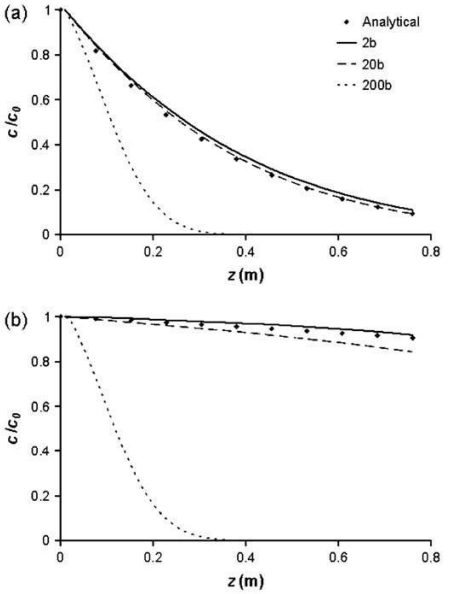

Figure 5. Comparison of MT3DMS results with the analytical solution for concentration along the fracture at $t = 4$ d: (a) $D' = 10^{-6}$ cm²/s and (b) 10^{-10} cm²/s.

along the fracture and (2) in time when using $\Delta x_{min} = 20b$ and $2b$. Results for the finer grid ($\Delta x_{min} = 2b$) are close to the analytical solution for both $D' = 10^{-10}$ and 10^{-6} cm²/s. The coarser grid ($\Delta x_{min} = 20b$) is able to reproduce the analytical solution for $D' = 10^{-6}$ cm²/s but is clearly unable to match the analytical solution of the less diffusive scenario where $D' = 10^{-10}$ cm²/s.

A sensitivity analysis was conducted to assess whether the numerical schemes chosen for the simulations had contributed to the requirement for such fine discretization at the FMI. All possible combinations of CVFE/Galerkin finite element/finite-difference discretization techniques with upstream/central/downstream advective weighting and central (Crank-Nicolson)/fully implicit time weighting were tested in HydroGeoSphere. Simulations were run for $D' = 10^{-10}$ cm²/s, with $\Delta x_{min} = 2b$ and $20b$ and concentrations compared after 4 d at $z = 0.76$ m. In results not shown here, all numerical combinations produced good results when $\Delta x_{min} = 2b$, falling within 2% of the analytical solution and 0.052% of each other. All combinations produced very poor results when $\Delta x_{min} = 20b$, falling 25% from the analytical solution but within 0.17% of each other. Therefore, it is apparent that regardless of the numerical methods used to calculate the solution in HydroGeoSphere, a very fine grid is required at the FMI to match the analytical solution under the physical conditions simulated in the model.

MT3DMS results presented in Figure 5 confirm that the HydroGeoSphere results are not a code-specific phenomenon. It is immediately obvious that both models require extremely fine discretization to match analytical results for low-diffusion coefficients but that less strict discretization requirements can be tolerated for a higher diffusion coefficient. It is also of interest to note the performance of MT3DMS when the element size immediately adjacent to the fracture is $200b$, which is still a fine grid compared to that used for most field-scale simulations. The predicted migration of the solute through the fracture is severely underestimated, in particular for the case with lower diffusion ($D' = 10^{-10}$ cm²/s). Erroneously, the value of the diffusion coefficient itself has little effect on the model prediction, further emphasizing the importance of fine grid discretization in discrete-fracture modeling. Given the results for the range of numerical schemes tested in HydroGeoSphere, plus the TVD scheme used in MT3DMS, it appears that the requirement for fine gridding at the FMI under conditions of low diffusion is neither a phenomenon of the codes nor the numerical schemes used in them.

Figure 6 shows simulated concentrations normalized by their corresponding analytical values as a function of $\Delta x_{min}/2b$. It is readily apparent that highly diffusive cases are able to achieve better agreement between numerical and analytical solutions for larger element sizes, but that for low-diffusivity cases, $\Delta x_{min}/2b \approx 1$ is required for a match. All cases converge once $\Delta x_{min}/2b$ reduces to 1 ($\Delta x_{min} = 2b$), but the converged values of $c_{modeled}/c_{Tang}$ are not all exactly 1. This could be due to the approximation made in the analytical model that diffusion occurs

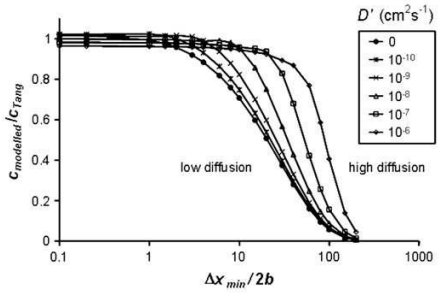

Figure 6. Ratio of modeled to analytical solute concentration (t = 4 d, z = 0.76 m) in the fracture as a function of $\Delta x_{min}/2b$.

only perpendicular to the FMI. In reality, diffusion creates arrowhead-like concentration contours that are inherently 2D in nature, as shown in Figure 3. Such a concentration distribution creates concentration gradients that are not perpendicular to the fracture wall as is assumed in the analytical approach used by Tang et al. (1981). Thus, minor discrepancies should be expected, especially for large diffusion coefficients.

It is apparent that the ability to match the analytical solution with coarser grids is strongly dependent on the magnitude of matrix diffusion. Highly diffusive cases are easily matched with coarser grids. However, as the magnitude of diffusion is reduced, the discretization at the FMI necessarily becomes finer. Previously mentioned studies have matched analytical solutions for solute transport in fractured rock without requiring the very fine discretization identified in this study. Thus, it is useful to examine the quantitative disparity between numerical and analytical results as a function of the relative importance of matrix diffusion as a means of solute transport. Lever and Bradbury (1985) defined the ratio of matrix diffusion to mechanical dispersion in the fracture by their associated timescales:

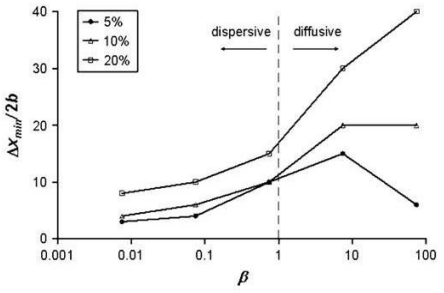

Figure 7. $\Delta x_{min}/2b$ required to reach 5, 10, and 20% accuracy relative to the analytical solution (t = 4 d, z = 0.76 m) as a function of β.

$$\beta = \frac{z^{3/2}}{4A^2\nu\sqrt{\alpha}}. \quad (9)$$

A β value greater than 1 indicates a diffusive scenario, whereas a value less than 1 indicates a dispersive scenario. It should be noted that β is not an exact measure of the transport mode in a fracture-matrix system because it assumes matrix diffusion and mechanical dispersion as independent processes. However, it is very useful as an indicator of the relative strength of these two processes. Results for this study were obtained by altering A only while α, v, and z were held constant. Figure 7 shows the maximum $\Delta x_{min}/2b$ required to simulate concentrations with an accuracy of 5, 10, and 20% relative to the analytical solution as a function of β. Simulations were run at discrete values of Δx_{min}, and as such the critical values are not exact. Clearly, scenarios where matrix diffusion is more significant (points on the right of this graph) can tolerate coarser discretization. This is easily explained by the way a finite-element model simulates reality. The concentration gradient is calculated as the difference in concentration between one node and the next divided by the distance between them. Any resultant transport occurs directly into the node downgradient. In the case of the fracture-matrix system simulated here, a gradient exists from the fracture into the matrix. Thus, a solute flux occurs from the common node in the fracture to the closest node that is purely a porous media node. If this node is located farther into the matrix than the length scale associated with real matrix diffusion in a given time step, the model will overestimate matrix diffusion. Since solute penetrates farther into the matrix in more diffusive scenarios, these cases are less sensitive to the grid discretization at the FMI, allowing the use of larger elements. Additionally, it can be inferred that scenarios with higher v or α will require finer discretization because transport along the fracture is more rapid, reducing solute contact time with the matrix. Reduced contact time results in a smaller length for diffusion into the matrix, and subsequently finer discretization is required in that direction to ensure that solute is not spread to a distance greater into the matrix than it should be. For a given set of physical parameters, both the timescale of the model and the time steps used will also impact the discretization requirements. Because the necessary discretization at the FMI is related to the length scale for diffusion over a time step, simulations that use longer time steps will be able to use larger nodal spacings. Additionally, results generated after longer periods of simulation may be accurate even if early time results are not because solute diffuses further into the matrix as time progresses.

In Figure 7, the point farthest to the right on the 5% accuracy plot (corresponding to $D' = 10^{-6}$ cm^2/s) requires finer discretization than the less diffusive scenario to its left. Figure 6 shows that the $D' = 10^{-6}$ cm^2/s does not plateau at the analytical value. As mentioned previously, this may be due to the approximation in the analytical solution of a diffusion gradient exactly perpendicular to the FMI. The $D' = 10^{-6}$ cm^2/s scenario is the

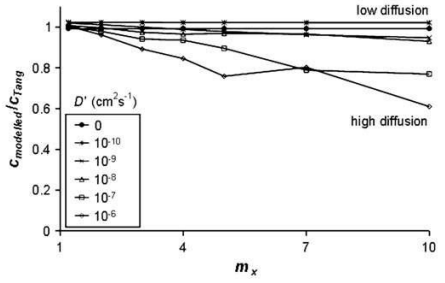

Figure 8. Ratio of modeled to analytical solute concentration (t = 4 d, z = 0.76 m) in the fracture as a function of m_x, where $\Delta x_{min} = 2b = 1.2 \times 10^{-4}$ m.

most diffusive case tested and thus differs most from this approximation.

We now consider the rate at which element size can increase into the matrix (m_x). Given the very fine discretization required for the elements immediately adjacent to the fracture, it is desirable that elements can rapidly increase away from the fracture to save CPU time and memory. Figure 8 shows the effect of the grid spacing multiplier, m_x, on simulated concentrations normalized by their analytical values. Increasing m_x leads to reduced simulated concentrations for $D' = 10^{-6}$ and 10^{-7} cm^2/s but has little effect on scenarios where diffusion is smaller even up to a large value of $m_x = 10$. This is because in less diffusive scenarios, solutes do not reach very far into the matrix during the 4 d simulation, making fine grid discretization away from the fracture unnecessary. Therefore, while scenarios with low diffusion require very fine elements near the fracture, they can tolerate a very large grid multiplier and thus fewer elements in the matrix. However, it should be noted that (for any given time step size) to simulate transport over longer times when solute penetrates farther into the matrix, such large increases in grid spacing may not be acceptable.

In summary, as expected, both the discretization at the FMI (Δx_{min}) and the grid multiplier perpendicular to the FMI (m_x) affect simulation of solute transport in fractured rock. For the relatively short durations simulated in this study, low-diffusion scenarios require very fine elements near the fracture (Δx_{min}) but can tolerate a very large grid multiplier (m_x) and thus fewer elements within the matrix. On the other hand, high-diffusion scenarios can be simulated with bigger elements near the fracture (Δx_{min}) but with more matrix elements (m_x). These discretization requirements are summarized in Table 2.

Table 2
Summary of Grid Requirements Δx_{min} and m_x for Dispersive and Diffusive Scenarios

	$\beta < 1$ Dispersive Scenario	$\beta > 1$ Diffusive Scenario
Necessary discretization at the FMI	Smaller Δx_{min}	Larger Δx_{min}
Necessary grid multiplier perpendicular to the FMI	Larger m_x	Smaller m_x

Discussion

This study has shown using two different numerical models and several numerical methods that in some cases very fine spatial discretization (on the order of the fracture aperture, $2b$) perpendicular to the FMI is required in order to match analytical results. This requirement for such extremely fine discretization has not been reported by previous authors. The results indicate that scenarios with high matrix diffusion (i.e., slower water flow, higher porosity or diffusion coefficient, smaller aperture, longer times) do not require such small elements. On the other hand, scenarios with low matrix diffusion require extremely fine grids (Table 2). The aforementioned studies of Sudicky and McLaren (1992) and Cook et al. (2005) in which elements 250 times the fracture aperture were used to match the analytical solution of Sudicky and Frind (1982) were conducted using parameters that equate to β values of 0.143 and 885, respectively. These represent a slightly dispersive scenario and a highly diffusive scenario and combined with their long simulation periods of around 27.5 and 55 years in the case of Sudicky and McLaren (1992) and approximately 50 years for Cook et al. (2005) explain why they were able to use such large elements without encountering significant errors.

Thus, in many cases, solute transport may be simulated accurately without discretization on the order of the fracture aperture. However, when simulating scenarios involving high water velocity (e.g., forced gradient tracer tests), small diffusion coefficients (e.g., large compounds such as uranium), low matrix porosity, or very large fractures, simulations are prone to error and a rigorous sensitivity analysis of solutions to grid discretization is warranted.

As a consequence of the inherent discretization required for some practical scenarios, the use of discrete-fracture network models in the simulation of catchment-scale phenomena may be severely limited by computing capacity. With current computing capabilities, models requiring discretization on the scale of the fracture aperture will be limited to incorporation of very few fractures and/or small-scale model dimensions.

Conclusions

This study has examined the spatial discretization required perpendicular to the FMI in a discrete-fracture model in order to demonstrate how simulation accuracy and required discretization are influenced by the diffusive-dispersive nature of the problem being considered. Comparison with the analytical solution of Tang et al. (1981) has indicated the following:

1. Finite difference and element grids need to be designed according to the relative dominance of advection and dispersion in the fracture to diffusion in the matrix.
2. Diffusive scenarios ($\beta > 1$) tolerate larger elements close to the FMI (large Δx_{min}) but require the growth of matrix elements moving away from the fracture to be gradual (small m_x), a result not reported in previous literature.
3. Dispersive scenarios ($\beta < 1$) require small elements close to the FMI (small Δx_{min}) but are able to employ larger matrix elements (large m_x) for relatively short timescales, before solute penetrates far into the matrix, a result not reported in previous literature.
4. Results were compared from a wide range of numerical schemes and two different numerical codes. The requirement for fine discretization at the FMI was found to be neither a phenomenon of the codes nor the numerical schemes used within them.
5. Minor discrepancies between numerical and analytical results were observed, especially for diffusive scenarios. These are assumed to be due to the assumption made in the analytical solution that matrix diffusion occurs only perpendicular to the FMI but which is inherently 2D in the numerical framework considered here.
6. While it has previously been reported that fine discretization is required to simulate solute transport in discretely fractured media, this study has quantified the relationship between Δx_{min} and β, showing that the grid discretization required for low matrix diffusion scenarios can be on the order of the size of the fracture aperture ($\Delta x_{min} \approx 2b$). This necessary grid spacing requirement is extremely fine and has not been reported previously in the literature.
7. While the discretization requirements at the FMI and in the adjacent matrix are related to the physical parameters of the system being modeled (e.g., D', v, z), they are also tied to the timescales used for individual time steps and overall model duration.

The results of this study clearly indicate that caution must be taken when modeling solute transport in discrete-fracture systems using a numerical model. Careful attention must be given to the diffusive-to-dispersive ratio in the system under consideration. Critically, the results of this study provide guidance on the choice of Δx_{min} and m_x that should be employed for the varying cases of diffusive/dispersive effects in the physical system under consideration. These results are demonstrative and indicative only, and we wish to exercise some caution in overgeneralizing results here. However, it is abundantly clear that a sensitivity analysis must be conducted to determine the precise spatial and temporal discretization required in any given model of solute transport in fractured porous media.

Acknowledgments

The authors gratefully acknowledge project funding from Land and Water Australia, the Canadian Water Network, and the Natural Sciences and Engineering Research Council of Canada. We thank the anonymous reviewer for their constructive comments. D.W. thanks the Centre for Groundwater Studies for a research stipend and Flinders University for a research scholarship.

References

Anderson, M.P., and W.W. Woessner. 1992. *Applied Groundwater Modeling: Simulation of Flow and Advective Transport*. San Diego, California: Academic Press Inc.

Chan, T., N.W. Scheier, and V. Guvanasen. 1999a. MOTIF Version 3.2 Theory Manual, 06819-REP-01200-0091-R00. Toronto, Ontario, Canada: Nuclear Waste Management Division, Ontario Power Generation Inc.

Chan, T., N.W. Scheier, and F.W. Stanchell. 1999b. MOTIF Code Version 3.2 User's Manual, 06819-REP-01200-0090-R00. Toronto, Ontario, Canada: Nuclear Waste Management Division, Ontario Power Generation Inc.

Clift, S.S., E.F. D'Azevedo, P.A. Forsyth, and J.R. Knightly. 1996. WATSIT-1 and WATSIT-B Waterloo Sparse Iterative Matrix Solvers. User's Guide with Developer Notes for Version 2.0.0. Waterloo, Canada: University of Waterloo.

Cook, P.G., A.J. Love, N.I. Robinson, and C.T. Simmons. 2005. Groundwater ages in fractured rock aquifers. *Journal of Hydrology* 308, no. 1–4: 284–301.

Diodato, D.M. 1994. *A Compendium of Fracture Flow Models*. Argonne, Illinois: Argonne National Laboratory.

England, R.L., N.W. Kline, K.J. Ekblad, and R.G. Baca. 1985. MAGNUM-2D Computer Code: User's Guide, RHO-BW-CR-143P. Richland, Washington: Rockwell Hanford Operations.

Graf, T., and R. Therrien. 2005. Variable-density groundwater flow and solute transport in porous media containing nonuniform discrete fractures. *Advances in Water Resources* 28, no. 12: 1351–1367.

Grisak, G.E., and J.F. Pickens. 1980. Solute transport through fractured media 1: The effect of matrix diffusion. *Water Resources Research* 16, no. 4: 719–730.

HSI-GeoTrans. 2000. *Theory and Implementation for SWIFT for Windows: The Sandia Waste-Isolation Flow and Transport Model for Fractured Media*. Sterling, Virginia: HSI GeoTrans.

Huyakorn, P.S., and G.F. Pinder. 1983. *Computational Methods in Subsurface Flow*. Orlando, Florida: Academic Press Inc.

Lever, D.A., and M.H. Bradbury. 1985. Rock-matrix diffusion and its implications for radionuclide migration. *Mineralogical Magazine* 49, no. 351: 245–254.

Neuman, S.P. 2005. Trends, prospects and challenges in quantifying flow and transport through fractured rocks. *Hydrogeology Journal* 13, no. 1: 124–147.

Piessens, R., and R. Huysmans. 1984. Algorithm 619. Automatic numerical inversion of the Laplace transform. *Association of Computer Machinery Transactions on Mathematical Software* 10, no. 3: 348–353.

Rausch, R., W. Schafer, R. Therrien, and C. Wagner. 2005. *Solute Transport Modelling: An Introduction to Models and Solution Strategies*. Stuttgart, Baden-Württemberg: Borntraeger.

Reynolds, D.A., and B.H. Kueper. 2002. Numerical examination of the factors controlling DNAPL migration through a single fracture. *Ground Water* 40, no. 4: 368–377.

Robinson, N.I., and J.M. Sharp. 1997. Analytical solution for solute transport in a finite set of parallel fractures with matrix diffusion, CMIS C23/97. Adelaide, South Australia, Australia: CSIRO.

Runchal, A. 2002. PORFLOW User's Manual, Version 5. Bel Air, California: Analytic & Computational Research Inc.

Slough, K.J., E.A. Sudicky, and P.A. Forsyth. 1999. Grid refinement for modeling multiphase flow in discretely fractured porous media. *Advances in Water Resources* 23, no. 3: 261–269.

Sudicky, E.A., and E.O. Frind. 1982. Contaminant transport in fractured porous media: analytical solutions for a system of parallel fractures. *Water Resources Research* 18, no. 6: 1634–1642.

Sudicky, E.A., and R.G. McLaren. 1998. *FRACTRAN User's Guide. An Efficient Simulator for Two-Dimensional, Saturated Groundwater Flow and Solute Transport in Porous or Discretely-Fractured Porous Formations*. Waterloo, Ontario, Canada: Groundwater Simulations Group, Waterloo Centre for Groundwater Research, University of Waterloo.

Sudicky, E.A., and R.G. McLaren. 1992. The Laplace transform Galerkin technique for large-scale simulation of mass transport in discretely fractured porous formations. *Water Resources Research* 28, no. 2: 499–514.

Tang, D.H., E.O. Frind, and E.A. Sudicky. 1981. Contaminant transport in fractured porous media: Analytical solution for a single fracture. *Water Resources Research* 17, no. 3: 555–564.

Therrien, R., and E.A. Sudicky. 1996. Three-dimensional analysis of variably-saturated flow and solute transport in discretely-fractured porous media. *Journal of Contaminant Hydrology* 23, no. 1–2: 1–44.

Therrien, R., E.A. Sudicky, R.G. McLaren, and S.M. Panday. 2005. *HydroGeoSphere: A Three-Dimensional Numerical Model Describing Fully-Integrated Subsurface and Surface Flow and Solute Transport. User's Guide*. Waterloo, Ontario, Canada: Groundwater Simulations Group.

Travis, B.J., and K.H. Birdsell. 1991. *TRACR3D: A Model of Flow and Transport in Porous Media, Model Description and User's Manual*. Los Alamos, New Mexico: Los Alamos National Laboratory.

VanderKwaak, J.E., and E.A. Sudicky. 1996. Dissolution of non-aqueous-phase liquids and aqueous-phase contaminant transport in discretely-fractured porous media. *Journal of Contaminant Hydrology* 23, no. 1–2: 45–68.

Zheng, C. 1990. *MT3D: A Modular Three-Dimensional Transport Model for Simulation of Advection, Dispersion and Chemical Reactions of Contaminants in Groundwater Systems*. Rockville, Maryland: S.S. Papadopulos and Associates Inc.